ACS NANO

www.acsnano.org

PERSPECTIVE

Applying Spatiotemporal Modeling of Cell Dynamics to Accelerate Drug Development

Xindong Chen, Shihao Xu, Bizhu Chu, Jing Guo, Huikai Zhang, Shuyi Sun, Le Song, and Xi-Qiao Feng*

Cite This: *ACS Nano* 2024, 18, 29311−29336

Read Online

ACCESS | Metrics & More | Article Recommendations

ABSTRACT: **Cells act as physical computational programs that utilize input signals to orchestrate molecule-level protein−protein interactions (PPIs), generating and responding to forces, ultimately shaping all of the physiological and pathophysiological behaviors. Genome editing and molecule drugs targeting PPIs hold great promise for the treatments of diseases. Linking genes and molecular drugs with protein-performed cellular behaviors is a key yet challenging issue due to the wide range of spatial and temporal scales involved. Building predictive spatiotemporal modeling systems that can describe the dynamic behaviors of cells intervened by genome editing and molecular drugs at the intersection of biology, chemistry, physics, and computer science will greatly accelerate pharmaceutical advances. Here, we review the mechanical roles of cytoskeletal proteins in orchestrating cellular behaviors alongside significant advancements in biophysical modeling while also addressing the limitations in these models. Then, by integrating generative artificial intelligence (AI) with spatiotemporal multiscale biophysical modeling, we propose a computational pipeline for developing virtual cells, which can simulate and evaluate the therapeutic effects of drugs and genome editing technologies on various cell dynamic behaviors and could have broad biomedical applications. Such virtual cell modeling systems might revolutionize modern biomedical engineering by moving most of the painstaking wet-laboratory effort to computer simulations, substantially saving time and alleviating the financial burden for pharmaceutical industries.**

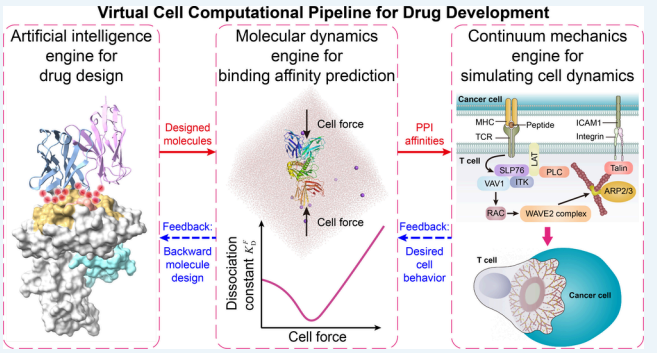

KEYWORDS: *cytoskeletal proteins, cell dynamics, protein−protein interactions, molecular dynamics simulation, artificial intelligence, gene therapy, drug design, virtual cell*

INTRODUCTION

Cells are active physical objects that perform a wide range of physiological functions by generating, transmitting, and sensing various types of mechanical forces.[1−4] Cytoskeleton is a highly dynamic network assembled by a substantial number of proteins.[5] Besides providing structural and mechanical support to cells, the cytoskeleton is a direct player of innumerable cellular dynamic behaviors, ranging from embryo development,[6,7] cell movement,[8−12] cell division,[13−15] immunological synapse formation,[16−19] and intracellular transport[20,21] to phagocytosis,[22−24] endocytosis,[25−27] and macropinocytosis.[28,29] The branched actin network, for example, is a primary propulsive force-generating machinery.[4,11] Through actin filament polymerization, it produces pushing forces to drive cell migrations (Figure 1a),[4,5,8,30] carry out endocytosis for drug and vaccine uptakes (Figure 1b),[25,27,31,32] perform macropinocytosis for antigen presentations (Figure 1c),[29,33] and boost cytotoxic T cell killing target cells (Figure 1d).[16,17,34] Dysfunctions of cytoskeletal proteins lead to a variety of diseases and disorders, including some cancers, neurodegenerations, and immune system disorders. For example, overexpression of the Arp2/3 complex, which assembles the branched actin network, is correlated with tumor metastasis and poor patient survival in lung,[35] breast,[36] pancreatic,[37] and colorectal cancers.[38] Moreover, dysfunction of the tau protein, which disrupts the formation of the microtubule network in neurons, is thought to be related with the development of Alzheimer's disease (Figure 1e).[39−42] Since the cytoskeletons play key roles in many physiological and pathological behaviors of cells, some of FDA-approved drugs target cytoskeletal

Received: September 8, 2024
Revised: October 2, 2024
Accepted: October 8, 2024
Published: October 18, 2024

https://doi.org/10.1021/acsnano.4c12599
ACS Nano 2024, 18, 29311−29336

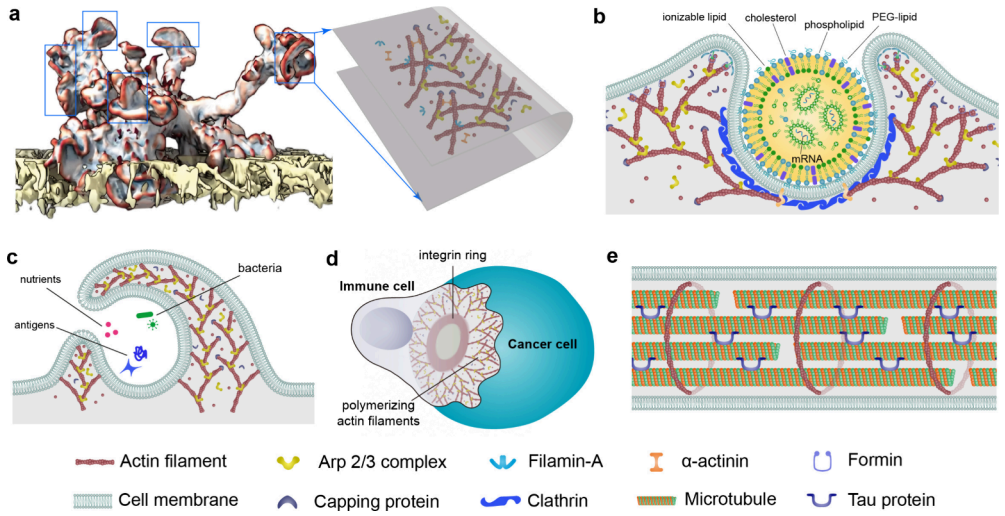

Figure 1. The cytoskeleton performs various cellular functions. (a) Migrating cells generate a lot of lamellipodial protrusions (in blue boxes) and employ the polymerization of lamellipodial branched actin networks to overcome the confinements of the 3D collagen matrix. Reprinted in part with permission from ref 71. Copyright 2019, Springer Nature. (b) Polymerizing branched actin filaments carry out clathrin-mediated endocytosis for cellular uptake of lipid nanoparticle−mRNA vaccine. The clathrin-mediated endocytosis forms vesicles with diameter of 60−200 nm.[72−74] (c) Polymerizing branched actin filaments generate membrane ruffles and conduct macropinocytosis to ingest extracellular bacteria, nutrients, and antigens. In immune responses, antigen-processing cells, like macrophages and immature dendritic cells, use macropinocytosis to sample potential antigens for presentation to T cells.[29,33,75] The diameters of macropinosomes are normally 0.2−5 μm.[76] (d) Cytotoxic T cells use the polymerizing branched actin network to form immunological synapse and exert mechanical forces on target cancer cells. The force enhances perforin activity and thus potentiates cytotoxicity for killing cancer cells.[17,34] (e) Microtubules, tau proteins, and cortical actin rings form a long axonal cytoskeletal network. Mechanical stability of the network not only plays a key role in transporting nutrients and proteins into the growing cones (driven by polymerizing branched and bundled actin filaments), but also helps to sustain the normal functions of nervous system.

proteins directly[43−45] or indirectly via upstream signaling pathways (Table 1).[46−50]

In the recent years, significant advances have been made in experimental techniques for measuring mechanical properties of proteins and cellular forces,[51−55] and imaging the dynamic behaviors of protein-stained living cells[56−58] that interact with extracellular microenvironments (ECMs). These techniques provide an increasing correlation knowledge between protein molecules, cell behaviors, and ECMs. On the basis of these findings, more and more predictive biophysical models[5,15,31,59−66] from the subcellular to multicellular scales have been proposed at the intersection of biology, mathematics, physics, and computer science. Because of their huge advantages in performing quantitative analysis of cellular processes, the biophysical models have effectively elucidated the underlying mechanisms of many complicated biological questions that are difficult for traditional experiments. On the other hand, drug discovery and development is a highly expensive and intricate process, typically spanning over 10 years and demanding substantial financial investment, while also bearing a significant risk of failure.[67,68] None of those models currently simulating cellular dynamic behaviors can be applied to pharmaceutical engineering to accelerate the drug discovery and development process. This challenge arises from the intricate spatiotemporal cross-scale computational hurdles between molecular ligand−protein interactions and dynamic cellular behaviors. Furthermore, it stems from the simultaneous involvement of numerous proteins in single-cellular functions, particularly in contexts where the cytoskeleton undergoes highly kinetic and stochastic remodeling due to the coupling of mechanical forces and biochemical cues. Consequently, although developing the spatiotemporal multiscale cellular models applicable to pharmaceutical engineering presents enormous opportunities to accelerate healthcare advancements,[69,70] a computational framework to realize this goal is still missing.

In this work, we first introduce the main cytoskeleton proteins, their elasticity and dynamic properties, and different types of cytoskeletal networks that perform distinct cellular functions. Then, we review the major biophysical advances in simulating protein-based cellular dynamic behaviors, ranging from subcellular to multicellular scales for studying endocytosis, cancer invasion, and embryonic development. Finally, we discuss the limitations of the present models and propose a comprehensive computational pipeline for developing virtual cells by combining generative artificial intelligence (AI) technology with spatiotemporal multiscale modeling. The proposed pipeline can be applied to different cellular scenarios with complicated mechano-chemo-biological mechanisms and offers significant potential for accelerating drug discovery and development in pharmaceutical engineering. By shifting a substantial portion of labor-intensive wet-laboratory efforts to computer simulations, the pipeline might shorten drug development time, improve success rate, alleviate the financial burden for pharmaceutical industries, and thus revolutionize modern biomedicine.

CYTOSKELETAL PROTEIN ELASTICITY AND NETWORKS

Cytoskeletal Filament Elasticity. Cytoskeletons are mainly composed of three kinds of cytoskeletal filaments, i.e., actin filaments, microtubules (MTs), and intermediate filaments (IFs).[108−110] They are assisted by various binding proteins, organizing into different types of cytoskeletal networks (Figure 2). The cytoskeletal networks' mechanical properties and interactions with ECMs determine cell

https://doi.org/10.1021/acsnano.4c12599
ACS Nano 2024, 18, 29311−29336

Table 1. FDA-Approved Drugs That Target Cytoskeletal Proteins Directly or Indirectly via Upstream Signaling Pathways

Drug Name	Target	Disease	Company
Paclitaxel	Tubulin (stabilize MTs and thereby stop mitosis).[43−45]	Breast cancer, ovarian cancer, lung cancer	Bristol−Myers Squibb, Pfizer, Hospira, Novartis
Cilengitide	Integrin (inhibit cell adhesion and thereby angiogenesis).[77−79]	Glioblastoma, melanoma	Merck KGaA
Ixabepilone	Tubulin (stabilize microtubules and prevent their depolymerization).[80,81]	Advanced breast cancer	Bristol−Myers Squibb
Ripasudil	Rho kinase (inhibit the Rho-associated protein kinase pathway and thus reduce actomyosin contractility and actin bundle formation).[82,83]	Glaucoma, ocular hypertension	Kowa
Docetaxel	Tubulin (prevent MT depolymerization and thereby stop mitosis).[84−86]	Breast cancer, prostate cancer, lung cancer, stomach cancer	Sanofi
Vinblastine	Tubulin (inhibit its polymerization and disrupt MT dynamics).[87,88]	Hodgkin's lymphoma, testicular cancer, breast cancer	Pfizer
Fasudil	Rho-kinase enzyme (inhibit Rho-associated protein kinase to decrease phosphorylation of myosin light chain and LIM kinase, resulting in reduced actomyosin contractility).[89,90]	Vasospasm, pulmonary arterial hypertension	Bayer, Daiichi Sankyo
Epothilones	Tubulin (stabilize MTs, disrupt mitosis and induce cell death).[91,92]	Breast cancer, non-small cell lung cancer, prostate cancer	Bristol−Myers Squibb
Imatinib	Tyrosine kinase BCR-ABL (affect downstream targets, including focal adhesion kinase and Rho GTPases, which are key regulators of cytoskeletal organization).[46−50]	Leukemia, gastrointestinal stromal tumor	Novartis
Dasatinib	BCR-ABL, c-Kit, Src family (disrupt Rho GTPase signaling pathways and inhibit Src pathways to reduce actin cytoskeleton polymerizations and focal adhesion turnover).[93−95]	Leukemia	Bristol−Myers Squibb
Gefitinib	Epidermal growth factor receptor (inhibit the formation of actin stress fibers and focal adhesions).[96]	Non-small cell lung cancer	AstraZeneca
Erlotinib	Epidermal growth factor receptor (disrupt actin cytoskeleton dynamics).[97,98]	Nonsmall cell lung cancer, pancreatic cancer	Roche, Genentech
Crizotinib	ALK (alter downstream signaling of RhoA and Rac1 to regulate cytoskeletal dynamics).[99,100]	Nonsmall cell lung cancer	Pfizer
Carvedilol	Beta-adrenergic receptors (reduce protein kinase A activation to reduce actomyosin network contractions).[101,102]	Hypertension, heart failure	GlaxoSmithKline
Entrectinib	NTRK, ROS1 (inhibit downstream signaling of Rho GTPases and disrupt actin dynamic).[103,104]	Nonsmall cell lung cancer, solid tumors	Rozlytrek, Genentech
Propranolol	Beta-adrenergic receptors (reduce protein kinase A activation to reduce actomyosin network contractions).[102,105]	Hypertension, angina	Wyeth
Memantine	NMDA receptor antagonist (increase the expression of genes related to cytoskeletal organization in hippocampus).[106,107]	Alzheimer's disease	Allergan, Lundbeck, Merz Pharma

behaviors, modulate cell fate, direct tissue development, and instruct postnatal functions.[111−117] Actin filaments, MTs, and IFs are all semi-flexible,[118] and their mechanical properties can be described by the characteristic persistence length l_p, which is defined as the average length at which significant bending fluctuations occur under thermal fluctuations and quantifies the bending stiffness of the cytoskeletal filaments. l_p can be calculated from in vitro experimental measurements according to $\langle \tau \rightarrow (0) \tau \rightarrow (s) \rangle = \langle \cos \theta(s) \rangle = \exp(-s/l_p)$ where $\tau \rightarrow (s)$ is the unit tangent vector at position s along the contour of the filament chains, $\theta(s)$ is the angle between the two tangent vectors at positions 0 and s, and $\langle\ \rangle$ represents taking the average value in statistic mechanics. Based on l_p, the Young's modulus E of the filaments can also be approximately obtained according to $EI = l_p k_B T$ where I is the moment of inertia of the cross section, k_B is the Boltzmann's constant, and T is the absolute temperature. The implied Young's modulus E is 0.5−1.0 GPa for actin filaments and MTs, and is 6.4−200 MPa for IFs based on protein types (Table 2).[119] It should be mentioned that cytoskeletal filaments, especially IFs,[120,121] are viscoelastic, and thus their mechanical responses to loading are frequency-dependent. In eukaryotic cells, the typical contour lengths of actin filaments and MTs are normally much shorter than their characteristic persistence lengths (Table 2). As a result, the curved states they exhibit in cells are primarily due to external forces acting upon them. The stiffnesses, lengths, and diameters of the three major types of cytoskeletal filaments and their binding proteins for organizing different cytoskeletal networks for distinct biological functions are summarized in Table 2, Table 3, and Figure 2.

Actin Dynamics. Actin dynamics plays a critical role in driving cell membrane deformation impacting on diverse biological functions.[132−134] Actin filaments are polar biopolymers and have two ends, namely, barbed end and pointed end.[30] The barbed end is much more active in actin polymerization, and thus its elongation rate is 10 times faster than that of the pointed end.[135] The polymerization rate is proportional to the concentration of actin monomers. Growth velocity V_g of actin filaments based on polymerization can be simply expressed by $V_g = \delta(k_{on}C_a - k_{off})$, where $\delta \approx 2.7$ nm and is the growth length by adding an actin monomer to the barbed end, C_a is the concentration of actin monomers, and k_{on} and k_{off} are polymerization and depolymerization rate constants, respectively.[136−138] Actin filament polymerization is terminated by capping protein binding to its barbed end.[139] Thus, the growth length of actin filaments is determined by the ratio of single-molecule polymerization rate and capping rate.[1] In a steady state where actin nucleation rate is equal to capping rate, the growth length of actin filaments $L_f = \delta(k_{on}C_a - k_{off})/(k_{cap}C_{cap})$ where k_{cap} and C_{cap} are capping rate constant and capping protein concentration, respectively.[140] It should be noted that actin polymerization is also modulated by other protein molecules, such as formin[141,142] and VASP,[143,144] which improve polymerization rate or protect from capping. They regulate actin filaments to grow to different lengths for different functions.

https://doi.org/10.1021/acsnano.4c12599
ACS Nano 2024, 18, 29311−29336

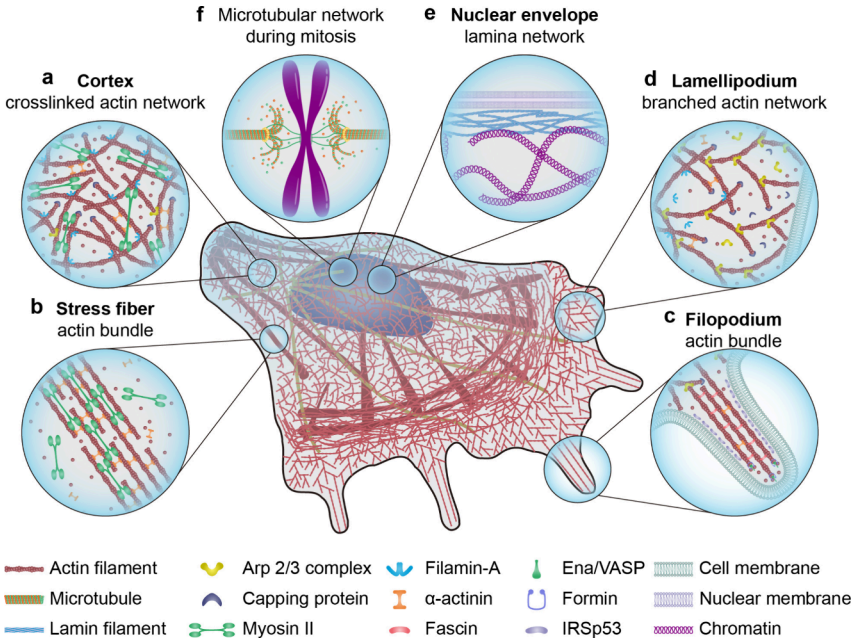

Figure 2. Overview of typical cytoskeletal networks and their locations in cells. (a) The cross-linked actin network is mainly assembled in cell cortex and is a thin layer actin network with a thickness of 100−500 nm.[60] Contraction of myosin motors in it regulates cortical tension, ranging from 100−3000 pN/μm,[60] which then modulates deformations and movements of the cell and nucleus. The lengths of actin filaments and myosin minifilaments in the network are normally 500−1500 nm[60] and 280−330 nm.[194,195] (b) The stress fiber is an actin bundled network, which is mainly assembled by actin filaments, myosins, and cross-linking proteins, such as α-actinins. Contraction of myosin motors in the stress fiber generates pulling forces. During cell migration, in the front of the cell, the contraction pulls the nucleus forward,[196] and in the back of the cell, the contraction pulls the detachments of integrin-based focal adhesions.[197] (c) The filopodial actin bundled network is a finger-like, and drives cell migration through actin filament polymerizations at the leading edge. It normally grows out from a branched actin network. (d) The lamellipodial branched actin network is a sheet-like structure with a thickness of around 150−200 nm, and is extensively assembled along the leading edge of migrating cells (Figure 1a). Because of its high stiffness[1,5] and polymerization force-regulated actin filament−Arp2/3 complex interaction,[4] it not only plays a critical role in driving cell migrations[8] but also acts as a mechano-sensor of cells for figuring out the complex ECMs.[4] (e) The lamina network is a type of IF network, and is formed under the nuclear membrane. It provides mechanical stability for the nucleus, and serves a platform for anchoring nuclear pore complexes[198] for molecular transportations between the nucleus and cytoplasm, including mRNA and nutrients. Additionally, it also tightly interacts with chromatins,[199,200] and variations of mechanical properties regulate gene fates.[201] (f) The microtubular network exists throughout the cytoplasm, and is the key player of sustaining cell body stability and molecular transportations in cytoplasm. During mitosis, it forms a mitotic spindle and exerts forces on chromosomes based on disassembly, pulling them apart. In neurons, it provides the main structural support for axons (Figure 1e).

Table 2. Globular Proteins, Dimensions, Persistence Lengths, and Elasticities of Cytoskeletal Filaments and DNA[118,122−131]

Type	Globular proteins	Diameter (nm)	Persistence length (μm)	Young's modulus (GPa)	Contour length (μm, position)	
F-actin	actin	7	17	0.5−1.0	0.1−0.5 (cortex, lamellipodia)	1−20 (filopodia, stress fibers)
MTs	α-tubulin & β-tubulin	13 (inner) 25 (outer)	1×10^3 to 5×10^3	0.5−1.0	1−10 (in cytoplasm)	50−100 (axons)
IFs	vimentin; lamin; keratin	10	0.2−2.1	6×10^{-2} to 0.2	0.1−0.5 (nuclear lamina network)	1−10 (in cytoplasm)
DNA	nucleotide	2	5×10^{-2}	0.3−1.0	2×10^6	

Actin Networks and Cellular Functions. By connecting with different actin binding proteins, actin filaments can organize into three kinds of networks, i.e., branched actin networks (Figure 2d), cross-linked actin networks (Figure 2a), and actin filament bundles (Figure 2b and c). Branched actin networks are mainly initiated by the Arp2/3 complex.[145−147] They are not structurally isotropic, but with most of the polymerizing barbed ends toward one direction (Figure 2d),[5,30,148] which is closely related with cellular propulsive functions.[149] Polymerization of branched actin filaments is one of the most important ways for cells to generate propulsive forces to interact with ECMs and hence accomplish physiological as well as pathophysiological functions. Thus, the branched actin network participates in driving cell migration and cancer invasion (Figure 1a),[8,38] leading dendritic spine formation,[133] conducting clathrin-mediated endocytosis and macropinocytosis for various size nanoparticle uptakes (Figure 1b and c),[29,150] and enhancing cytotoxic T cells to kill target cells (Figure 1d).[34] Strikingly, one important function of the branched actin network is that it can sense mechanical resistance from the ECM[4] and adjust the filament density accordingly to ensure the fulfillment of cellular functions.[8,151] Finite element simulations based on a multiscale assembling model (Figure 3a) demonstrate that the branched

https://doi.org/10.1021/acsnano.4c12599
ACS Nano 2024, 18, 29311−29336

Table 3. Typical Cytoskeletal Networks, Their Main Component Proteins, and Cellular Functions

Type of cytoskeletal networks	Main component proteins	Cellular functions
Branched actin network	Arp2/3 complex, actin filament, capping protein (also include a little bit of cross-linking proteins, i.e., filamin-A and α-actinin).[202,203]	Lamellipodia-based cell migration;[5,8] endocytosis;[24,31] macropinocytosis;[29] immune cells kill cancer cells;[34,204,205] formation of neuronal dendrites;[206,207] DNA repair and chromatin organization;[208−210] nucleus deformation.[211]
Cortical cross-linked actomyosin network	Myosin, actin filament, filamin-A, α-actinin, capping protein (also include a little bit of Arp2/3 complex).[194]	Regulate cell membrane tension and cell shape;[60] adapt nucleus deformation;[9,10] immune cells kill cancer cells.[17,155]
Actin filament bundle	Actin filament, fascin, α-actinin, capping protein (also include myosin in stress fibers connected with adhesions).[212,213]	Filopodia-based cell migration;[214,215] contractile stress fiber for cell migration;[216] communication between remote cells;[163] contractile ring for mitosis;[217] actin ring in axon;[218] tissue morphogenesis.[161,219]
MT network	MT, tau[218] (tau[220] and ACF7[218] can cross-link microtubules with actin filaments).	Mitosis;[221,222] axon formation;[223,224] maintain cell shape;[225,226] nucleus movements;[227,228] intracellular transport.[229]
IF network	Intermediate filament, filaggrin,[230] kinesin, plectin (kinesin[231,232] and plectin[233] cross-link IFs with MTs).	Nucleus deformation;[234,235] regulate chromatin organization[191,200] and gene expressions;[201,236] maintain cell shape;[190,237] embryonic development.[6]

actin networks exhibit higher sensitivity to the variations of filamentous actin concentrations and greater stiffness than cross-linked actin networks,[5] due to the relatively rigid Arp2/3 branched junctions.[152] The stiffness of branched actin networks primarily depends on cross-linking proteins (filamin-A and α-actinin) at low Arp2/3 concentration and actin filaments at high Arp2/3 concentration.[5] The cross-linked actin network is another kind of actin network that is organized by various cross-linking proteins, such as myosin, filamin-A, and α-actinin (Figure 2a). The cortical cross-linked actin network is anchored to the plasma membrane through ERM proteins and is involved in controlling cell shape[153] and maintaining mechanical integrity.[60,110] During cell migration, the cross-linked actin network can significantly regulate cell morphology, nucleus deformation, and cytoplasm bleb formation through myosin contractions, facilitating the cell to squeeze through narrow pores in ECMs.[9,10,56] In addition, due to the abundance of force-sensitive proteins on the cell membrane, the cross-linked actin network, by modulating cell membrane tension force, participates in many other crucial cell behaviors, such as activation of signaling molecules[154] and formation of perforin pores during immune response.[17,155] The last type of actin network is actin filament bundles, which are composed of parallel or antiparallel actin filaments cross-linked by proteins, like fascin and α-actinin (Figure 2c). They are finger-like structures with a diameter ranging from 50 to 300 nm,[156,157] and can grow over 30 μm by actin polymerization. They not only drive cell migrations and steer the growths of nervous cells in tissues[158−161] but also serve as communicating bridges between remote cells.[162] Besides the protrusion, filopodial actin bundles can retract to generate pulling forces for up-taking drugs[76] and viruses.[163] Moreover, when cross-linked with myosin, actin filament bundles form contractile stress fibers that attach to focal adhesions, exerting pulling forces to regulate cell behaviors (Figure 2b).[164]

MT Dynamics and Cellular Functions. MTs are assembled from α-β tubulin heterodimers, which stack head-to-tail to form polar protofilaments.[165,166] In each MT, 13 protofilaments associate laterally in parallel to form a hollow cylindrical structure. Therefore, MTs are the stiffest among the three main types of cytoskeletal filaments, with a persistence length that can reach 5 mm.[167] This stiffness enables MTs to provide the primary structural support for cells,[129] contribute cellular polarity,[168] and facilitate neuronal migration,[169,170] as well as act as linear tracks for intracellular trafficking.[167,171] MTs are highly dynamic,[172,173] and can abruptly switch between growth and catastrophe (shrinkage).[174−177] Such dynamic instability stems from the peculiar chiral structures and enables their tips to explore the cellular environment and capture chromosomes during cell division.[178] By disassembling and shortening, MTs exert pulling forces to separate chromosomes into two sets, accomplishing cell division (Figure 2f).[179] Because of their dominating role in cell division, many anticancer drugs perturbing their dynamics, such as taxane paclitaxel and nocodazole, have been developed to prevent tumor development and exhibit good clinical effects (Table 1).[178] The biophysical mechanism of the high dynamic instability of MTs can be explained from the perspective of mechanics. According to the principle of minimum internal energy, the α-β tubulin heterodimers that compose a protofilament have intrinsic properties that cause the protofilament to preferentially adopt a bent conformation. In the MT lattice structure, however, the 13 protofilaments are

https://doi.org/10.1021/acsnano.4c12599
ACS Nano 2024, 18, 29311−29336

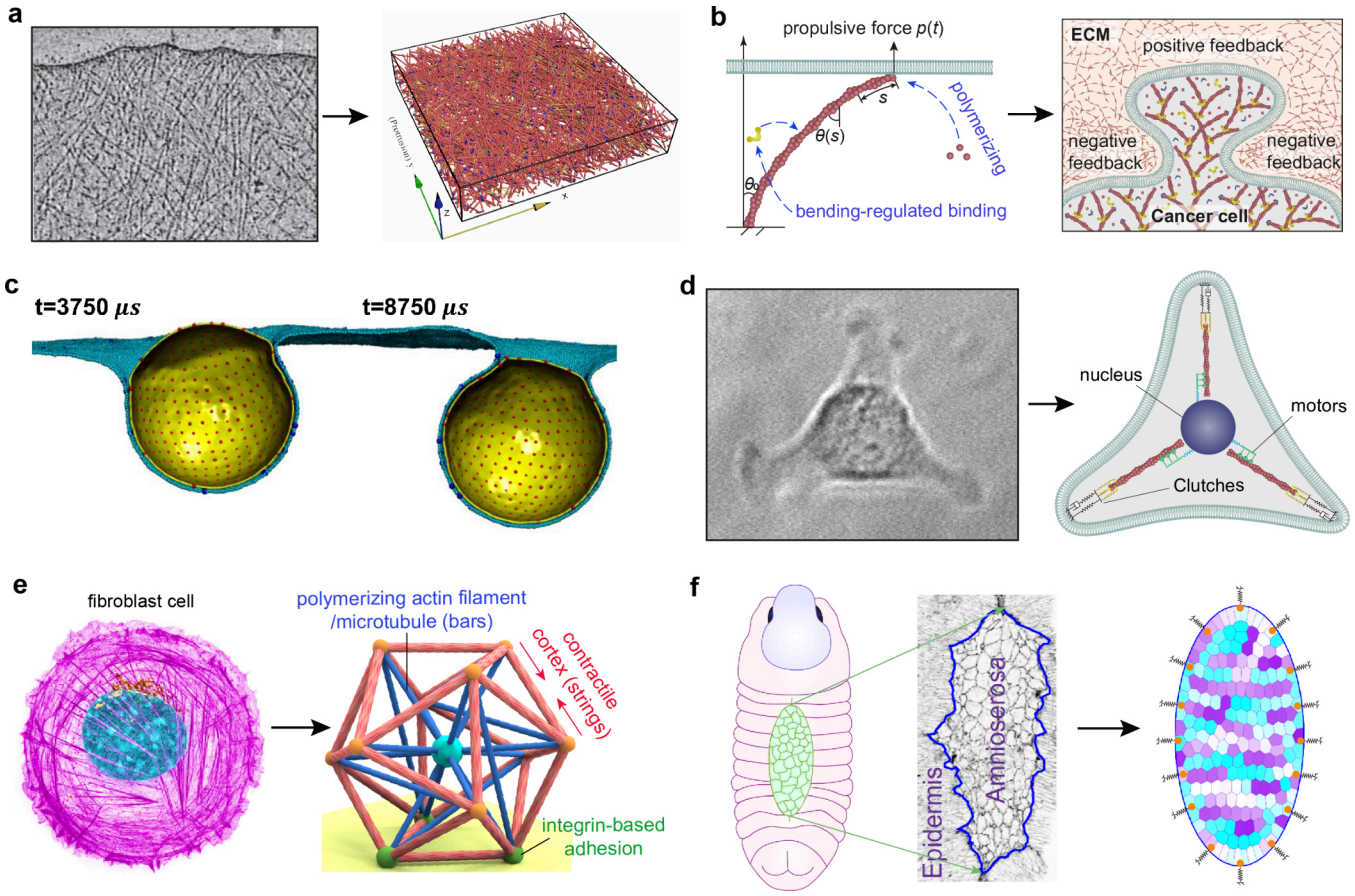

Figure 3. Subcellular, single-cell, and multicellular models for investigating cell dynamics. (a) Protein-based assembling branched actin network model investigates the dominating proteins in modulating lamellipodial stiffness. Adapted with permission under a Creative Commons CC BY License from ref 5. Copyright 2020, Springer Nature. (b) Spatiotemporal RAP model investigates how protein molecules dynamically regulate self-adaptive cancer cell invasions in complex ECMs. Adapted with permission under a Creative Commons CC BY-NC-ND License from ref 4. Copyright 2023, National Academy of Sciences. (c) The coarse-grained molecular dynamics model studies the endocytosis of nanoparticles with different elasticities, sizes, and shapes. The polymerizing actin filaments that generate a propulsive force are neglected. Reprinted with permission from ref 258. Copyright 2019, American Chemical Society. (d) The motor-clutch model is used to investigate cell migrations on substrates with different mechanical properties. (e) The biochemomechanical tensegrity model of cytoskeleton is applied to study the single-cell oscillations. Adapted with permission from ref 272. Copyright 2023, Elsevier. (f) The vertex model investigates oscillatory morphodynamics of multicellular system during embryonic development. Reprinted with permission from ref 278. Copyright 2017, National Academy of Sciences.

straightened by the lateral interacting forces between them.[166,180] These lateral forces result in MTs being prestressed structures, which store elastic strain energy U. The energy can be expressed by

$$U = \frac{1}{2}\sum_{m=1}^{13}\sum_{n=1}^{N_m}[k_{long}(l_{long} - l_{long}^0)^2 + k_{lat}(d_{lat} - d_{lat}^0)^2 + k_{bend}(\theta_{bend} - \theta_{bend}^0)^2 + k_{tor}(\theta_{tor} - \theta_{tor}^0)^2] \quad (1)$$

where N_m is the number of α-β tubulin heterodimers along the mth protofilament; k_{long}, k_{lat}, k_{bend}, and k_{tor} are coefficients of the longitudinal stretching, lateral stretching, bending, and torsional stiffness for a α-β tubulin heterodimer, respectively; l_{long}, d_{lat}, θ_{bend}, and θ_{tor} are the longitudinal length, lateral width, bending angle, and torsional angle of a dimer in the MT lattice structure, respectively; and the superscript 0 represents their counterparts in the bent protofilament at the equilibrium state. Such a tensegrity-like structure lies at the heart of MT dynamic instability. Once the β-subunit GTP hydrolyzes by releasing Pi, the tubulin dimers in the MT lattice structure produce unevenly distributed deformations, tightening longitudinal and loosening lateral interdimer contacts.[128,165] Consequently, the lateral bonding can no longer counteract the strain energy stored in each tubulin dimers, thereby triggering the microtubule disassembling catastrophe.[181] Although structural studies indicate the seam protofilament site is the weakest in the MT lattice, the seam is not the primary initiator of the lattice opening, and MT catastrophe initiates at any of the 13 protofilament interfaces.[128,165,180]

IF and Cellular Functions. IFs are named because they have an intermediate diameter compared to actin filaments and MTs.[182] They are composed of a family of related proteins, such as keratins, vimentins, neurofilaments, and lamins.[6,183−186] They widely distribute from cytoplasm to the nucleus.[182,187] Their dysfunctions result in more than 30 diseases, most of which are difficult to treat.[182] Compared to actin filaments and MTs, they are nonpolar, are much softer, and have greater stability.[188] They can be extended to two or three times of their resting lengths without breaking, allowing them to absorb large amounts of energy.[120,121,189] Since actin filaments and MTs disassemble under moderate strains, IFs

https://doi.org/10.1021/acsnano.4c12599
ACS Nano 2024, 18, 29311−29336

play a significant role in resisting severe deformations of both cells and nuclei, and in maintaining their mechanical integrities.[190] Mechanical loadings on a single IF demonstrate that IFs exhibit strong viscoelastic properties.[121] Under a slow loading rate, they are very soft, while a faster loading rate leads to a substantial stiffening effect. Lamin IFs are the main components of nuclear networks within the nuclear envelope (Figure 2e). They are not only the primary mechanically supports of nucleus,[127,184] but also are engaged in the organization of heterochromatin.[191,192] Nuclear IF meshwork also serves as a crucial platform for the assembly of nuclear pore complexes, and fixes these complexes to the nuclear envelope for transporting mRNA as well as various proteins between the nucleus and cytoplasm.[187,193] In addition to nuclear lamin IFs, keratin IFs are the first major components of the embryo cytoskeleton that display prominent cell-to-cell variability, regulating cell lineage specifications in mammalian development.[6]

SPATIOTEMPORAL SIMULATIONS OF PROTEIN-BASED CELL DYNAMICS

Subcellular Simulations. Dynamic mechanical behaviors of cytoskeletal networks determine the cellular performance in biological functions. Overexpression, under-expression, or aberration of cytoskeletal protein result in many diseases, including cancer invasions, liver cirrhosis, pulmonary fibrosis, and cardiovascular disease syndromes.[40,182,237−239] A promising approach for identifying therapeutic targets for these diseases is to construct spatiotemporal multiscale subcellular models based on the behavior of single proteins and then develop a corresponding dynamic biophysical computational engine to reveal the key factors that govern cellular dynamic behaviors.[69] For example, to investigate how complicated self-adaptive cell migration behaviors in complex ECMs emerge from the millisecond-scale assembling activities of protein molecules, a spatiotemporal 'resistance-adaptive propulsion' (RAP) theory and a dynamic multiscale modeling system were developed.[4] This model considers the polymerization-induced conformational changes of actin filaments (eq 2 and Figure 3b) and force-regulated PPIs

$$\frac{\partial\theta(t,s)}{\partial s} = \int_s^{l(t)} \frac{p(t)}{EI} \sin[\theta(t,s) + \theta_0]\, ds \tag{2}$$

where t, θ, l, and p are the polymerization time, bending angle, length, and polymerization force of an actin filament, respectively; θ_0 is the initial angle between the straight actin filament and the normal vector of the local cell membrane. This modeling system successfully overcame the spatiotemporal cross-scale challenges between single molecular proteins and the cell, and revealed the biophysical molecular mechanism that underlies how migrating cells mechano-sense and make adaptive responses to complex ECMs.[1,8,12,240] Specifically, the polymerization force-regulated actin filament-Arp2/3 complex binding interaction remodels the density of the polymerizing branched actin filaments based on the magnitude of ECM resistance, thereby adjusting the propulsive force and dominating self-adaptive cell migrations in complex ECMs. It demonstrates that Arp2/3 might be a key target protein for developing anticancer drugs, especially for patients in the advanced stages of cancer. Additionally, in order to reduce computational complexity, some other simplified subcellular models[171,241−244] were also proposed to investigate cell dynamic behaviors. For instance, to elucidate the biophysical mechanism underlying the complex kinetics of growing axons, an active viscoelastic rod model of axonal growth, which considers myosin, actin filaments, and MTs, was recently proposed.[171] It shows that it is the interplay between cytoskeletal dynamics and axon−substrate adhesion that determines the axonal state transition between growth, stalling, and collapse. Moreover, cells work under highly dynamic in vivo environments. To maintain functional stability and allow time for adaptive response, cells show viscoelastic behaviors, resisting suddenly imposed deformations.[245] To investigate these behaviors, some subcellular multiscale actin network models[246,247] were constructed. By using the combined finite element and Langevin dynamics method, these computational models systematically demonstrate the underlying mechanisms of how the binding kinetics, deformability, and bond types of cross-linking proteins affect the viscoelastic behaviors of actin networks during cell deformation. Specifically, continuous breakage and rebinding of cross-linking proteins lead to a locally peaked loss modulus in the rheology spectrum of the network, indicating the maximal energy dissipation when the driving frequency aligns with cross-linking molecule dissociation/association rates.[246] Because of the stabilizing effect of forces on catch bond cross-linking proteins, the peak position of the network's loss modulus shifts to lower driving frequencies with increasing applied prestress, which is in contrast to the networks with slip-bond cross-linking proteins.[247] These computational results are in good agreement with experimental observations and demonstrate the underlying mechanisms of viscoelastic behaviors of cells.[245,248]

Clathrin-mediated endocytosis is the main mechanism by which cells ingest nanoparticles that carry drugs, genes, mRNA vaccines, and nutrients.[27,249−252] Based on actin polymerization force, a cell membrane wraps nanoparticles, whose safe entry into cells is an essential step for achieving high-yield therapeutic efficiency. Therefore, a fundamental understanding of the biophysical interactions between cell membrane and elastic nanoparticles is critical for designing highly efficient nanoparticle carriers for delivering mRNA vaccines, drugs, and genes.[253−257] A coarse-grained molecular dynamics model (Figure 3c) was applied to systematically investigate the endocytosis of nanoparticles with different elasticities, sizes, and shapes.[258] It shows that the cell membrane wrapping efficiency of nanoparticles is determined by a competing relation between receptor diffusion kinetics and driving force. Compared to the rigid nanoparticles, soft ones have less efficiency in wrapping because of elastic deformations. Owing to the oblate ellipsoid nanoparticles' prominent large binding area, they present a higher endocytic rate than sphere ones.[258] In addition, some theoretical models based on continuum mechanics were also developed to investigate the dynamic uptake processes of endocytosis.[31,32,259−261] These models treat the lipid bilayer cell membrane as a thin elastic shell, and the deformation energy during the wrapping process is expressed by a modified form of the Helfrich energy

$$W = \kappa(\theta^\alpha)[H - C(\theta^\alpha)]^2 + \kappa_G(\theta^\alpha)K \tag{3}$$

where W, H, and K are the deformation energy per unit area, the local mean curvature, and the local Gaussian curvature, respectively; $C(\theta^\alpha)$, $k(\theta^\alpha)$, and $k_G(\theta^\alpha)$ are the spontaneous curvature, bending modulus, and Gaussian modulus, respectively; θ^α represents the cell membrane surface coordinates. During the endocytosis process, the deformation of the cell

https://doi.org/10.1021/acsnano.4c12599
ACS Nano 2024, 18, 29311−29336

membrane follows a force balance $\nabla\cdot\boldsymbol{\sigma} + p_d\mathbf{n} = \mathbf{f}$ where ∇ and $\boldsymbol{\sigma}$ are surface divergence and stress vector, respectively; p_d is the pressure difference between the inside and outside of the cell membrane; $\mathbf{n}$ is the unit normal vector of the cell membrane surface; $\mathbf{f}$ is the polymerization force generated by actin filaments. Spatiotemporal simulations reveal that the cell membrane tension $\boldsymbol{\sigma}$ plays an important role in endocytosis. More specifically, while high membrane tension increases the difficulty of membrane endocytic internalization, the high tension also directs more growing and pronounced bending actin filaments toward the endocytic pit to increase the polymerizing force, contributing to the endocytosis.[31,32]

Single-Cell Simulations. Cells migrate, oscillate, and divide by coordinating the cytoskeletal actions, such as adhesions,[262] protrusions,[4] and contractions,[217] originating from different parts of the cellular body. However, the whole-cell cytoskeleton is too complex to be fully constructed and computed. To achieve single-cell mechanical dynamic simulations for interpreting biophysical mechanisms of cellular behaviors, most existing models simplify the cytoskeleton by representing its detailed network structures with different mechanical components. These components typically include actomyosin-based contractile elements, integrin-based adhesion elements, and actin filament and MT polymerization-based elements. Since the cytoskeleton undergoes frequent remodeling due to the interplay of mechanical forces and biochemical cues, it is critical to consider the biochemomechanical factors in these representing elements.[3,61,263] Motor-clutch models[242,264−266] (Figure 3d) are often employed to investigate cell migration behaviors in ECMs with different viscoelastic properties. They have demonstrated that the match between cellular adhesive binding time scales and ECM viscoelasticity determines cell migration velocity and direction, suggesting viscous dissipation plays an important role in determining cell response.[242,264,266,267] Change of ECM viscoelasticity is a factor inducing disease progressions, and might be a potent target that contributes to the development of cell therapeutics.[265,268,269] Because the cytoskeleton exhibits both compressive and tensile forces and shares a high similarity to tensegrity structures, tensegrity-based cytoskeletal models are also often applied to investigate complicated single-cell dynamic behaviors.[270−272] Recently, for instance, a biochemo-mechanical tensegrity-based cytoskeletal model (Figure 3e),[272] which incorporates the reaction and diffusion of myosin and RhoA, and the mechanical-chemical feedback mechanisms, was proposed to explore the cellular oscillating behaviors that appear in embryonic development.[273] Elastic strings and bars are utilized to simulate the actomyosin network contractions and the MTs and actin bundle polymerizations, respectively. The results show that the spontaneous oscillations of cells are a consequence of the feedback loop between the active contractile forces and chemical reactions. Additionally, shell-like single-cell models based on simplified two-dimensional multiscale cytoskeletal models[14,15,63] and the Kirchhoff−Love plate theory[64,274] were also developed to investigate the dynamic morphological evolutions of cells during asymmetric polarization and division. These models revealed that the plane of cell division tends to be perpendicular to the direction of the maximum principal stress in the nucleus[14,15] and explained the biophysical mechanisms by which cells use torsional deformation induced by chemical factors to carry out divisions in confined spaces.[274]

Multicellular Simulations. Collective cellular dynamics plays a crucial role in processes such as embryonic development, tumor metastasis, and wound healing.[275] To simulate these behaviors, modified dynamic vertex models (Figure 3f) that incorporate biochemical cues have shown promise as a physical framework, and has been used successfully in various multicellular studies.[275−277] Based on the vertex model, the mechanical energy in a monolayer cells is described by[278,279]

$$U = \sum_J \frac{1}{2}K_c(A_J - A_0)^2 + \sum_J \frac{1}{2}k_{mJ}m_J L_J^2 + \sum_{\langle i,j\rangle}\Lambda l_{ij} \quad (4)$$

where K_c is the area stiffness of cells regulated by the cytoskeleton, nucleus, and cytoplasm;[237] A_J and A_0 are the current and preferred areas of the Jth cell, respectively; k_{mJ}, m_J, and L_J denote the elastic coefficient of cortical actomyosin network,[60] the contractile activity of myosin, and the perimeter of cell J, respectively; Λ is the interfacial tension between two adjacent cells due to adhesive junctions of cadherin molecules;[280] l_{ij} is the edge length between vertices i and j. Then, the collective cell mechanical dynamic behaviors can be simulated based on the force balance equation ($\eta \mathrm{d}r_i/\mathrm{d}t = -\partial U/(\partial r_i)$) at each vertex where r_i and η are the coordinates of vertex i and the friction efficient from ECM, respectively. Since the dynamic vertex models, as demonstrated by the above equations, can effectively integrate all major biophysical factors of a multicellular system, they are widely employed to investigate the biophysical mechanisms that underlie collective cell behaviors, including oscillatory dynamics,[278] curvature-dependent cell migrations,[276,281] and morphological development of tissues.[275,282] Oscillatory morphodynamics of collective cells is an essential phenomenon in embryonic development that occurs in many living systems. A study that employed a dynamic vertex model (Figure 3f),[278] which incorporates myosin activity through the Hill function, successfully replicated the collective cell oscillations of amnioserosa in the *Drosophila* embryo. This study found that the oscillatory behavior results from a chemomechanical Hopf bifurcation that relies on myosin-regulated contractile forces, cell stiffness, and boundary conditions. Recently, a stress fiber-reinforced vertex model[283] was also developed to explore the mechanisms by which the number of apical stress fibers scales with cell area, ultimately limiting cell elongation.[284] It is revealed that imposed anisotropic biaxial stretching facilitates cell rearrangement within the epithelial monolayer, resulting in size-dependent elongation of the cells. Concurrently, the formation of stress fibers aligning primarily with the main stretching direction in cells aids in resisting the imposed stretching, ultimately reducing the size dependency of their deformation.[283] These results show the vital role of dynamic vertex models in comprehensively elucidating the complex biophysical mechanisms that underlie collective cell behaviors.

A General Computational Pipeline for Developing Spatiotemporal Multiscale Cell Models for Pharmaceutical Applications. A thorough comprehension of cell mechanical and dynamic behaviors derived via the cytoskeleton is crucial for advancing our understanding of cell biology and human health. Existing spatiotemporal models (see refs 5, 14, 15, 31, 32, 171, 241, 243, 264, 266, 274, 276, 278, 279, 281, 282, 285−288) have exhibited powerful abilities to reveal the biophysical mechanisms and dominant factors involved in various physiological and pathophysiological processes. However, none of them can be applied to pharmaceutical

https://doi.org/10.1021/acsnano.4c12599
ACS Nano 2024, 18, 29311−29336

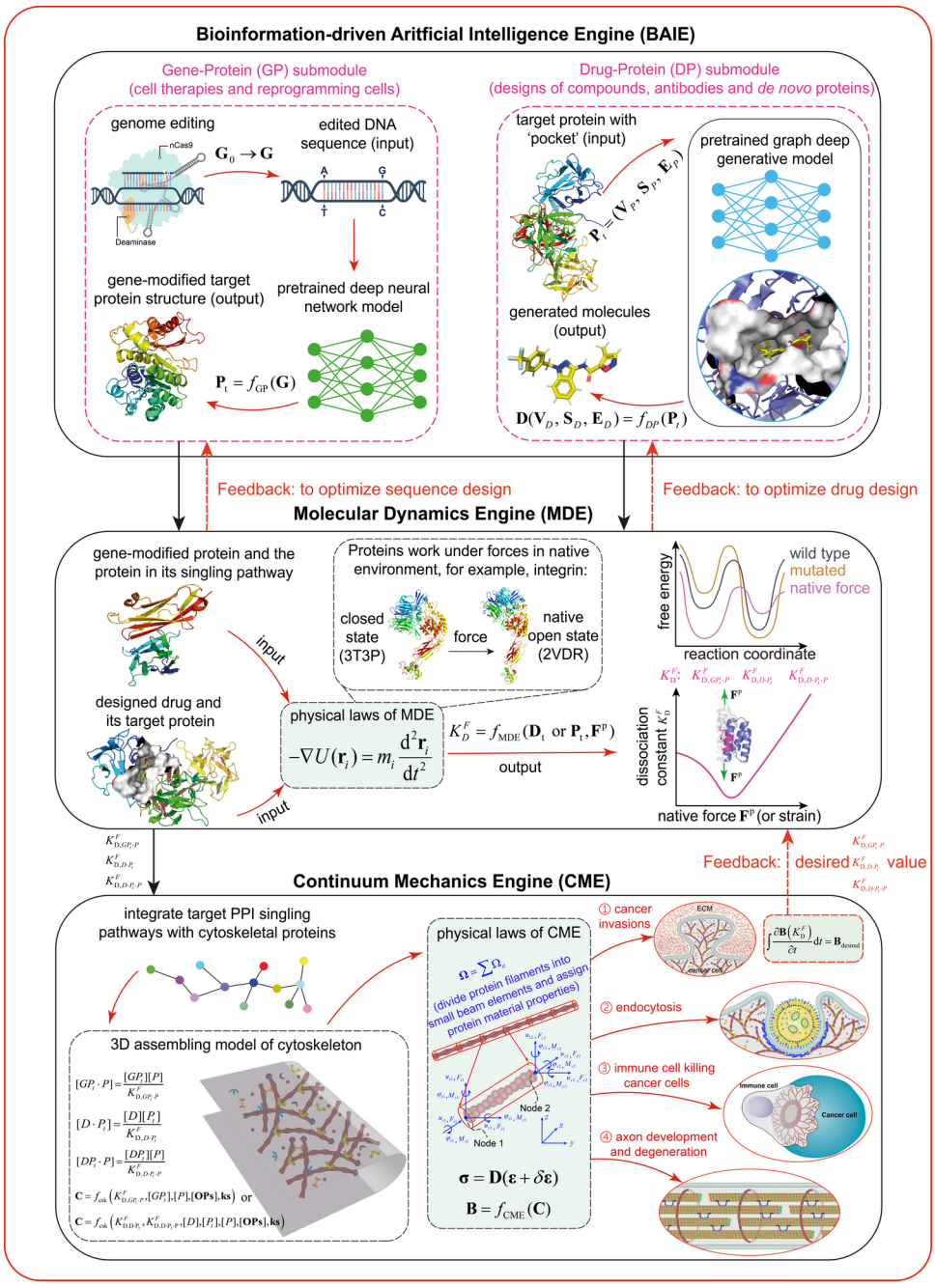

Figure 4. A general spatiotemporal cross-scale computational pipeline automatically designs genome editing bases and drugs, and virtually tests their therapeutic effects on cellular pathophysiological dynamic behaviors and generates quantitative feedbacks to optimize their designs. Note that if there is no mechanical force acting on the protein in the native environment, the mechanical force is zero in the parameters. This pipeline overcomes the spatiotemporal cross-scale challenges between molecules and cells. By moving most of the painstaking wet-laboratory effort to computer simulations, it would substantially save time and alleviate the financial burden of pharmaceutical industries, significantly accelerating biomedical engineering advances.

engineering, such as investigating the effects of drugs on cancer invasion or neurodegeneration behaviors, to accelerate pharmaceutical advances. A primary reason for their limitations is that they are developed based on significant simplifications of biological factors, without quantitatively considering the precise working mechanisms as well as the highly kinetic interactions of enzymes, ion channels, ligands, and receptors. Even though the spatiotemporal RAP modeling system[4] is based on single protein level and conformational change-induced protein−protein interactions (PPIs), it does not incorporate the exact folding structures of proteins, making it unsuitable for pharmaceutical engineering applications.

The discovery and development of an approved drug typically entail staggering costs, amounting to 2−3 billion US dollars, and a lengthy process spanning over a decade.[68,289,290] This substantial investment of time and resources is mainly because the wet-laboratory experiments are quite time-consuming and often yield disparate results between in vitro and in vivo conditions.[289] On the other hand, biomedical engineering is at a historic juncture, where a convergence of

https://doi.org/10.1021/acsnano.4c12599
ACS Nano 2024, 18, 29311−29336

biotechnologies and AI to address diseases through the precise editing of specific base pairs or segments of DNA or designing more effective drugs with generative AI.[291,292] These pharmaceutical challenges and the epochal advances in biotechnology-based and AI-driven therapeutics inspire us to ask whether we can develop spatiotemporal multiscale modeling systems that can replicate and predict cell dynamic behaviors driven by complicated molecular protein interactions in the real physical world for biomedical applications. Such virtual cell modeling systems integrating AI with biophysical calculations can move most of the painstaking wet-laboratory effort to computer simulations for testing the cellular effects of drugs or gene-edited DNA sequences targeting specific proteins and then generate quantitative feedback to optimize the drug designs or gene-editing base pairs. To realize this ambitious and promising goal, here we propose a general spatiotemporal cross-scale computational pipeline, consisting of three interconnected modules (Figure 4): a bioinformation-driven artificial intelligence engine (BAIE), a molecular dynamic engine (MDE), and a continuum mechanics engine (CME). By leveraging the power of computation, we believe that this virtual cell simulation pipeline could substantially reduce both the time and the financial cost of pharmaceutical industries and thereby may revolutionize both modern therapeutic engineering and basic biomedical researches.

BAIE. Proteins, composed of amino acids, are fundamental building blocks of life and synthesized in two key stages: transcription and translation.[293] During transcription, genetic information encoded by DNA is transcribed into mRNA, which is then transported to ribosomes where it assembles a polypeptide chain by linking amino acids together in a specific order, while losing water molecules.[294] The resulting polypeptide chain undergoes post-translational modifications[295−298] and folds into its unique three-dimensional (3D) structure, which ultimately determines the function of protein.[298−302] As a result, any alterations to the DNA and RNA sequences encoding a protein[303] or the binding of molecular drugs to the protein may significantly change its folding structure, and consequently modify its functional role in performing cellular behaviors.[293,304] On this basis, our BAIE are designed to have two independent submodules: the gene−protein submodule (GP), and the drug−protein submodule (DP). The GP submodule utilizes a deep learning AI platform to establish quantitative correlations between specific DNA sequences (or RNA) and their corresponding protein folding structures. The DP submodule is a deep generative AI platform for molecular design tasks to discover the potential chemical compounds, antibodies, or de novo proteins that interact with target proteins based on existing pharmaceutical libraries.

GP Submodule. Over the past few years, significant biomedical breakthroughs have been made in two areas. First, CRISPR-Cas gene-editing technology has enabled precise manipulation of cellular DNA sequences to alter cell fates through gene insertion, replacement, or deletion.[305,306] Second, the rapid development of deep learning models, such as AlphaFold2,[299] RoseTTAFold,[300] and AlphaFold3,[307] enables accurate prediction of the three-dimensional atomic coordinates of folded structures of proteins and protein complexes from their amino acid sequences.[301,308−310] Many human diseases, such as some kinds of cancers (breast cancer caused by BRCA1 and BRCA2 gene mutations, lung cancer caused by KRAS gene mutations, and so on), Huntington's chorea, hemophilia, and cystic fibrosis, stem from mutations in genetic information.[311,312] These mutations alter amino acid sequences, leading to defective protein folding structures and destructive consequences in cellular functions. Hence, the convergence of two breakthrough technologies holds great potential to reshape the treatment of diseases. Their combination can quantitatively operate the behaviors of target proteins and, thereby, cellular behaviors toward a designated performance. Thus, the deep learning GP submodule $P = F(G, \{W_i^g\})$ outputs the three-dimensional atomic coordinates of proteins P based on the input of modified genetic sequence G. Then, it delivers the structural information on proteins to the MDE and CME modules for further predicting the effects of gene-editing based therapy on cell behaviors. The function $F(G,\{W_i^g\})$ represents deep neural networks where W_i^g is the parameter matrix to be learned. The obtained proteins were fed into the MDE for investigating PPIs. In addition to curing diseased cells, the GP → MDE → CME pipeline can be applied to test and optimize the performance of reprogrammed cells for a specific function, such as chimeric antigen receptor (CAR) T-cells, which are reprogrammed by adding a gene to express a CAR to recognize the specific cancer cell antigen and then attack the cancer cells.[313−319]

DP Submodule. Diseases are derived from aberrant behaviors of proteins.[293,320−322] Discovery of drug molecules that can bind specifically and with high affinity to target proteins for achieving desired therapeutic effects is a grand challenge. This is because the size of the chemical space is enormous. For small molecular compounds, it is estimated to be on the order of 10exp(60) spaces.[68,323] For antibody or T-cell receptor drugs, complementarity determining regions with 20 amino acids have a 20exp(20) mutation spaces. These spaces are far beyond the realm of what can be practically screened and synthesized in laboratories.[324] However, by using computational methods to explore chemical or amino acid mutation space, promising molecules for target proteins can be more efficiently identified.[68,324−330] In fact, structure-based virtual screening of molecular compounds[68,324−326,331] and designs of antibodies and de novo proteins[332,333] based on artificial intelligence has gained great advances in recent years.

The DP submodule is a graph-based molecular generative AI platform for drug design by predicting potential drug candidates and binding scores for target pockets of proteins. Although many generative AI models[334] based on recurrent neural networks,[335−337] variational autoencoders,[338−340] and generative adversarial networks[341,342] has been proposed, most of them only generate one-dimensional (SMILES)[343,344] or two-dimensional (graph)[334,345−347] representations of molecules without using the structural and interactions information on target pockets of proteins. The molecular generative AI platform of the DP submodule requires a large data set of known drug molecules, which should include information on the structure, pharmacological properties, and the interacting region of target proteins. It generates drugs $\mathbf{D} = (\mathbf{V}_D, \mathbf{S}_D, \mathbf{E}_D)$ with desired properties based on the binding information on target proteins $\mathbf{P}_t = (\mathbf{V}_P, \mathbf{S}_P, \mathbf{E}_P)$ where $\mathbf{V}_D \in \mathbb{R}^{N_D \times T}$ and $\mathbf{V}_P \in \mathbb{R}^{N_P \times T}$ represent one-hot atom types of the generated drug and the target protein, respectively (N_D is the number of drug atoms; N_P is the number of the protein atoms; T is the number of the atom types.); $\mathbf{S}_P \in \mathbb{R}^{N_P \times 3}$ and $\mathbf{S}_P \in \mathbb{R}^{N_P \times 3}$ represent 3D coordinates of atoms in the drug and protein, respectively; $\mathbf{E}_D \in \mathbb{R}^{N_D \times N_D}$ and $\mathbf{E}_P \in \mathbb{R}^{N_P \times N_P}$ denote bond features between atoms in the drug and its target protein,

https://doi.org/10.1021/acsnano.4c12599
ACS Nano 2024, 18, 29311−29336

respectively. This deep generative AI model can be developed based on diffusion probabilistic approaches, which include a forward diffusion process and a reverse generative process that are defined as Markov chains.[348,349] The diffusion process gradually introduces noise into the drug data from $\mathbf{D}_0$ ($\mathbf{D}$) to $\mathbf{D}_R$ in R steps with $q(\mathbf{D}_{1:R}|\mathbf{D}_0,\mathbf{P}_t) = \prod_{r=1}^{R} q(\mathbf{D}_r|\mathbf{D}_{r-1},\mathbf{P}_t)$, and the generative process is to learn a graph neural network model p_θ to reconstruct the drug data $\mathbf{D}_0$ from the injected noise distribution $\mathbf{D}_R$ with $p_\theta(\mathbf{D}_{0:R-1}|\mathbf{D}_R,\mathbf{P}_t) = \prod_{r=1}^{R} p_\theta(\mathbf{D}_{r-1}|\mathbf{D}_r,\mathbf{P}_t)$. To encourage docking with the target protein, the model can be trained by minimizing the weighted sums of Kullback–Leibler divergences of atom coordinates, atom types, and chemical bonds. The generated molecules were stored and fed into the MDE module for validations.

MDE. PPIs underlie all cellular processes and ultimately control physiological behaviors.[350,351] Numerous diseases result from their changes.[322,324] While AI algorithms have been applied to predict the complex network of PPIs,[352,353] they have limitations in accurately predicting the specificity and binding affinity of these interactions due to the insufficient data available.[354,355] Particularly, many PPIs are regulated by mechanical forces during cell dynamic behaviors. This leads to force-dependent behaviors of their binding affinity, which is commonly described by the force-dependent dissociation constant K_D^F.[62,302,356−360] For example, during cell migration, forces from cytoskeleton stretch integrin and open its bent-closed conformation[361,362] (Figure 4). This conformation change improves integrin–fibronectin binding affinity and thus strengthen adhesion formation to provide sufficient forces for cell migrations.[361,362] Moreover, stretching of DNA leads to changes in the binding of DNA-interacting proteins[363−365] and regulates gene expressions.[366] In fact, force-dependent K_D^F is the essential mechanism by which cells obtain feedback from extracellular environments and generate adaptive responses to fulfill their functions. For instance, polymerization force of actin filaments regulates their conformational changes[359,360] and then modifies the binding affinity of the Arp2/3 complex[4,367,368] to remodel the actin network. Relying on this mechanism, cells can sense magnitudes of ECM resistances and accurately determine the appropriate force generation for fulfilling their functions.[4] However, current AI models for protein designs, including RF diffusion[332] and Chroma,[333] are unable to capture these force-regulated PPI behaviors that happen in native environments.[369] Additionally, due to a lack of training data, AI models often encounter challenges in accurately predicting atomic-level conformational dynamic changes in proteins upon molecule binding. Understanding these dynamic changes and elucidating the subsequent interactions between the resultant drug–protein complex and the protein within the signaling pathway are important for the development of efficacious treatments such as the study of antibody–drug conjugates. MD simulations[294,370,371] can achieve this continuous dynamic view and detailed understanding of these PPIs, drug–protein interactions (DPIs), and drug–protein–protein interactions (DPPIs). They are important methods for discovering the key amino acid residues and identifying their precise interacting mechanisms.

Our MDE module is designed for performing MD simulations of gene-modified PPIs (from the GP submodule), DPIs, and DPPIs (from the DP submodule). MD relies on force fields to calculate the interactions between atoms, including covalent bonds, hydrogen bonds, van der Waals forces, electrostatic forces, hydrophobic interactions, salt bridges, disulfide bonds, and $\pi-\pi$ interactions. The most popular force fields that are commonly used in MD simulations for proteins are AMBER,[62,294,372] CHARMM,[373,374] GROMOS,[375−377] OPLS,[378,379] and MARTINI (coarse-grained MD).[380,381] Force fields describe the potential energy of the system as a function of the positions and velocities of all atoms, allowing prediction of the dynamic behavior of the system over time. The potential energy can be expressed as

$$U = \underbrace{\frac{1}{2}\sum_{\text{bonds}} k_i^{\text{bond}}(r_i - r_0)^2}_{U_{\text{bond}}} + \underbrace{\frac{1}{2}\sum_{\text{angles}} k_i^{\text{angle}}(\theta_i - \theta_0)^2}_{U_{\text{angle}}} + \underbrace{\frac{1}{2}\sum_{\text{dihedrals}} k_i^{\text{dihe}}[1 + \cos(n_i\phi_i + \gamma_i)]}_{U_{\text{dihedral}}} + \underbrace{\sum_i \sum_{j>i} 4e_{ij}\left[\left(\frac{\delta_{ij}}{r_{ij}}\right)^{12} + \left(\frac{\delta_{ij}}{r_{ij}}\right)^{6}\right] + \sum_i \sum_{j>i} \frac{q_i q_j}{4\pi e_0 r_{ij}}}_{U_{\text{nonbond}}} \tag{5}$$

where k_i^{bond}, r_i, and r_0 are the bond stretching strength parameter, bond length, and the equilibrium bond length for each pair atoms, respectively; k_i^{angel}, θ_i, and θ_0 are the bending strength parameter, bending angle, and the equilibrium bending angle for each triple atoms, respectively; k_i^{dihe}, n_i, ϕ_i, and γ_i are the torsion strength parameter, multiplicity, dihedral angle, and phase angle for each quadruple atoms, respectively; e_{ij}, δ_{ij}, and r_{ij} are the well depth, atom diameter, and the distance between two atoms, respectively; q_i and q_j are atom electrostatic charges; e_0 is the permittivity of free space. The equilibrium configuration of molecules can be computed by minimizing the potential energy through solving the Newton's equations of motions $-\nabla U(\mathbf{r}_i) = m_i \frac{d^2\mathbf{r}_i}{dt^2}$ with numerical iteration algorithms based on Taylor expansion and finite difference method where ∇, m_i, $\mathbf{r}_i$, and t are the Nabla operator, atom mass, atom motion vector, and time, respectively. It should be mentioned that since proteins often involve a large number of degrees of freedom and have complex energy landscapes with numerous local minima separated by high-energy barriers, standard MD simulations may get trapped in local energy minima and fail to explore the full conformational space. Enhanced sampling techniques[382] including replica exchange molecular dynamics, umbrella sampling, metadynamics, and simulated annealing are often used to explore rare events or large conformational changes in protein systems. These methods introduce biases or additional potentials to accelerate the exploration of specific regions of configuration space or enhance the sampling of rare events.

Once the GP submodule has generated gene-modified proteins or the DP submodule has produced drugs (including compounds, antibodies, and de novo proteins) for target proteins, they will be inputted into the MDE module to calculate PPIs, DPIs, or DPPIs. It should be noted that protein conformations are very sensitive to forces,[4,357,383] and many of them work based on force regulations in the native cellular environments.[17] For example, stretching and bending of cell membrane can trigger the different behaviors of G protein-coupled receptors for cell dynamics, such as immune system activities.[384] In absence of forces, isolated proteins tend to

https://doi.org/10.1021/acsnano.4c12599
ACS Nano 2024, 18, 29311−29336

undergo conformational collapse toward energetically favorable compact states, which can lead to the burial of critical residues that are involved in binding interactions with drug molecules or other proteins. Thus, in MD simulations of our MDE module, in vivo forces acting on proteins during cell dynamics should be applied properly, which is crucial to increasing the likelihood of successful drug discovery outcomes, and identifying the real interacting amino acid residues of proteins that happen in the in vivo environments. By applying steered MD simulations,[385] force-dependent dissociation constants of gene-mutated PPIs $K^F_{D,GP_t\cdot P}$, DPIs $K^F_{D,D.P_t}$, and DPPIs $K^F_{D,D.P_t\cdot P}$ can be obtained by calculating the changes of free energy ΔG.[62] In theory, the Helmholtz free energy G is given by

$$G = -k_B T \ln Z \tag{6}$$

$$Z = \frac{1}{N!h^{3N}} \iint \exp\left(-\frac{H(\mathbf{p},\mathbf{r})}{k_B T}\right) d\mathbf{p}d\mathbf{r} = \frac{1}{N!h^{3N}} \int \exp\left(-\frac{U(\mathbf{r})}{k_B T}\right) d\mathbf{r} \int \exp\left(-\frac{E_{kin}(\mathbf{p})}{k_B T}\right) d\mathbf{p} \tag{7}$$

where Z is the partition function of the system; N is the number of atoms in the system; and $H(\mathbf{p},\mathbf{r})$ is the Hamiltonian total energy for a given configuration described by conjugate momenta $\mathbf{p}$ and position $\mathbf{r}$. $U(\mathbf{r})$ and $E_{kin}(\mathbf{p})$ are the potential and kinetic energies of the system, respectively. However, since the protein systems normally include a large number of atom interactions, it is hard to get the analytical formulas of the partition functions Z to calculate their absolute free energies G and the changes of the absolute free energies ΔG upon receptor−ligand binding.[386] Molecular mechanics Poisson−Boltzmann surface area (MMPBSA) is an end-state method to calculate the free energy changes ΔG of ligand−receptor binding in solution.[387−389] Because the primary free energy is contributed from water molecule interactions, and this energy fluctuation is normally an order of magnitude greater than the binding energy, the calculation requires a considerable amount of time to converge. Thus, MMPBSA divides the simulation system into a vacuum state and a solvated state based on the thermodynamic cycle. The binding free energy ΔG is calculated by.

$$\Delta G = \Delta U_{vac} + \Delta G_{sol,p} + \Delta G_{sol,np} - T\Delta S_{vac} \tag{8}$$

where ΔU_{vac} is the potential energy change of the molecules upon binding in vacuum state and can be calculated by eq 5; $\Delta G_{sol,p}$ and $\Delta G_{sol,np}$ are the solvation free energy differences contributed by the polar electrostatic interactions and the nonpolar van der Waals hydrophobic interactions, respectively; ΔS_{vac} is the change of entropy. To compute the polar solvation free energy term $\Delta U_{sol,p}$, it is necessary to first determine the distribution of electrostatic potential $\varphi(\mathbf{r})$ by solving the Poisson−Boltzmann equation (PBE). PBE is derived by employing a mean-field approximation to the system's average potential of mean force and is expressed by[386,390]

$$\nabla\varepsilon(\mathbf{r})\nabla\varphi(\mathbf{r}) + 4\pi\lambda(\mathbf{r}) \sum_i c_i z_i e \exp\left(-\frac{z_i e\varphi(\mathbf{r})}{k_B T}\right) = -4\pi\rho(\mathbf{r}) \tag{9}$$

where $\varepsilon(\mathbf{r})$ is the dielectric distribution in the MD system; $\lambda(\mathbf{r})$ is the predefined ion-exclusion function; c_i and z_i are the bulk number density and the charge of the ion type i, respectively; $\rho(\mathbf{r})$ is the charge density distribution of ligand, receptor, or their complex; $z_i e\varphi(\mathbf{r})$ is the potential of mean force of the ion type i. The electrostatic potential distribution can be determined by solving the PBE by using the finite difference method. When the absolute value of ions' electrostatic potential is very small, the PBE can be simplified to Debye−Hückel Equation by $\exp[(-z_i e\varphi(\mathbf{r})/(k_B T)] = 1 - (z_i e\varphi(\mathbf{r})/(k_B T))$ through Taylor expansion. With the electrostatic potential distribution, the polar solvation free energy difference can be calculated by $\Delta G_{sol,p} = \int \varphi_{RL}(\mathbf{r}_{RL})\rho_{RL}(\mathbf{r}_{RL})d\mathbf{r}_{RL} - \int \varphi_R(\mathbf{r}_R)\rho_R(\mathbf{r}_R)d\mathbf{r}_R - \int \varphi_L(\mathbf{r}_L)\rho_L(\mathbf{r}_L)d\mathbf{r}_L$ where the subscripts R, L, and RL denote the receptor, ligand, and receptor−ligand complex molecules, respectively. The nonpolar solvation free energy term consists of two highly different interactions. One component is the repulsive free energy, which is approximately proportional to the solvent accessible surface area (SASA) of the receptor, ligand, and their complex. The other one U_{vdw} is the van der Waals attractive interaction potential energy between solute (ligand, receptor or complex) and water molecules. Thus, $\Delta G_{sol,np} = \gamma(SASA_{RL} - SASA_R - SASA_L) + b + (U_{vdw,RL} - U_{vdw,R} - U_{vdw,L})$ where γ is surface tension and takes a value of 0.0378 kcal/(mol·Å^2); b is a correction term of SASA and takes a value of −0.569 kcal/mol.[391] $U_{vdw} = \sum_{k=1}^{N_s} \int \rho_{kw}(\mathbf{r}_{kw})V_{vdw}(\mathbf{r}_{kw})d\mathbf{r}_{kw}$ where N_s is the total number of solute atoms, ρ_{kw} is a solvent distribution function around solute atom k at a given distance $\mathbf{r}_{kw}$, and V_{vdw} is the attractive van der Waals potential.[392] Entropy is a measure of the disorder of a system. Thus, the final entropy energy term can be computed as $-T\Delta S = k_B T \ln\langle\exp((\Delta U_{p,np})/(k_B T)\rangle$ where $\Delta U_{p,np} = U_{p,np} - \langle U_{p,np}\rangle$ represents the fluctuation of the electrostatic and van der Waals potential energies around the ensemble average energies.[393] It should be mentioned that although MMPBSA is an effective method and can be applied to study both the external force-induced and drug-variation-induced binding affinity changes, its solving process of PBE is normally based on approximation, and this affects its accuracy, particularly for strongly charged molecular systems. Additionally, MMPBSA treats water molecules implicitly.[388,389,394] Thus, its prediction accuracy can be further improved by considering the potential structural water molecules.

For the drug-variation-induced affinity variation conditions, free energy perturbation (FEP) and thermodynamic integration (TI) methods also can be employed. The two alchemical methods are theoretically more rigorous and accurate, albeit at the expense of considerably higher computational costs. Although it is challenging to compute the absolute free energy with eqs 6 and 7, the free energy difference ΔG due to drug change can be calculated. For example, an antibody is mutated from a to b. Based on the FEP method, its free energy difference can be expressed by[395−397]

$$\Delta G_{ba} = G_b - G_a = -k_B T \ln \frac{\int \exp[-U_b(\mathbf{r})/k_B T]d\mathbf{r}}{\int \exp[-U_a(\mathbf{r})/k_B T]d\mathbf{r}} \tag{10}$$

The kinetic energy from momenta $\mathbf{p}$ does not contribute to the energy difference after equilibrium. Therefore, only potential energy $U(\mathbf{r})$ exists in eq 10. The free energy difference can be reformulated into the following form for calculations[398]

https://doi.org/10.1021/acsnano.4c12599
ACS Nano 2024, 18, 29311−29336

$$\Delta G_{ba} = -k_B T \ln \left\langle \exp\left[\frac{U_a(\mathbf{r}) - U_b(\mathbf{r})}{k_B T}\right]\right\rangle_i = -k_B T \ln \left\langle \exp\left[\frac{\Delta U_{ba}(\mathbf{r})}{k_B T}\right]\right\rangle_i \quad (11)$$

By sampling both the systems a and b, the following Bennett acceptance ratio method[399,400] can also be applied to calculate the free energy difference ΔG_{ba}, and it has a better statistic accuracy.

$$\left\langle \frac{1}{1 + \exp\left[\frac{\Delta U_{ab}(\mathbf{r}) - \Delta G_{ba}}{k_B T}\right]}\right\rangle_i = \left\langle \frac{1}{1 + \exp\left[\frac{\Delta U_{ba}(\mathbf{r}) + \Delta G_{ba}}{k_B T}\right]}\right\rangle_j \quad (12)$$

FEP theory requires the two systems a and b to be sufficiently similar so that their microstates $\mathbf{r}$ can largely overlap, which is important for accuracy. Therefore, in FEP calculations, a hybrid structure in the variant region needs to be constructed to ensure that systems a and b have an identical atom set. Then, by introducing a series of λ ($0 = \lambda_1 < \lambda_2 \cdots < \lambda_i < \cdots \lambda_M = 1$) to perturb the hybrid local structure, intermediate systems that gradually morph a to b can be defined in a series of steps.[400] During the calculation process, Hamiltonian replica exchange is utilized to exchange replicas between neighboring systems to calculate potential energy changes $\Delta U = [U(\mathbf{r}_{i+1},\lambda_i) + U(\mathbf{r}_i,\lambda_{i+1})] - [U(\mathbf{r}_i,\lambda_i) + U(\mathbf{r}_{i+1},\lambda_{i+1})]$. Finally, the free energy difference is $\Delta G_{ba} = \sum_0^M \Delta G_{i+1,i}$. It should be noted that λ is an implicit variable in the FEP method. The free energy difference can also be computed with the TI method, where λ is directly employed to perturb the Hamiltonian. Thus, the TI free energy difference $\Delta G_{ba} = \int_0^1 \left\langle \frac{\partial U(\mathbf{r},\lambda)}{\partial \lambda}\right\rangle d\lambda$. After obtaining the free energy difference of receptor−ligand complex $\Delta G_{ba,\mathrm{RL}}$ in a vacuum environment and the free energy difference of ligand $\Delta G_{ba,\mathrm{L}}$ in a water environment, the ligand-variation-induced affinity change can be computed with $\Delta\Delta G_{ba} = \Delta G_{\mathrm{ba,RL}} - \Delta G_{ba,\mathrm{L}}$ according to the thermodynamic cycle.

On the basis of MMPBSA, FEP, or TI calculation results, the amino acid residues or the small molecule chains at the binding sites that contribute to the binding free energy of PPIs, DPIs, and DPPIs can be analyzed. The obtained $K^F_{\mathrm{D,GP_t\cdot P}}$, $K^F_{\mathrm{D,D\cdot P_t}}$, and $K^F_{\mathrm{D,D\cdot P_t\cdot P}}$ and the identified key amino acid residues in the MDE module will give feedback to the DP and GP submodules to optimize the gene-editing sequences or the design of drug molecules for the target proteins. After the desired gene-modified proteins or drug molecules are obtained, they will be fed into the CME module to examine the impact of genome editing or drugs on cellular physiological and pathophysiological dynamics. It should be mentioned that MD simulations currently still remain slow in computational speed, and it is impractical to compute the interactions between a large number of proteins in the singling pathways. However, the efficiency of MD simulations is significantly improving under the assistance of AI and supercomputer development;[401] and in the future, it will be feasible to carry out extensive protein−protein interaction calculations with technology advances.

CME. CME is a continuum mechanics engine that simulates cell mechanical dynamic behaviors spatiotemporally from PPIs at the single protein level. It connects the signaling dynamics, involving protein phosphorylation, calcium influx, and the activation of transcription factors, with the mechanical dynamics of the cytoskeletal proteins (Figure 4), which ultimately determines the behaviors of cells,.[16,133,402,403] While signaling dynamics and mechanical dynamics opterate differently, they are closely interconnected: signaling pathways can modulate the cytoskeleton, and cytoskeletal proteins can influence signaling by generating force. Their connections (Figure 4) are essentially important for understanding cell behaviors and building physical virtual cells. The cytoskeletal proteins are normally rod-like structures. From the principle of continuum mechanics, they can be regarded as beams in mechanical calculations.[5,404,405] Based on the $K^F_{\mathrm{D,GP_t\cdot P}}$, $K^F_{\mathrm{D,D\cdot P_t}}$, and $K^F_{\mathrm{D,D\cdot P_t\cdot P}}$ of the target protein and drug and their interactions with cytoskeletal proteins in signaling pathway network, the three-dimensional kinetic assembling model of the cytoskeleton can be constructed[5,406] through the mathematical function of biochemical reactions $\mathbf{C} = f_{\mathrm{csk}}(K^F_{\mathrm{D,GP_t\cdot P}},[GP_t],[P],[\mathbf{OPs}],\mathbf{ks})$ (for the GP → MDE → CME pipeline) or $\mathbf{C} = f_{\mathrm{csk}}(K^F_{\mathrm{D,D.P_t}},K^F_{\mathrm{D,D.P_t\cdot P}},[D],[P_t],[P],[\mathbf{OPs}],\mathbf{ks})$ (for the DP → MDE → CME pipeline) where $[GP_t]$, $[P_t]$, $[P]$, $[D]$, and $[\mathbf{OPs}]$ represent molar concentrations of gene-edited target protein, target protein, the protein that directly interacts with the target protein, drug, and a series of other proteins in the signaling pathway network of cellular PPIs; $\mathbf{ks}$ represents a series of on-rate k_{on} and off-rate k_{off} constants of other proteins and can be obtained from experimental results.

The calculation process of CME is performed in 4 steps. In the first step, the assembled cytoskeleton, cell membrane, and ECM at time t_m are divided into small different elements. For instance, the cytoskeleton is regarded as the topological structure composed of a lot of beams, where each actin filament, MTs, IFs, and cross-linking proteins can be divided into beam elements.[4,5] Then the geometric non-linear 3D Euler−Bernoulli[4,407] or Timoshenko beam[408] theory is applied to describe their deformation behaviors including stretch, compression, bending, and twist during cell mechanical dynamics. In the second step, we establish the field functions of displacement, strain, and stress of elements. Generally, the displacement vector field in a beam element is $\mathbf{u}_{e,t_m} = \mathbf{N}(\mathbf{x})\mathbf{q}_{e,t_m}$, where $\mathbf{N}(\mathbf{x})$ is the matrix of shape function and $\mathbf{q}_{e,t_m}$ is the nodal displacement field at the time t_m. According to the strain−displacement relationship, such as $\varepsilon_{ij} = (u_{i,x_j} + u_{j,x_i} + u_{k,x_i} u_{k,x_j})/2$ where $u_{i,x_j} = \partial u_i/\partial x_j$ represents the gradient in the 3D space $\mathbf{x}$ and $i,j = 1,2,3$, the strain filed is written as $\varepsilon_{e,t_m} = \mathbf{B}(\mathbf{x})\mathbf{q}_{e,t_m}$, where $\mathbf{B}(\mathbf{x})$ is the strain matrix that contains linear $\mathbf{B}_1(\mathbf{x})$ and non-linear $\mathbf{B}_{\mathrm{nl}}(\mathbf{x})$ components. The stress field $\boldsymbol{\sigma}_{e,t_m}$ can be obtained based on the stress−strain relationship $\boldsymbol{\sigma}_{e,t_m} = \mathbf{D}(E,\nu)\boldsymbol{\varepsilon}_{e,t_m}$ where $\mathbf{D}(E,\nu)$ is the elastic matrix and E, ν are the material Young's modulus and Poisson's ratio, respectively, which are measured from experiments.[5,383] In the third step, according to the principle of minimum potential energy $\partial\Pi(\mathbf{q}_{e,t_m})/\partial\mathbf{q}_{e,t_m} = 0$,[409] the final governing equation of the element is $\sum_{e=1}^N [(\mathbf{T}_e)^{\mathrm{T}}\mathbf{k}\mathbf{T}_e]\mathbf{q}_{e,t_m} = \sum_{e=1}^N \mathbf{T}_e\mathbf{P}_{e,t_m}$ where N is the total number of elements; $\mathbf{P}_{e,t_m}$ is the vector of the element nodal force at the time t_m; $\mathbf{k}$ is the element stiffness matrix that is composed of the linear $\mathbf{k}_0$ and non-linear $\mathbf{k}_{\mathrm{nl}}$ components; and $\mathbf{T}_e$ is the element coordinate transformation matrix.[409] By

https://doi.org/10.1021/acsnano.4c12599
ACS Nano 2024, 18, 29311−29336

solving the nonlinear govern equation with iteration methods, the whole displacement field $\mathbf{q}_{t_m}$ of the cytoskeleton and cell membrane at the time t_m can be calculated. In addition, the strain $\boldsymbol{\varepsilon}_{p,t_m}$ and stress σ_{p,t_m} fields of each cytoskeletal protein (actin filament, MT, IF, and cross-linking protein) can also be calculated via the strain−displacement relationship and stress−strain relationship, respectively. In the fourth step, the cytoskeleton at time t_{m+1} remodels $\mathbf{C}_{t_{m+1}} = \mathbf{C}_{t_m} + \boldsymbol{\delta}\mathbf{C}_{t_m}$ based on the force-induced deformation ($\boldsymbol{\varepsilon}_{p,t_m}$)-dependent PPIs ($K^F_{\mathrm{D,GP_t\cdot P}}$, $K^F_{\mathrm{D,D\cdot P_t}}$, and $K^F_{\mathrm{D,D\cdot P_t\cdot P}}$). Then, the remodeled cytoskeleton $\mathbf{C}_{t_{m+1}}$ will be computed in the next cycle (steps 1−4) to obtain the $\mathbf{q}_{t_m}$, ε_{p,t_m}, and $\boldsymbol{\sigma}_{p,t_m}$ at the time t_{m+1}. The dynamic behaviors of the cell $\mathbf{B} = f_{\mathrm{CME}}(\mathbf{C}_{t_m}, \mathbf{C}_{t_{m+1}}, \mathbf{C}_{t_{m+2}}, \cdots, \mathbf{C}_{t_{m+n}})$ driven by PPIs from the time t_m to t_{m+n} in a millisecond scale[4] can be obtained, and is described by a series displacement fields $\mathbf{B} = [\mathbf{q}_{t_m}, \mathbf{q}_{t_{m+1}}, \mathbf{q}_{t_{m+2}}, \cdots, \mathbf{q}_{t_{m+n}}]$.

Although calculating the dynamics of a whole cell at the level of single protein behavior is difficult because of the complexity of cells, CME can be readily applied to simulate the local behaviors of cells. As most of cellular behaviors, such as endocytosis for drug and mRNA vaccine uptake,[53,254,410−412] lamellipodial and filopodial protrusions for cell migrations,[4] macropinocytosis,[29,76] and immune cells for killing cancer cells synapses,[17,19,155,205,413,414] are driven by local cellular cytoskeletons, CME has a wide range of applications in studying cell dynamics. The spatiotemporal cellular modeling system in our previous work[4] is developed based on CME. Here, we take it as an example to demonstrate how our BAIE (GP/DP) → MDE → CME computational system can be applied to pharmaceutical engineering. Polymerization of Arp2/3 complex-branched actin filament network at the leading edge is an essential way that drives cancer invasions[35−38,415,416] and immune cell migrations[19,58,71,204] in ECMs. In cells, the behavior of Arp2/3 complex assembling the branched actin filament network is simultaneously regulated by two opposite mechanisms, Rac-Arpin-Arp2/3 inhibitory circuit and Rac-WAVE-Arp2/3 activatory circuit.[417] Both Arpin and WAVE have a C-helix that binds to the barbed end of Arp3,[418] influencing the Arp2/3 complex's binding to actin filaments and thus cell migrations. Based on the GP → MDE → CME subpipeline, we can directly investigate how to reprogram immune cells by modifying the DNA sequence of the gene encoding Arpin, WAVE, or Arp2/3 complex to manipulate their PPIs to enhance immune cell migration ability. This is significant for the immunotherapy of solid tumors because the tumor physical environments often impede immune cells from penetrating the tissues and thus pose a challenge for the effective immunotherapy.[419,420] Based on the DP → MDE → CME subpipeline, we can design drug molecules targeting the Arp2/3 complex, Arpin or WAVE to regulate their PPIs, and test their effectiveness in reducing the invasive ability of cancer cells. Although here we mainly employ actin as examples to elucidate the applications of our computational pipeline, other cytoskeletal proteins, such as MTs, IFs, and myosin filaments, play equally crucial roles in various cellular functions. For instance, during cancer invasion, the nucleus, as the largest organelle, is the final determining factor of migration through ECM pores.[9,10,71,421,422] Myosin contraction,[9,10] nuclear lamina network stiffness,[421,422] and polymerizing MTs[227] all play roles in regulating nuclear deformations, enabling the nucleus to adapt its shape and squeeze through narrow pores in ECMs. With the GP → MDE → CME subpipeline, we can explore how to modify the amino acid sequences of lamins to increase the lamina filament interactions for improving nuclear lamina network stiffness to impede nuclear deformation, thereby confining cancer cells to their original locations. Similarly, with the DP → MDE → CME subpipeline, the drugs disrupting myosin contraction or MT polymerization can also be designed to reduce the pushing pressures powering nucleues adaption to ECM pores. Consequently, our pipeline can also be applied to investigate the gene-editing and drug effects on nuclear behaviors by targeting nuclear lamin, myosin, MT, or their upstream singling pathways. Overall, by integrating AI with physics, our BAIE (GP/DP) → MDE → CME computational pipeline links genes and molecule designs with protein-driven cellular dynamics, effectively overcoming the spatiotemporal cross-scale challenges between them. It has versatile and broad applications in the usage of gene-editing technology[311] and the designs of drugs,[370,423] antibodies,[319,424] molecular glue degraders[425,426] and de novo proteins[351,427] for cell therapies. Its combination with wet-laboratory experimental validations may substantially save time, improve success rate, and alleviate the financial burden of pharmaceutical industries, accelerating the biomedical advances. It should be mentioned that cells for different functions are normally much different from each other due to DNA methylation and epigenetic modifications. Since it is the mechanical forces that shape many physiological and pathological behaviors of cells and all the behaviors are fundamentally driven by atom interactions,[2] this general computational pipeline might be applied able to different scenarios of cell dynamics and constitutes an essential step toward building virtual cells, which will revolutionize both biomedical engineering and researches in the future.

AUTHOR INFORMATION

Corresponding Author

Xi-Qiao Feng − *Institute of Biomechanics and Medical Engineering, Department of Engineering Mechanics, Tsinghua University, Beijing 100084, China;* orcid.org/0000-0001-6894-7979; Email: fengxq@tsinghua.edu.cn

Authors

Xindong Chen − *Institute of Biomechanics and Medical Engineering, Department of Engineering Mechanics, Tsinghua University, Beijing 100084, China; BioMap, Beijing 100144, China;* orcid.org/0000-0003-2498-1280

Shihao Xu − *Institute of Biomechanics and Medical Engineering, Department of Engineering Mechanics, Tsinghua University, Beijing 100084, China;* orcid.org/0000-0003-0522-5252

Bizhu Chu − *School of Pharmacy, Shenzhen University, Shenzhen 518055, China; Medical School, Shenzhen University, Shenzhen 518055, China;* orcid.org/0000-0002-3111-7653

Jing Guo − *Department of Medical Oncology, Xiamen Key Laboratory of Antitumor Drug Transformation Research, The First Affiliated Hospital of Xiamen University, Xiamen 361000, China*

Huikai Zhang − *Institute of Biomechanics and Medical Engineering, Department of Engineering Mechanics, Tsinghua University, Beijing 100084, China*

https://doi.org/10.1021/acsnano.4c12599
ACS Nano 2024, 18, 29311−29336

Shuyi Sun − *Institute of Biomechanics and Medical Engineering, Department of Engineering Mechanics, Tsinghua University, Beijing 100084, China;* orcid.org/0000-0001-7201-8152

Le Song − *BioMap, Beijing 100144, China*

Complete contact information is available at: https://pubs.acs.org/10.1021/acsnano.4c12599

Notes

The authors declare no competing financial interest.

REFERENCES

(1) Bieling, P.; Li, T. D.; Weichsel, J.; McGorty, R.; Jreij, P.; Huang, B.; Fletcher, D. A.; Mullins, R. D. Force Feedback Controls Motor Activity and Mechanical Properties of Self-Assembling Branched Actin Networks. *Cell* **2016**, *164*, 115−127.

(2) Dance, A. The Secret Forces That Squeeze and Pull Life into Shape. *Nature* **2021**, *589*, 186−188.

(3) Sun, S.-Y.; Zhang, H.; Fang, W.; Chen, X.; Li, B.; Feng, X.-Q. Bio-Chemo-Mechanical Coupling Models of Soft Biological Materials: A Review. *Advances in Applied Mechanics* **2022**, *55*, 309−392.

(4) Chen, X.; Li, Y.; Guo, M.; Xu, B.; Ma, Y.; Zhu, H.; Feng, X.-Q. Polymerization Force-Regulated Actin Filament-Arp2/3 Complex Interaction Dominates Self-Adaptive Cell Migrations. *Proc. Natl. Acad. Sci. U. S. A.* **2023**, *120*, No. e2306512120.

(5) Chen, X.; Zhu, H.; Feng, X.; Li, X.; Lu, Y.; Wang, Z.; Rezgui, Y. Predictive Assembling Model Reveals the Self-Adaptive Elastic Properties of Lamellipodial Actin Networks for Cell Migration. *Communications biology* **2020**, *3*, 616.

(6) Lim, H. Y. G.; Alvarez, Y. D.; Gasnier, M.; Wang, Y.; Tetlak, P.; Bissiere, S.; Wang, H.; Biro, M.; Plachta, N. Keratins Are Asymmetrically Inherited Fate Determinants in the Mammalian Embryo. *Nature* **2020**, *585*, 404−409.

(7) Valet, M.; Siggia, E. D.; Brivanlou, A. H. Mechanical Regulation of Early Vertebrate Embryogenesis. *Nat. Rev. Mol. Cell Biol.* **2022**, *23*, 169−184.

(8) Mueller, J.; Szep, G.; Nemethova, M.; de Vries, I.; Lieber, A. D.; Winkler, C.; Kruse, K.; Small, J. V.; Schmeiser, C.; Keren, K.; et al. Load Adaptation of Lamellipodial Actin Networks. *Cell* **2017**, *171*, 188−200.

(9) Lomakin, A.; Cattin, C.; Cuvelier, D.; Alraies, Z.; Molina, M.; Nader, G.; Srivastava, N.; Saez, P.; Garcia-Arcos, J.; Zhitnyak, I.; et al. The Nucleus Acts as a Ruler Tailoring Cell Responses to Spatial Constraints. *Science* **2020**, *370*, No. eaba2894.

(10) Venturini, V.; Pezzano, F.; Castro, F. C.; Häkkinen, H.-M.; Jiménez-Delgado, S.; Colomer-Rosell, M.; Marro, M.; Tolosa-Ramon, Q.; Paz-López, S.; Valverde, M. A.; et al. The Nucleus Measures Shape Changes for Cellular Proprioception to Control Dynamic Cell Behavior. *Science* **2020**, *370*, No. eaba2644.

(11) Mehidi, A.; Kage, F.; Karatas, Z.; Cercy, M.; Schaks, M.; Polesskaya, A.; Sainlos, M.; Gautreau, A. M.; Rossier, O.; Rottner, K.; et al. Forces Generated by Lamellipodial Actin Filament Elongation Regulate the Wave Complex during Cell Migration. *Nat. Cell Biol.* **2021**, *23*, 1148−1162.

(12) Bera, K.; Kiepas, A.; Godet, I.; Li, Y.; Mehta, P.; Ifemembi, B.; Paul, C. D.; Sen, A.; Serra, S. A.; Stoletov, K.; et al. Extracellular Fluid Viscosity Enhances Cell Migration and Cancer Dissemination. *Nature* **2022**, *611*, 365−373.

(13) Chakrabortty, B.; Willemsen, V.; de Zeeuw, T.; Liao, C.-Y.; Weijers, D.; Mulder, B.; Scheres, B. A Plausible Microtubule-Based Mechanism for Cell Division Orientation in Plant Embryogenesis. *Curr. Biol.* **2018**, *28*, 3031−3043.

(14) Liu, Z.-Y.; Li, B.; Zhao, Z.-L.; Xu, G.-K.; Feng, X.-Q.; Gao, H. Mesoscopic Dynamic Model of Epithelial Cell Division with Cell-Cell Junction Effects. *Phys. Rev. E* **2020**, *102*, 012405.

(15) Zhao, Z.-L.; Liu, Z.-Y.; Du, J.; Xu, G.-K.; Feng, X.-Q. A Dynamic Biochemomechanical Model of Geometry-Confined Cell Spreading. *Biophys. J.* **2017**, *112*, 2377−2386.

(16) Fritzsche, M.; Fernandes, R. A.; Chang, V. T.; Colin-York, H.; Clausen, M. P.; Felce, J. H.; Galiani, S.; Erlenkämper, C.; Santos, A. M.; Heddleston, J. M.; et al. Cytoskeletal Actin Dynamics Shape a Ramifying Actin Network Underpinning Immunological Synapse Formation. *Science advances* **2017**, *3*, No. e1603032.

(17) Basu, R.; Whitlock, B. M.; Husson, J.; Le Floc'h, A.; Jin, W.; Oyler-Yaniv, A.; Dotiwala, F.; Giannone, G.; Hivroz, C.; Biais, N.; et al. Cytotoxic T Cells Use Mechanical Force to Potentiate Target Cell Killing. *Cell* **2016**, *165*, 100−110.

(18) Hammer, J. A.; Wang, J. C.; Saeed, M.; Pedrosa, A. T. Origin, Organization, Dynamics, and Function of Actin and Actomyosin Networks at the T Cell Immunological Synapse. *Annu. Rev. Immunol.* **2019**, *37*, 201−224.

(19) Markey, K. A.; Gartlan, K. H.; Kuns, R. D.; MacDonald, K. P.; Hill, G. R. Imaging the Immunological Synapse between Dendritic Cells and T Cells. *J. Immunol. Methods* **2015**, *423*, 40−44.

(20) Zenker, J.; White, M. D.; Templin, R.; Parton, R.; Thorn-Seshold, O.; Bissiere, S.; Plachta, N. A Microtubule-Organizing Center Directing Intracellular Transport in the Early Mouse Embryo. *Science* **2017**, *357*, 925−928.

(21) Siddiqui, N.; Zwetsloot, A. J.; Bachmann, A.; Roth, D.; Hussain, H.; Brandt, J.; Kaverina, I.; Straube, A. Ptpn21 and Hook3 Relieve Kif1c Autoinhibition and Activate Intracellular Transport. *Nat. Commun.* **2019**, *10*, 2693.

(22) Freeman, S. A.; Goyette, J.; Furuya, W.; Woods, E. C.; Bertozzi, C. R.; Bergmeier, W.; Hinz, B.; Van Der Merwe, P. A.; Das, R.; Grinstein, S. Integrins Form an Expanding Diffusional Barrier That Coordinates Phagocytosis. *Cell* **2016**, *164*, 128−140.

(23) Egami, Y.; Kawai, K.; Araki, N. Rhoc Regulates the Actin Remodeling Required for Phagosome Formation during Fcγr-Mediated Phagocytosis. *J. Cell Sci.* **2017**, *130*, 4168−4179.

(24) Jaumouillé, V.; Cartagena-Rivera, A. X.; Waterman, C. M. Coupling of B2 Integrins to Actin by a Mechanosensitive Molecular Clutch Drives Complement Receptor-Mediated Phagocytosis. *Nat. Cell Biol.* **2019**, *21*, 1357−1369.

(25) Jin, M.; Shirazinejad, C.; Wang, B.; Yan, A.; Schöneberg, J.; Upadhyayula, S.; Xu, K.; Drubin, D. G. Branched Actin Networks Are Organized for Asymmetric Force Production during Clathrin-Mediated Endocytosis in Mammalian Cells. *Nat. Commun.* **2022**, *13*, 3578.

(26) Kumari, A.; Pineau, J.; Sáez, P. J.; Maurin, M.; Lankar, D.; San Roman, M.; Hennig, K.; Boura, V. F.; Voituriez, R.; Karlsson, M. C.; et al. Actomyosin-Driven Force Patterning Controls Endocytosis at the Immune Synapse. *Nat. Commun.* **2019**, *10*, 2870.

(27) Sindhwani, S.; Syed, A. M.; Ngai, J.; Kingston, B. R.; Maiorino, L.; Rothschild, J.; MacMillan, P.; Zhang, Y.; Rajesh, N. U.; Hoang, T.; et al. The Entry of Nanoparticles into Solid Tumours. *Nat. Mater.* **2020**, *19*, 566−575.

(28) Rotty, J. D.; Brighton, H. E.; Craig, S. L.; Asokan, S. B.; Cheng, N.; Ting, J. P.; Bear, J. E. Arp2/3 Complex Is Required for Macrophage Integrin Functions but Is Dispensable for Fcr Phagocytosis and in Vivo Motility. *Dev. Cell* **2017**, *42*, 498−513.

(29) Mylvaganam, S.; Freeman, S. A.; Grinstein, S. The Cytoskeleton in Phagocytosis and Macropinocytosis. *Curr. Biol.* **2021**, *31*, R619−R632.

(30) Pollard, T. D.; Borisy, G. G. Cellular Motility Driven by Assembly and Disassembly of Actin Filaments. *Cell* **2003**, *112*, 453−465.

(31) Akamatsu, M.; Vasan, R.; Serwas, D.; Ferrin, M. A.; Rangamani, P.; Drubin, D. G. Principles of Self-Organization and Load Adaptation by the Actin Cytoskeleton during Clathrin-Mediated Endocytosis. *Elife* **2020**, *9*, No. e49840.

(32) Hassinger, J. E.; Oster, G.; Drubin, D. G.; Rangamani, P. Design Principles for Robust Vesiculation in Clathrin-Mediated Endocytosis. *Proc. Natl. Acad. Sci. U. S. A.* **2017**, *114*, E1118−E1127.

(33) Canton, J. Macropinocytosis: New Insights into Its Underappreciated Role in Innate Immune Cell Surveillance. *Frontiers in Immunology* **2018**, *9*, 2286.
(34) Tamzalit, F.; Wang, M. S.; Jin, W.; Tello-Lafoz, M.; Boyko, V.; Heddleston, J. M.; Black, C. T.; Kam, L. C.; Huse, M. Interfacial Actin Protrusions Mechanically Enhance Killing by Cytotoxic T Cells. *Science Immunology* **2019**, *4*, No. eaav5445.
(35) Semba, S.; Iwaya, K.; Matsubayashi, J.; Serizawa, H.; Kataba, H.; Hirano, T.; Kato, H.; Matsuoka, T.; Mukai, K. Coexpression of Actin-Related Protein 2 and Wiskott-Aldrich Syndrome Family Verproline-Homologous Protein 2 in Adenocarcinoma of the Lung. *Clin. Cancer Res.* **2006**, *12*, 2449−2454.
(36) Kazazian, K.; Go, C.; Wu, H.; Brashavitskaya, O.; Xu, R.; Dennis, J. W.; Gingras, A.-C.; Swallow, C. J. Plk4 Promotes Cancer Invasion and Metastasis through Arp2/3 Complex Regulation of the Actin Cytoskeleton. *Cancer Res.* **2017**, *77*, 434−447.
(37) Juin, A.; Spence, H. J.; Martin, K. J.; McGhee, E.; Neilson, M.; Cutiongco, M. F. A.; Gadegaard, N.; Mackay, G.; Fort, L.; Lilla, S.; Kalna, G.; Thomason, P.; Koh, Y. W. H.; Norman, J. C.; Insall, R. H.; Machesky, L. M. N-Wasp Control of Lpar1 Trafficking Establishes Response to Self-Generated Lpa Gradients to Promote Pancreatic Cancer Cell Metastasis. *Dev. Cell* **2019**, *51*, 431−445.
(38) Frentzas, S.; Simoneau, E.; Bridgeman, V. L.; Vermeulen, P. B.; Foo, S.; Kostaras, E.; Nathan, M. R.; Wotherspoon, A.; Gao, Z.-h.; Shi, Y.; et al. Vessel Co-Option Mediates Resistance to Anti-Angiogenic Therapy in Liver Metastases. *Nat. Med.* **2016**, *22*, 1294−1302.
(39) Esteves, A.; Palma, A.; Gomes, R.; Santos, D.; Silva, D.; Cardoso, S. Acetylation as a Major Determinant to Microtubule-Dependent Autophagy: Relevance to Alzheimer's and Parkinson Disease Pathology. *Biochimica et Biophysica Acta (BBA)-Molecular Basis of Disease* **2019**, *1865*, 2008−2023.
(40) Van Dyck, C. H.; Swanson, C. J.; Aisen, P.; Bateman, R. J.; Chen, C.; Gee, M.; Kanekiyo, M.; Li, D.; Reyderman, L.; Cohen, S.; et al. Lecanemab in Early Alzheimer's Disease. *N. Engl. J. Med.* **2023**, *388*, 9−21.
(41) Abbott, A. Could Drugs Prevent Alzheimer's? These Trials Aim to Find Out. *Nature* **2022**, *603*, 216−219.
(42) Kellogg, E. H.; Hejab, N. M.; Poepsel, S.; Downing, K. H.; DiMaio, F.; Nogales, E. Near-Atomic Model of Microtubule-Tau Interactions. *Science* **2018**, *360*, 1242−1246.
(43) Horwitz, S. Taxol (Paclitaxel): Mechanisms of Action. *Annals of oncology: official journal of the European Society for Medical Oncology* **1994**, *5*, S3−6.
(44) Wattanathamsan, O.; Thararattanobon, R.; Rodsiri, R.; Chanvorachote, P.; Vinayanuwattikun, C.; Pongrakhananon, V. Tubulin Acetylation Enhances Lung Cancer Resistance to Paclitaxel-Induced Cell Death through Mcl-1 Stabilization. *Cell Death Discovery* **2021**, *7*, 67.
(45) Müller-Deku, A.; Meiring, J. C. M.; Loy, K.; Kraus, Y.; Heise, C.; Bingham, R.; Jansen, K. I.; Qu, X.; Bartolini, F.; Kapitein, L. C.; Akhmanova, A.; Ahlfeld, J.; Trauner, D.; Thorn-Seshold, O. Photoswitchable Paclitaxel-Based Microtubule Stabilisers Allow Optical Control over the Microtubule Cytoskeleton. *Nat. Commun.* **2020**, *11*, 4640.
(46) Popow-Woźniak, A.; Woźniakowska, A.; Kaczmarek, Ł.; Malicka-Błaszkiewicz, M.; Nowak, D. Apoptotic Effect of Imatinib on Human Colon Adenocarcinoma Cells: Influence on Actin Cytoskeleton Organization and Cell Migration. *Eur. J. Pharmacol.* **2011**, *667*, 66−73.
(47) Wang, X.; Bleher, R.; Wang, L.; Garcia, J.; Dudek, S.; Shekhawat, G.; Dravid, V. Imatinib Alters Agonists-Mediated Cytoskeletal Biomechanics in Lung Endothelium. *Sci. Rep.* **2017**, *7*, 1−14.
(48) Preisinger, C.; Kolch, W. The Bcr-Abl Kinase Regulates the Actin Cytoskeleton Via a Gads/Slp-76/Nck1 Adaptor Protein Pathway. *Cell. Signal.* **2010**, *22*, 848−856.
(49) Puissant, A.; Dufies, M.; Fenouille, N.; Ben Sahra, I.; Jacquel, A.; Robert, G.; Cluzeau, T.; Deckert, M.; Tichet, M.; Chéli, Y. Imatinib Triggers Mesenchymal-Like Conversion of Cml Cells Associated with Increased Aggressiveness. *J. Mol. Cell Biol.* **2012**, *4*, 207−220.
(50) Kumar, R.; Pereira, R. S.; Zanetti, C.; Minciacchi, V. R.; Merten, M.; Meister, M.; Niemann, J.; Dietz, M. S.; Rüssel, N.; Schnütgen, F.; et al. Specific, Targetable Interactions with the Microenvironment Influence Imatinib-Resistant Chronic Myeloid Leukemia. *Leukemia* **2020**, *34*, 2087−2101.
(51) Evans, E. A.; Calderwood, D. A. Forces and Bond Dynamics in Cell Adhesion. *Science* **2007**, *316*, 1148−1153.
(52) Kaya, M.; Higuchi, H. Nonlinear Elasticity and an 8-Nm Working Stroke of Single Myosin Molecules in Myofilaments. *Science* **2010**, *329*, 686−689.
(53) Abella, M.; Andruck, L.; Malengo, G.; Skruzny, M. Actin-Generated Force Applied during Endocytosis Measured by Sla2-Based Fret Tension Sensors. *Dev. Cell* **2021**, *56*, 2419−2426.
(54) Prass, M.; Jacobson, K.; Mogilner, A.; Radmacher, M. Direct Measurement of the Lamellipodial Protrusive Force in a Migrating Cell. *J. Cell Biol.* **2006**, *174*, 767−772.
(55) Yu, M.; Yuan, X.; Lu, C.; Le, S.; Kawamura, R.; Efremov, A. K.; Zhao, Z.; Kozlov, M. M.; Sheetz, M.; Bershadsky, A.; et al. Mdia1 Senses Both Force and Torque during F-Actin Filament Polymerization. *Nat. Commun.* **2017**, *8*, 1650.
(56) Li, D.; Shao, L.; Chen, B.-C.; Zhang, X.; Zhang, M.; Moses, B.; Milkie, D. E.; Beach, J. R.; Hammer, J. A.; Pasham, M.; et al. Extended-Resolution Structured Illumination Imaging of Endocytic and Cytoskeletal Dynamics. *Science* **2015**, *349*, aab3500.
(57) Mahamid, J.; Pfeffer, S.; Schaffer, M.; Villa, E.; Danev, R.; Cuellar, L. K.; Förster, F.; Hyman, A. A.; Plitzko, J. M.; Baumeister, W. Visualizing the Molecular Sociology at the Hela Cell Nuclear Periphery. *Science* **2016**, *351*, 969−972.
(58) Liu, T.-l.; Upadhyayula, S.; Milkie, D. E.; Singh, V.; Wang, K.; Swinburne, I. A.; Mosaliganti, K. R.; Collins, Z. M.; Hiscock, T. W.; Shea, J.; et al. Observing the Cell in Its Native State: Imaging Subcellular Dynamics in Multicellular Organisms. *Science* **2018**, *360*, No. eaaq1392.
(59) Beroz, F.; Jawerth, L. M.; Münster, S.; Weitz, D. A.; Broedersz, C. P.; Wingreen, N. S. Physical Limits to Biomechanical Sensing in Disordered Fibre Networks. *Nat. Commun.* **2017**, *8*, 16096.
(60) Chugh, P.; Clark, A. G.; Smith, M. B.; Cassani, D. A.; Dierkes, K.; Ragab, A.; Roux, P. P.; Charras, G.; Salbreux, G.; Paluch, E. K. Actin Cortex Architecture Regulates Cell Surface Tension. *Nat. Cell Biol.* **2017**, *19*, 689.
(61) Deshpande, V. S.; McMeeking, R. M.; Evans, A. G. A Bio-Chemo-Mechanical Model for Cell Contractility. *Proc. Natl. Acad. Sci. U. S. A.* **2006**, *103*, 14015−14020.
(62) Wang, Y.; Yao, M.; Baker, K. B.; Gough, R. E.; Le, S.; Goult, B. T.; Yan, J. Force-Dependent Interactions between Talin and Full-Length Vinculin. *J. Am. Chem. Soc.* **2021**, *143*, 14726−14737.
(63) Qin, Y.; Li, Y.; Zhang, L.-Y.; Xu, G.-K. Stochastic Fluctuation-Induced Cell Polarization on Elastic Substrates: A Cytoskeleton-Based Mechanical Model. *Journal of the Mechanics and Physics of Solids* **2020**, *137*, 103872.
(64) Yin, S.; Li, B.; Feng, X.-Q. Bio-Chemo-Mechanical Theory of Active Shells. *Journal of the Mechanics and Physics of Solids* **2021**, *152*, 104419.
(65) Mak, M.; Zaman, M. H.; Kamm, R. D.; Kim, T. Interplay of Active Processes Modulates Tension and Drives Phase Transition in Self-Renewing, Motor-Driven Cytoskeletal Networks. *Nat. Commun.* **2016**, *7*, 10323.
(66) Lin, S.-Z.; Ye, S.; Xu, G.-K.; Li, B.; Feng, X.-Q. Dynamic Migration Modes of Collective Cells. *Biophys. J.* **2018**, *115*, 1826−1835.
(67) DiMasi, J. A.; Grabowski, H. G.; Hansen, R. W. Innovation in the Pharmaceutical Industry: New Estimates of R&D Costs. *J. Health Econ.* **2016**, *47*, 20−33.
(68) Gorgulla, C.; Boeszoermenyi, A.; Wang, Z.-F.; Fischer, P. D.; Coote, P. W.; Padmanabha Das, K. M.; Malets, Y. S.; Radchenko, D. S.; Moroz, Y. S.; Scott, D. A.; et al. An Open-Source Drug Discovery

Platform Enables Ultra-Large Virtual Screens. *Nature* **2020**, *580*, 663−668.
(69) Singla, J.; McClary, K. M.; White, K. L.; Alber, F.; Sali, A.; Stevens, R. C. Opportunities and Challenges in Building a Spatiotemporal Multi-Scale Model of the Human Pancreatic B Cell. *Cell* **2018**, *173*, 11−19.
(70) Maritan, M.; Autin, L.; Karr, J.; Covert, M. W.; Olson, A. J.; Goodsell, D. S. Building Structural Models of a Whole Mycoplasma Cell. *J. Mol. Biol.* **2022**, *434*, 167351.
(71) Renkawitz, J.; Kopf, A.; Stopp, J.; de Vries, I.; Driscoll, M. K.; Merrin, J.; Hauschild, R.; Welf, E. S.; Danuser, G.; Fiolka, R.; et al. Nuclear Positioning Facilitates Amoeboid Migration Along the Path of Least Resistance. *Nature* **2019**, *568*, 546.
(72) Kaksonen, M.; Roux, A. Mechanisms of Clathrin-Mediated Endocytosis. *Nat. Rev. Mol. Cell Biol.* **2018**, *19*, 313−326.
(73) Sochacki, K. A.; Dickey, A. M.; Strub, M.-P.; Taraska, J. W. Endocytic Proteins Are Partitioned at the Edge of the Clathrin Lattice in Mammalian Cells. *Nat. Cell Biol.* **2017**, *19*, 352−361.
(74) Obashi, K.; Sochacki, K. A.; Strub, M.-P.; Taraska, J. W. A Conformational Switch in Clathrin Light Chain Regulates Lattice Structure and Endocytosis at the Plasma Membrane of Mammalian Cells. *Nat. Commun.* **2023**, *14*, 732.
(75) Bloomfield, G.; Kay, R. R. Uses and Abuses of Macropinocytosis. *J. Cell Sci.* **2016**, *129*, 2697−2705.
(76) Behzadi, S.; Serpooshan, V.; Tao, W.; Hamaly, M. A.; Alkawareek, M. Y.; Dreaden, E. C.; Brown, D.; Alkilany, A. M.; Farokhzad, O. C.; Mahmoudi, M. Cellular Uptake of Nanoparticles: Journey inside the Cell. *Chem. Soc. Rev.* **2017**, *46*, 4218−4244.
(77) Mas-Moruno, C.; Rechenmacher, F.; Kessler, H. Cilengitide: The First Anti-Angiogenic Small Molecule Drug Candidate. Design, Synthesis and Clinical Evaluation. *Anti-Cancer Agents in Medicinal Chemistry* **2010**, *10*, 753−768.
(78) Burke, P. A.; DeNardo, S. J.; Miers, L. A.; Lamborn, K. R.; Matzku, S.; DeNardo, G. L. Cilengitide Targeting of Avβ3 Integrin Receptor Synergizes with Radioimmunotherapy to Increase Efficacy and Apoptosis in Breast Cancer Xenografts. *Cancer Res.* **2002**, *62*, 4263−4272.
(79) Reardon, D. A.; Fink, K. L.; Mikkelsen, T.; Cloughesy, T. F.; O'Neill, A.; Plotkin, S.; Glantz, M.; Ravin, P.; Raizer, J. J.; Rich, K. M.; et al. Randomized Phase Ii Study of Cilengitide, an Integrin-Targeting Arginine-Glycine-Aspartic Acid Peptide, in Recurrent Glioblastoma Multiforme. *J. Clin. Oncol.* **2008**, *26*, 5610−5617.
(80) Dumontet, C.; Jordan, M. A.; Lee, F. F. Ixabepilone: Targeting Biii-Tubulin Expression in Taxane-Resistant Malignancies. *Mol. Cancer Ther.* **2009**, *8*, 17−25.
(81) Lee, F. Y.; Borzilleri, R.; Fairchild, C. R.; Kamath, A.; Smykla, R.; Kramer, R.; Vite, G. Preclinical Discovery of Ixabepilone, a Highly Active Antineoplastic Agent. *Cancer Chemother. Pharmacol.* **2008**, *63*, 157−166.
(82) Testa, V.; Della Giustina, P.; Traverso, C.; Iester, M. An Update on Ripasudil for the Treatment of Glaucoma and Ocular Hypertension. *Drugs of Today (Barcelona, Spain: 1998)* **2020**, *56*, 599−608.
(83) Kaneko, Y.; Ohta, M.; Inoue, T.; Mizuno, K.; Isobe, T.; Tanabe, S.; Tanihara, H. Effects of K-115 (Ripasudil), a Novel Rock Inhibitor, on Trabecular Meshwork and Schlemm's Canal Endothelial Cells. *Sci. Rep.* **2016**, *6*, 19640.
(84) Cheetham, P.; Petrylak, D. P. Tubulin-Targeted Agents Including Docetaxel and Cabazitaxel. *Cancer Journal* **2013**, *19*, 59−65.
(85) Morse, D. L.; Gray, H.; Payne, C. M.; Gillies, R. J. Docetaxel Induces Cell Death through Mitotic Catastrophe in Human Breast Cancer Cells. *Mol. Cancer Ther.* **2005**, *4*, 1495−1504.
(86) Ploussard, G.; Terry, S.; Maillé, P.; Allory, Y.; Sirab, N.; Kheuang, L.; Soyeux, P.; Nicolaiew, N.; Coppolani, E.; Paule, B.; et al. Class Iii B-Tubulin Expression Predicts Prostate Tumor Aggressiveness and Patient Response to Docetaxel-Based Chemotherapy. *Cancer Res.* **2010**, *70*, 9253−9264.
(87) Gigant, B.; Wang, C.; Ravelli, R. B.; Roussi, F.; Steinmetz, M. O.; Curmi, P. A.; Sobel, A.; Knossow, M. Structural Basis for the Regulation of Tubulin by Vinblastine. *Nature* **2005**, *435*, 519−522.
(88) Dhyani, P.; Quispe, C.; Sharma, E.; Bahukhandi, A.; Sati, P.; Attri, D. C.; Szopa, A.; Sharifi-Rad, J.; Docea, A. O.; Mardare, I.; et al. Anticancer Potential of Alkaloids: A Key Emphasis to Colchicine, Vinblastine, Vincristine, Vindesine, Vinorelbine and Vincamine. *Cancer Cell International* **2022**, *22*, 206.
(89) Negoro, N.; Hoshiga, M.; Seto, M.; Kohbayashi, E.; Ii, M.; Fukui, R.; Shibata, N.; Nakakoji, T.; Nishiguchi, F.; Sasaki, Y.; et al. The Kinase Inhibitor Fasudil (Ha-1077) Reduces Intimal Hyperplasia through Inhibiting Migration and Enhancing Cell Loss of Vascular Smooth Muscle Cells. *Biochem. Biophys. Res. Commun.* **1999**, *262*, 211−215.
(90) Mohri, M.; Shimokawa, H.; Hirakawa, Y.; Masumoto, A.; Takeshita, A. Rho-Kinase Inhibition with Intracoronary Fasudil Prevents Myocardial Ischemia in Patients with Coronary Microvascular Spasm. *J. Am. Coll. Cardiol.* **2003**, *41*, 15−19.
(91) Nettles, J. H.; Li, H.; Cornett, B.; Krahn, J. M.; Snyder, J. P.; Downing, K. H. The Binding Mode of Epothilone a on A, ß-Tubulin by Electron Crystallography. *Science* **2004**, *305*, 866−869.
(92) Kowalski, R. J.; Giannakakou, P.; Hamel, E. Activities of the Microtubule-Stabilizing Agents Epothilones a and B with Purified Tubulin and in Cells Resistant to Paclitaxel (Taxol®). *J. Biol. Chem.* **1997**, *272*, 2534−2541.
(93) Calizo, R. C.; Bhattacharya, S.; van Hasselt, J. C.; Wei, C.; Wong, J. S.; Wiener, R. J.; Ge, X.; Wong, N. J.; Lee, J.-J.; Cuttitta, C. M.; et al. Disruption of Podocyte Cytoskeletal Biomechanics by Dasatinib Leads to Nephrotoxicity. *Nat. Commun.* **2019**, *10*, 2061.
(94) Pichot, C.; Hartig, S.; Xia, L.; Arvanitis, C.; Monisvais, D.; Lee, F.; Frost, J.; Corey, S. Dasatinib Synergizes with Doxorubicin to Block Growth, Migration, and Invasion of Breast Cancer Cells. *Br. J. Cancer* **2009**, *101*, 38−47.
(95) Kreutzman, A.; Colom-Fernández, B.; Jiménez, A. M.; Ilander, M.; Cuesta-Mateos, C.; Pérez-García, Y.; Arévalo, C. D.; Brück, O.; Hakanen, H.; Saarela, J.; et al. Dasatinib Reversibly Disrupts Endothelial Vascular Integrity by Increasing Non-Muscle Myosin Ii Contractility in a Rock-Dependent Mannerdasatinib Disrupts Adhesive Structures on Endothelial Cells. *Clin. Cancer Res.* **2017**, *23*, 6697−6707.
(96) Lin, T.-C. Gefitinib Modulates Stress Fibers and Tubular-Like Structure Formation and Attenuates Angiogenesis in an in Vivo Chicken Model of Chorioallantoic Membrane Angiogenesis. *Biochem. Biophys. Res. Commun.* **2020**, *526*, 568−573.
(97) Tang, Z.; Du, R.; Jiang, S.; Wu, C.; Barkauskas, D.; Richey, J.; Molter, J.; Lam, M.; Flask, C.; Gerson, S.; et al. Dual Met-Egfr Combinatorial Inhibition against T790m-Egfr-Mediated Erlotinib-Resistant Lung Cancer. *Br. J. Cancer* **2008**, *99*, 911−922.
(98) Wertheimer, C.; Liegl, R.; Kernt, M.; Docheva, D.; Kampik, A.; Eibl-Lindner, K. Egfr-Blockade with Erlotinib Reduces Egf and Tgf-B2 Expression and the Actin-Cytoskeleton Which Influences Different Aspects of Cellular Migration in Lens Epithelial Cells. *Curr. Eye Res.* **2014**, *39*, 1000−1012.
(99) Chuang, J. C.; Neal, J. W. Crizotinib as First Line Therapy for Advanced Alk -Positive Non-Small Cell Lung Cancers. *Translational Lung Cancer Research* **2015**, *4*, 639−641.
(100) Boulos, J. C.; Saeed, M. E.; Chatterjee, M.; Bülbül, Y.; Crudo, F.; Marko, D.; Munder, M.; Klauck, S. M.; Efferth, T. Repurposing of the Alk Inhibitor Crizotinib for Acute Leukemia and Multiple Myeloma Cells. *Pharmaceuticals* **2021**, *14*, 1126.
(101) Skobel, E.; Dannemann, O.; Reffelmann, T.; Bohm, V.; Weber, C.; Hanrath, P.; Uretsky, B. F.; Schwarz, E. R. Carvedilol Protects Myocardial Cytoskeleton during Hypoxia in the Rat Heart. *Journal of Applied Research in Clinical And Experimental Therapeutics* **2005**, *5*, 378.
(102) Bers, D. M. Cardiac Excitation-Contraction Coupling. *Nature* **2002**, *415*, 198−205.
(103) Cocco, E.; Schram, A. M.; Kulick, A.; Misale, S.; Won, H. H.; Yaeger, R.; Razavi, P.; Ptashkin, R.; Hechtman, J. F.; Toska, E.; et al. Resistance to Trk Inhibition Mediated by Convergent Mapk Pathway Activation. *Nat. Med.* **2019**, *25*, 1422−1427.

https://doi.org/10.1021/acsnano.4c12599
ACS Nano 2024, 18, 29311−29336

(104) Drilon, A.; Jenkins, C.; Iyer, S.; Schoenfeld, A.; Keddy, C.; Davare, M. A. Ros1-Dependent Cancers — Biology, Diagnostics and Therapeutics. *Nature Reviews Clinical Oncology* **2021**, *18*, 35−55.
(105) Solernó, L. M.; Sobol, N. T.; Gottardo, M. F.; Capobianco, C. S.; Ferrero, M. R.; Vásquez, L.; Alonso, D. F.; Garona, J. Propranolol Blocks Osteosarcoma Cell Cycle Progression, Inhibits Angiogenesis and Slows Xenograft Growth in Combination with Cisplatin-Based Chemotherapy. *Sci. Rep.* **2022**, *12*, 15058.
(106) Parsons, C. G.; Danysz, W.; Dekundy, A.; Pulte, I. Memantine and Cholinesterase Inhibitors: Complementary Mechanisms in the Treatment of Alzheimer's Disease. *Neurotox. Res.* **2013**, *24*, 358−369.
(107) Koola, M. M. Galantamine-Memantine Combination in the Treatment of Alzheimer's Disease and Beyond. *Psychiatry Res.* **2020**, *293*, 113409.
(108) Fletcher, D. A.; Mullins, R. D. Cell Mechanics and the Cytoskeleton. *Nature* **2010**, *463*, 485−492.
(109) Pollard, T. D. The Cytoskeleton, Cellular Motility and the Reductionist Agenda. *Nature* **2003**, *422*, 741−745.
(110) Blanchoin, L.; Boujemaa-Paterski, R.; Sykes, C.; Plastino, J. Actin Dynamics, Architecture, and Mechanics in Cell Motility. *Physiol. Rev.* **2014**, *94*, 235−263.
(111) Butcher, D. T.; Alliston, T.; Weaver, V. M. A Tense Situation: Forcing Tumour Progression. *Nat. Rev. Cancer* **2009**, *9*, 108−122.
(112) Paul, C. D.; Mistriotis, P.; Konstantopoulos, K. Cancer Cell Motility: Lessons from Migration in Confined Spaces. *Nat. Rev. Cancer* **2017**, *17*, 131−140.
(113) Stuelten, C. H.; Parent, C. A.; Montell, D. J. Cell Motility in Cancer Invasion and Metastasis: Insights from Simple Model Organisms. *Nat. Rev. Cancer* **2018**, *18*, 296−312.
(114) Engler, A. J.; Sen, S.; Sweeney, H. L.; Discher, D. E. Matrix Elasticity Directs Stem Cell Lineage Specification. *Cell* **2006**, *126*, 677−689.
(115) Discher, D. E.; Mooney, D. J.; Zandstra, P. W. Growth Factors, Matrices, and Forces Combine and Control Stem Cells. *Science* **2009**, *324*, 1673−1677.
(116) Watt, F. M.; Huck, W. T. Role of the Extracellular Matrix in Regulating Stem Cell Fate. *Nat. Rev. Mol. Cell Biol.* **2013**, *14*, 467−473.
(117) DuFort, C. C.; Paszek, M. J.; Weaver, V. M. Balancing Forces: Architectural Control of Mechanotransduction. *Nat. Rev. Mol. Cell Biol.* **2011**, *12*, 308−319.
(118) Broedersz, C. P.; MacKintosh, F. C. Modeling Semiflexible Polymer Networks. *Rev. Mod. Phys.* **2014**, *86*, 995.
(119) Fudge, D. S.; Gardner, K. H.; Forsyth, V. T.; Riekel, C.; Gosline, J. M. The Mechanical Properties of Hydrated Intermediate Filaments: Insights from Hagfish Slime Threads. *Biophys. J.* **2003**, *85*, 2015−2027.
(120) Janmey, P. A.; Euteneuer, U.; Traub, P.; Schliwa, M. Viscoelastic Properties of Vimentin Compared with Other Filamentous Biopolymer Networks. *J. Cell Biol.* **1991**, *113*, 155−160.
(121) Block, J.; Witt, H.; Candelli, A.; Peterman, E. J.; Wuite, G. J.; Janshoff, A.; Köster, S. Nonlinear Loading-Rate-Dependent Force Response of Individual Vimentin Intermediate Filaments to Applied Strain. *Phys. Rev. Lett.* **2017**, *118*, 048101.
(122) Block, J.; Schroeder, V.; Pawelzyk, P.; Willenbacher, N.; Köster, S. Physical Properties of Cytoplasmic Intermediate Filaments. *Biochimica et Biophysica Acta (BBA)-Molecular Cell Research* **2015**, *1853*, 3053−3064.
(123) Bloom, K. S. Beyond the Code: The Mechanical Properties of DNA as They Relate to Mitosis. *Chromosoma* **2008**, *117*, 103−110.
(124) Bear, J. E.; Svitkina, T. M.; Krause, M.; Schafer, D. A.; Loureiro, J. J.; Strasser, G. A.; Maly, I. V.; Chaga, O. Y.; Cooper, J. A.; Borisy, G. G.; et al. Antagonism between Ena/Vasp Proteins and Actin Filament Capping Regulates Fibroblast Motility. *Cell* **2002**, *109*, 509−521.
(125) Hylton, R. K.; Heebner, J. E.; Grillo, M. A.; Swulius, M. T. Cofilactin Filaments Regulate Filopodial Structure and Dynamics in Neuronal Growth Cones. *Nat. Commun.* **2022**, *13*, 2439.
(126) Turgay, Y.; Eibauer, M.; Goldman, A. E.; Shimi, T.; Khayat, M.; Ben-Harush, K.; Dubrovsky-Gaupp, A.; Sapra, K. T.; Goldman, R. D.; Medalia, O. The Molecular Architecture of Lamins in Somatic Cells. *Nature* **2017**, *543*, 261−264.
(127) Sapra, K. T.; Qin, Z.; Dubrovsky-Gaupp, A.; Aebi, U.; Müller, D. J.; Buehler, M. J.; Medalia, O. Nonlinear Mechanics of Lamin Filaments and the Meshwork Topology Build an Emergent Nuclear Lamina. *Nat. Commun.* **2020**, *11*, 6205.
(128) Alushin, G. M.; Lander, G. C.; Kellogg, E. H.; Zhang, R.; Baker, D.; Nogales, E. High-Resolution Microtubule Structures Reveal the Structural Transitions in Aβ-Tubulin Upon Gtp Hydrolysis. *Cell* **2014**, *157*, 1117−1129.
(129) Li, Y.; Kucera, O.; Cuvelier, D.; Rutkowski, D. M.; Deygas, M.; Rai, D.; Pavlovic, T.; Vicente, F. N.; Piel, M.; Giannone, G.; Vavylonis, D.; Akhmanova, A.; Blanchoin, L.; Thery, M. Compressive Forces Stabilize Microtubules in Living Cells. *Nat. Mater.* **2023**, *22*, 913−924.
(130) Wiggins, P. A.; van der Heijden, T.; Moreno-Herrero, F.; Spakowitz, A.; Phillips, R.; Widom, J.; Dekker, C.; Nelson, P. C. High Flexibility of DNA on Short Length Scales Probed by Atomic Force Microscopy. *Nat. Nanotechnol.* **2006**, *1*, 137−141.
(131) Piovesan, A.; Pelleri, M. C.; Antonaros, F.; Strippoli, P.; Caracausi, M.; Vitale, L. On the Length, Weight and Gc Content of the Human Genome. *BMC Res. Notes* **2019**, *12*, 106.
(132) Simon, C.; Kusters, R.; Caorsi, V.; Allard, A.; Abou-Ghali, M.; Manzi, J.; Di Cicco, A.; Lévy, D.; Lenz, M.; Joanny, J.-F.; et al. Actin Dynamics Drive Cell-Like Membrane Deformation. *Nat. Phys.* **2019**, *15*, 602−609.
(133) Pollard, T. D.; Cooper, J. A. Actin, a Central Player in Cell Shape and Movement. *Science* **2009**, *326*, 1208−1212.
(134) Kawska, A.; Carvalho, K.; Manzi, J.; Boujemaa-Paterski, R.; Blanchoin, L.; Martiel, J.-L.; Sykes, C. How Actin Network Dynamics Control the Onset of Actin-Based Motility. *Proc. Natl. Acad. Sci. U. S. A.* **2012**, *109*, 14440−14445.
(135) Pollard, T. D. Rate Constants for the Reactions of Atp-and Adp-Actin with the Ends of Actin Filaments. *J. Cell Biol.* **1986**, *103*, 2747−2754.
(136) Mogilner, A.; Oster, G. Cell Motility Driven by Actin Polymerization. *Biophys. J.* **1996**, *71*, 3030−3045.
(137) Mogilner, A.; Oster, G. Force Generation by Actin Polymerization Ii: The Elastic Ratchet and Tethered Filaments. *Biophys. J.* **2003**, *84*, 1591−1605.
(138) Boujemaa-Paterski, R.; Suarez, C.; Klar, T.; Zhu, J.; Guérin, C.; Mogilner, A.; Théry, M.; Blanchoin, L. Network Heterogeneity Regulates Steering in Actin-Based Motility. *Nat. Commun.* **2017**, *8*, 655.
(139) Hug, C.; Jay, P. Y.; Reddy, I.; McNally, J. G.; Bridgman, P. C.; Elson, E. L.; Cooper, J. A. Capping Protein Levels Influence Actin Assembly and Cell Motility in Dictyostelium. *Cell* **1995**, *81*, 591−600.
(140) Mullins, R. D.; Bieling, P.; Fletcher, D. A. From Solution to Surface to Filament: Actin Flux into Branched Networks. *Biophysical reviews* **2018**, *10*, 1537−1551.
(141) Courtemanche, N.; Lee, J. Y.; Pollard, T. D.; Greene, E. C. Tension Modulates Actin Filament Polymerization Mediated by Formin and Profilin. *Proc. Natl. Acad. Sci. U. S. A.* **2013**, *110*, 9752−9757.
(142) Pruyne, D.; Evangelista, M.; Yang, C.; Bi, E.; Zigmond, S.; Bretscher, A.; Boone, C. Role of Formins in Actin Assembly: Nucleation and Barbed-End Association. *Science* **2002**, *297*, 612−615.
(143) Barzik, M.; Kotova, T. I.; Higgs, H. N.; Hazelwood, L.; Hanein, D.; Gertler, F. B.; Schafer, D. A. Ena/Vasp Proteins Enhance Actin Polymerization in the Presence of Barbed End Capping Proteins. *J. Biol. Chem.* **2005**, *280*, 28653−28662.
(144) Graham, K.; Chandrasekaran, A.; Wang, L.; Ladak, A.; Lafer, E. M.; Rangamani, P.; Stachowiak, J. C. Liquid-Like Vasp Condensates Drive Actin Polymerization and Dynamic Bundling. *Nat. Phys.* **2023**, *19*, 574−585.
(145) Fäßler, F.; Dimchev, G.; Hodirnau, V.-V.; Wan, W.; Schur, F. K. M. Cryo-Electron Tomography Structure of Arp2/3 Complex in

https://doi.org/10.1021/acsnano.4c12599
ACS Nano 2024, 18, 29311−29336

Cells Reveals New Insights into the Branch Junction. *Nat. Commun.* **2020**, *11*, 6437.
(146) Chou, S. Z.; Chatterjee, M.; Pollard, T. D. Mechanism of Actin Filament Branch Formation by Arp2/3 Complex Revealed by a High-Resolution Cryo-Em Structureof the Branch Junction. *Proc. Natl. Acad. Sci. U. S. A.* **2022**, *119*, No. e2206722119.
(147) Ding, B.; Narvaez-Ortiz, H. Y.; Singh, Y.; Hocky, G. M.; Chowdhury, S.; Nolen, B. J. Structure of Arp2/3 Complex at a Branched Actin Filament Junction Resolved by Single-Particle Cryo-Electron Microscopy. *Proc. Natl. Acad. Sci. U. S. A.* **2022**, *119*, No. e2202723119.
(148) Rutkowski, D. M.; Vavylonis, D. Discrete Mechanical Model of Lamellipodial Actin Network Implements Molecular Clutch Mechanism and Generates Arcs and Microspikes. *PLoS Comput. Biol.* **2021**, *17*, No. e1009506.
(149) Jasnin, M.; Beck, F.; Ecke, M.; Fukuda, Y.; Martinez-Sanchez, A.; Baumeister, W.; Gerisch, G. The Architecture of Traveling Actin Waves Revealed by Cryo-Electron Tomography. *Structure* **2019**, *27*, 1211−1223.
(150) Arnold, M.; Cavalcanti-Adam, E. A.; Glass, R.; Blümmel, J.; Eck, W.; Kantlehner, M.; Kessler, H.; Spatz, J. P. Activation of Integrin Function by Nanopatterned Adhesive Interfaces. *ChemPhysChem* **2004**, *5*, 383−388.
(151) Plastino, J.; Blanchoin, L. Adaptive Actin Networks. *Dev. Cell* **2017**, *42*, 565−566.
(152) Blanchoin, L.; Amann, K. J.; Higgs, H. N.; Marchand, J.-B.; Kaiser, D. A.; Pollard, T. D. Direct Observation of Dendritic Actin Filament Networks Nucleated by Arp2/3 Complex and Wasp/Scar Proteins. *Nature* **2000**, *404*, 1007−1011.
(153) Wyatt, T. P.; Fouchard, J.; Lisica, A.; Khalilgharibi, N.; Baum, B.; Recho, P.; Kabla, A. J.; Charras, G. T. Actomyosin Controls Planarity and Folding of Epithelia in Response to Compression. *Nat. Mater.* **2020**, *19*, 109−117.
(154) Murugesan, S.; Hong, J.; Yi, J.; Li, D.; Beach, J. R.; Shao, L.; Meinhardt, J.; Madison, G.; Wu, X.; Betzig, E.; et al. Formin-Generated Actomyosin Arcs Propel T Cell Receptor Microcluster Movement at the Immune Synapse. *J. Cell Biol.* **2016**, *215*, 383−399.
(155) Wang, J. C.; Yim, Y.-I.; Wu, X.; Jaumouille, V.; Cameron, A.; Waterman, C. M.; Kehrl, J. H.; Hammer, J. A. A B-Cell Actomyosin Arc Network Couples Integrin Co-Stimulation to Mechanical Force-Dependent Immune Synapse Formation. *Elife* **2022**, *11*, No. e72805.
(156) Mogilner, A.; Rubinstein, B. The Physics of Filopodial Protrusion. *Biophys. J.* **2005**, *89*, 782−795.
(157) Claessens, M. M.; Bathe, M.; Frey, E.; Bausch, A. R. Actin-Binding Proteins Sensitively Mediate F-Actin Bundle Stiffness. *Nat. Mater.* **2006**, *5*, 748−753.
(158) Witte, H.; Bradke, F. The Role of the Cytoskeleton during Neuronal Polarization. *Curr. Opin. Neurobiol.* **2008**, *18*, 479−487.
(159) Dent, E. W.; Kwiatkowski, A. V.; Mebane, L. M.; Philippar, U.; Barzik, M.; Rubinson, D. A.; Gupton, S.; Van Veen, J. E.; Furman, C.; Zhang, J.; et al. Filopodia Are Required for Cortical Neurite Initiation. *Nat. Cell Biol.* **2007**, *9*, 1347−1359.
(160) Mattila, P. K.; Lappalainen, P. Filopodia: Molecular Architecture and Cellular Functions. *Nat. Rev. Mol. Cell Biol.* **2008**, *9*, 446−454.
(161) Bischoff, M. C.; Lieb, S.; Renkawitz-Pohl, R.; Bogdan, S. Filopodia-Based Contact Stimulation of Cell Migration Drives Tissue Morphogenesis. *Nat. Commun.* **2021**, *12*, 791.
(162) Sanders, T. A.; Llagostera, E.; Barna, M. Specialized Filopodia Direct Long-Range Transport of Shh during Vertebrate Tissue Patterning. *Nature* **2013**, *497*, 628−632.
(163) Chang, K.; Baginski, J.; Hassan, S. F.; Volin, M.; Shukla, D.; Tiwari, V. Filopodia and Viruses: An Analysis of Membrane Processes in Entry Mechanisms. *Frontiers in microbiology* **2016**, *7*, 300.
(164) Vignaud, T.; Copos, C.; Leterrier, C.; Toro-Nahuelpan, M.; Tseng, Q.; Mahamid, J.; Blanchoin, L.; Mogilner, A.; Théry, M.; Kurzawa, L. Stress Fibres Are Embedded in a Contractile Cortical Network. *Nat. Mater.* **2021**, *20*, 410−420.
(165) Zhang, R.; Alushin, G. M.; Brown, A.; Nogales, E. Mechanistic Origin of Microtubule Dynamic Instability and Its Modulation by Eb Proteins. *Cell* **2015**, *162*, 849−859.
(166) Gudimchuk, N. B.; Ulyanov, E. V.; O'Toole, E.; Page, C. L.; Vinogradov, D. S.; Morgan, G.; Li, G.; Moore, J. K.; Szczesna, E.; Roll-Mecak, A.; et al. Mechanisms of Microtubule Dynamics and Force Generation Examined with Computational Modeling and Electron Cryotomography. *Nat. Commun.* **2020**, *11*, 3765.
(167) Brangwynne, C. P.; MacKintosh, F. C.; Kumar, S.; Geisse, N. A.; Talbot, J.; Mahadevan, L.; Parker, K. K.; Ingber, D. E.; Weitz, D. A. Microtubules Can Bear Enhanced Compressive Loads in Living Cells Because of Lateral Reinforcement. *J. Cell Biol.* **2006**, *173*, 733−741.
(168) Gundersen, G. G.; Kreitzer, G.; Cook, T.; Liao, G. Microtubules as Determinants of Cellular Polarity. *Biological Bulletin* **1998**, *194*, 358−360.
(169) Parato, J.; Bartolini, F. The Microtubule Cytoskeleton at the Synapse. *Neurosci. Lett.* **2021**, *753*, 135850.
(170) Yu, W.; Baas, P. W. Changes in Microtubule Number and Length during Axon Differentiation. *J. Neurosci.* **1994**, *14*, 2818−2829.
(171) Zhang, H.; Zhang, K.; Li, M.; Shao, Y.; Feng, X.-Q. Force-Regulated State Transitions of Growing Axons. *Phys. Rev. Lett.* **2022**, *129*, 128101.
(172) Howard, J.; Hyman, A. A. Dynamics and Mechanics of the Microtubule Plus End. *Nature* **2003**, *422*, 753−758.
(173) Maurer, S. P.; Fourniol, F. J.; Bohner, G.; Moores, C. A.; Surrey, T. Ebs Recognize a Nucleotide-Dependent Structural Cap at Growing Microtubule Ends. *Cell* **2012**, *149*, 371−382.
(174) Mitchison, T.; Kirschner, M. Dynamic Instability of Microtubule Growth. *Nature* **1984**, *312*, 237.
(175) Kirschner, M.; Mitchison, T. Beyond Self-Assembly: From Microtubules to Morphogenesis. *Cell* **1986**, *45*, 329−342.
(176) Etienne-Manneville, S. Microtubules in Cell Migration. *Annu. Rev. Cell Dev. Biol.* **2013**, *29*, 471−499.
(177) Liao, G.; Nagasaki, T.; Gundersen, G. G. Low Concentrations of Nocodazole Interfere with Fibroblast Locomotion without Significantly Affecting Microtubule Level: Implications for the Role of Dynamic Microtubules in Cell Locomotion. *J. Cell Sci.* **1995**, *108*, 3473−3483.
(178) Gudimchuk, N. B.; McIntosh, J. R. Regulation of Microtubule Dynamics, Mechanics and Function through the Growing Tip. *Nat. Rev. Mol. Cell Biol.* **2021**, *22*, 777−795.
(179) Driver, J. W.; Geyer, E. A.; Bailey, M. E.; Rice, L. M.; Asbury, C. L. Direct Measurement of Conformational Strain Energy in Protofilaments Curling Outward from Disassembling Microtubule Tips. *Elife* **2017**, *6*, No. e28433.
(180) Igaev, M.; Grubmüller, H. Bending-Torsional Elasticity and Energetics of the Plus-End Microtubule Tip. *Proc. Natl. Acad. Sci. U. S. A.* **2022**, *119*, No. e2115516119.
(181) Manka, S. W.; Moores, C. A. The Role of Tubulin-Tubulin Lattice Contacts in the Mechanism of Microtubule Dynamic Instability. *Nat. Struct. Mol. Biol.* **2018**, *25*, 607−615.
(182) Omary, M. B.; Coulombe, P. A.; McLean, W. I. Intermediate Filament Proteins and Their Associated Diseases. *N. Engl. J. Med.* **2004**, *351*, 2087−2100.
(183) Duarte, S.; Viedma-Poyatos, Á.; Navarro-Carrasco, E.; Martínez, A. E.; Pajares, M. A.; Pérez-Sala, D. Vimentin Filaments Interact with the Actin Cortex in Mitosis Allowing Normal Cell Division. *Nat. Commun.* **2019**, *10*, 4200.
(184) Makarov, A. A.; Zou, J.; Houston, D. R.; Spanos, C.; Solovyova, A. S.; Cardenal-Peralta, C.; Rappsilber, J.; Schirmer, E. C. Lamin a Molecular Compression and Sliding as Mechanisms Behind Nucleoskeleton Elasticity. *Nat. Commun.* **2019**, *10*, 3056.
(185) Herrmann, H.; Aebi, U. Intermediate Filaments: Structure and Assembly. *Cold Spring Harb. Perspect. Biol.* **2016**, *8*, a018242.
(186) Pérez-Sala, D.; Oeste, C. L.; Martínez, A. E.; Carrasco, M. J.; Garzón, B.; Canada, F. J. Vimentin Filament Organization and Stress

https://doi.org/10.1021/acsnano.4c12599
ACS Nano 2024, 18, 29311−29336

Sensing Depend on Its Single Cysteine Residue and Zinc Binding. *Nat. Commun.* **2015**, *6*, 7287.
(187) Herrmann, H.; Bär, H.; Kreplak, L.; Strelkov, S. V.; Aebi, U. Intermediate Filaments: From Cell Architecture to Nanomechanics. *Nat. Rev. Mol. Cell Biol.* **2007**, *8*, 562−573.
(188) Guo, M.; Ehrlicher, A. J.; Mahammad, S.; Fabich, H.; Jensen, M. H.; Moore, J. R.; Fredberg, J. J.; Goldman, R. D.; Weitz, D. A. The Role of Vimentin Intermediate Filaments in Cortical and Cytoplasmic Mechanics. *Biophys. J.* **2013**, *105*, 1562−1568.
(189) Charrier, E. E.; Janmey, P. A. Mechanical Properties of Intermediate Filament Proteins. In *Methods in Enzymology*, Vol. *568*; Elsevier, 2016; pp 35−57.
(190) Hu, J.; Li, Y.; Hao, Y.; Zheng, T.; Gupta, S. K.; Parada, G. A.; Wu, H.; Lin, S.; Wang, S.; Zhao, X.; et al. High Stretchability, Strength, and Toughness of Living Cells Enabled by Hyperelastic Vimentin Intermediate Filaments. *Proc. Natl. Acad. Sci. U. S. A.* **2019**, *116*, 17175−17180.
(191) Bronshtein, I.; Kepten, E.; Kanter, I.; Berezin, S.; Lindner, M.; Redwood, A. B.; Mai, S.; Gonzalo, S.; Foisner, R.; Shav-Tal, Y.; et al. Loss of Lamin a Function Increases Chromatin Dynamics in the Nuclear Interior. *Nat. Commun.* **2015**, *6*, 8044.
(192) Chang, L.; Li, M.; Shao, S.; Li, C.; Ai, S.; Xue, B.; Hou, Y.; Zhang, Y.; Li, R.; Fan, X.; et al. Nuclear Peripheral Chromatin-Lamin B1 Interaction Is Required for Global Integrity of Chromatin Architecture and Dynamics in Human Cells. *Protein Cell* **2022**, *13*, 258−280.
(193) Xie, W.; Chojnowski, A.; Boudier, T.; Lim, J. S.; Ahmed, S.; Ser, Z.; Stewart, C.; Burke, B. A-Type Lamins Form Distinct Filamentous Networks with Differential Nuclear Pore Complex Associations. *Curr. Biol.* **2016**, *26*, 2651−2658.
(194) Truong Quang, B. A.; Peters, R.; Cassani, D. A.; Chugh, P.; Clark, A. G.; Agnew, M.; Charras, G.; Paluch, E. K. Extent of Myosin Penetration within the Actin Cortex Regulates Cell Surface Mechanics. *Nat. Commun.* **2021**, *12*, 6511.
(195) Shutova, M. S.; Spessott, W. A.; Giraudo, C. G.; Svitkina, T. Endogenous Species of Mammalian Nonmuscle Myosin Iia and Iib Include Activated Monomers and Heteropolymers. *Curr. Biol.* **2014**, *24*, 1958−1968.
(196) Burridge, K.; Guilluy, C. Focal Adhesions, Stress Fibers and Mechanical Tension. *Exp. Cell Res.* **2016**, *343*, 14−20.
(197) Livne, A.; Geiger, B. The Inner Workings of Stress Fibers-from Contractile Machinery to Focal Adhesions and Back. *J. Cell Sci.* **2016**, *129*, 1293−1304.
(198) Kittisopikul, M.; Shimi, T.; Tatli, M.; Tran, J. R.; Zheng, Y.; Medalia, O.; Jaqaman, K.; Adam, S. A.; Goldman, R. D. Computational Analyses Reveal Spatial Relationships between Nuclear Pore Complexes and Specific Lamins. *J. Cell Biol.* **2021**, *220*, No. e202007082.
(199) Briand, N.; Collas, P. Lamina-Associated Domains: Peripheral Matters and Internal Affairs. *Genome Biol.* **2020**, *21*, 85.
(200) Ulianov, S. V.; Doronin, S. A.; Khrameeva, E. E.; Kos, P. I.; Luzhin, A. V.; Starikov, S. S.; Galitsyna, A. A.; Nenasheva, V. V.; Ilyin, A. A.; Flyamer, I. M.; et al. Nuclear Lamina Integrity Is Required for Proper Spatial Organization of Chromatin in Drosophila. *Nat. Commun.* **2019**, *10*, 1176.
(201) Shah, P. P.; Lv, W.; Rhoades, J. H.; Poleshko, A.; Abbey, D.; Caporizzo, M. A.; Linares-Saldana, R.; Heffler, J. G.; Sayed, N.; Thomas, D.; et al. Pathogenic Lmna Variants Disrupt Cardiac Lamina-Chromatin Interactions and De-Repress Alternative Fate Genes. *Cell Stem Cell* **2021**, *28*, 938−954.
(202) Flanagan, L. A.; Chou, J.; Falet, H.; Neujahr, R.; Hartwig, J. H.; Stossel, T. P. Filamin a, the Arp2/3 Complex, and the Morphology and Function of Cortical Actin Filaments in Human Melanoma Cells. *J. Cell Biol.* **2001**, *155*, 511−518.
(203) Svitkina, T. M.; Borisy, G. G. Arp2/3 Complex and Actin Depolymerizing Factor/Cofilin in Dendritic Organization and Treadmilling of Actin Filament Array in Lamellipodia. *J. Cell Biol.* **1999**, *145*, 1009−1026.
(204) Leithner, A.; Altenburger, L. M.; Hauschild, R.; Assen, F. P.; Rottner, K.; Stradal, T. E.; Diz-Muñoz, A.; Stein, J. V.; Sixt, M. Dendritic Cell Actin Dynamics Control Contact Duration and Priming Efficiency at the Immunological Synapse. *J. Cell Biol.* **2021**, *220*, No. e202006081.
(205) Billadeau, D. D.; Nolz, J. C.; Gomez, T. S. Regulation of T-Cell Activation by the Cytoskeleton. *Nat. Rev. Immunol.* **2007**, *7*, 131−143.
(206) Wegner, A. M.; Nebhan, C. A.; Hu, L.; Majumdar, D.; Meier, K. M.; Weaver, A. M.; Webb, D. J. N-Wasp and the Arp2/3 Complex Are Critical Regulators of Actin in the Development of Dendritic Spines and Synapses. *J. Biol. Chem.* **2008**, *283*, 15912−15920.
(207) Rocca, D. L.; Amici, M.; Antoniou, A.; Suarez, E. B.; Halemani, N.; Murk, K.; McGarvey, J.; Jaafari, N.; Mellor, J. R.; Collingridge, G. L.; et al. The Small Gtpase Arf1Modulates Arp2/3-Mediated Actin Polymerization Via Pick1 to Regulate Synaptic Plasticity. *Neuron* **2013**, *79*, 293−307.
(208) Lamm, N.; Read, M. N.; Nobis, M.; Van Ly, D.; Page, S. G.; Masamsetti, V. P.; Timpson, P.; Biro, M.; Cesare, A. J. Nuclear F-Actin Counteracts Nuclear Deformation and Promotes Fork Repair during Replication Stress. *Nat. Cell Biol.* **2020**, *22*, 1460−1470.
(209) Caridi, C. P.; Plessner, M.; Grosse, R.; Chiolo, I. Nuclear Actin Filaments in DNA Repair Dynamics. *Nat. Cell Biol.* **2019**, *21*, 1068−1077.
(210) Schrank, B. R.; Aparicio, T.; Li, Y.; Chang, W.; Chait, B. T.; Gundersen, G. G.; Gottesman, M. E.; Gautier, J. Nuclear Arp2/3 Drives DNA Break Clustering for Homology-Directed Repair. *Nature* **2018**, *559*, 61−66.
(211) Thiam, H.-R.; Vargas, P.; Carpi, N.; Crespo, C. L.; Raab, M.; Terriac, E.; King, M. C.; Jacobelli, J.; Alberts, A. S.; Stradal, T.; et al. Perinuclear Arp2/3-Driven Actin Polymerization Enables Nuclear Deformation to Facilitate Cell Migration through Complex Environments. *Nat. Commun.* **2016**, *7*, 10997.
(212) Feld, L.; Kellerman, L.; Mukherjee, A.; Livne, A.; Bouchbinder, E.; Wolfenson, H. Cellular Contractile Forces Are Nonmechanosensitive. *Science advances* **2020**, *6*, No. eaaz6997.
(213) Parsons, J. T.; Horwitz, A. R.; Schwartz, M. A. Cell Adhesion: Integrating Cytoskeletal Dynamics and Cellular Tension. *Nat. Rev. Mol. Cell Biol.* **2010**, *11*, 633−643.
(214) Svitkina, T. M.; Bulanova, E. A.; Chaga, O. Y.; Vignjevic, D. M.; Kojima, S.-i.; Vasiliev, J. M.; Borisy, G. G. Mechanism of Filopodia Initiation by Reorganization of a Dendritic Network. *J. Cell Biol.* **2003**, *160*, 409−421.
(215) Vignjevic, D.; Kojima, S.-i.; Aratyn, Y.; Danciu, O.; Svitkina, T.; Borisy, G. G. Role of Fascin in Filopodial Protrusion. *J. Cell Biol.* **2006**, *174*, 863−875.
(216) Walcott, S.; Sun, S. X. A Mechanical Model of Actin Stress Fiber Formation and Substrate Elasticity Sensing in Adherent Cells. *Proc. Natl. Acad. Sci. U. S. A.* **2010**, *107*, 7757−7762.
(217) Cheffings, T. H.; Burroughs, N. J.; Balasubramanian, M. K. Actomyosin Ring Formation and Tension Generation in Eukaryotic Cytokinesis. *Curr. Biol.* **2016**, *26*, R719−R737.
(218) Dogterom, M.; Koenderink, G. H. Actin-Microtubule Crosstalk in Cell Biology. *Nat. Rev. Mol. Cell Biol.* **2019**, *20*, 38−54.
(219) Ventura, G.; Amiri, A.; Thiagarajan, R.; Tolonen, M.; Doostmohammadi, A.; Sedzinski, J. Multiciliated Cells Use Filopodia to Probe Tissue Mechanics during Epithelial Integration in Vivo. *Nat. Commun.* **2022**, *13*, 6423.
(220) Cabrales Fontela, Y.; Kadavath, H.; Biernat, J.; Riedel, D.; Mandelkow, E.; Zweckstetter, M. Multivalent Cross-Linking of Actin Filaments and Microtubules through the Microtubule-Associated Protein Tau. *Nat. Commun.* **2017**, *8*, 1981.
(221) Barisic, M.; Silva e Sousa, R.; Tripathy, S. K.; Magiera, M. M.; Zaytsev, A. V.; Pereira, A. L.; Janke, C.; Grishchuk, E. L.; Maiato, H. Microtubule Detyrosination Guides Chromosomes during Mitosis. *Science* **2015**, *348*, 799−803.
(222) Sawin, K. E.; LeGuellec, K.; Philippe, M.; Mitchison, T. J. Mitotic Spindle Organization by a Plus-End-Directed Microtubule Motor. *Nature* **1992**, *359*, 540−543.

https://doi.org/10.1021/acsnano.4c12599
ACS Nano 2024, 18, 29311−29336

(223) Atkins, M.; Nicol, X.; Fassier, C. Microtubule Remodelling as a Driving Force of Axon Guidance and Pruning. In *Seminars in Cell & Developmental Biology*, 2023; Elsevier, Vol. *140*, pp 35−53.
(224) Leterrier, C.; Dubey, P.; Roy, S. The Nano-Architecture of the Axonal Cytoskeleton. *Nat. Rev. Neurosci.* **2017**, *18*, 713−726.
(225) Chesarone, M. A.; DuPage, A. G.; Goode, B. L. Unleashing Formins to Remodel the Actin and Microtubule Cytoskeletons. *Nat. Rev. Mol. Cell Biol.* **2010**, *11*, 62−74.
(226) Jolly, A. L.; Kim, H.; Srinivasan, D.; Lakonishok, M.; Larson, A. G.; Gelfand, V. I. Kinesin-1 Heavy Chain Mediates Microtubule Sliding to Drive Changes in Cell Shape. *Proc. Natl. Acad. Sci. U. S. A.* **2010**, *107*, 12151−12156.
(227) Zhao, T.; Graham, O. S.; Raposo, A.; St Johnston, D. Growing Microtubules Push the Oocyte Nucleus to Polarize the Drosophila Dorsal-Ventral Axis. *Science* **2012**, *336*, 999−1003.
(228) Christophorou, N.; Rubin, T.; Bonnet, I.; Piolot, T.; Arnaud, M.; Huynh, J.-R. Microtubule-Driven Nuclear Rotations Promote Meiotic Chromosome Dynamics. *Nat. Cell Biol.* **2015**, *17*, 1388−1400.
(229) Caviston, J. P.; Holzbaur, E. L. Microtubule Motors at the Intersection of Trafficking and Transport. *Trends Cell Biol.* **2006**, *16*, 530−537.
(230) Steinert, P. M.; Marekov, L. N. The Proteins Elafin, Filaggrin, Keratin Intermediate Filaments, Loricrin, and Small Proline-Rich Proteins 1 and 2 Are Isodipeptide Cross-Linked Components of the Human Epidermal Cornified Cell Envelope (*). *J. Biol. Chem.* **1995**, *270*, 17702−17711.
(231) Liao, G.; Gundersen, G. G. Kinesin Is a Candidate for Cross-Bridging Microtubules and Intermediate Filaments: Selective Binding of Kinesin to Detyrosinated Tubulin and Vimentin. *J. Biol. Chem.* **1998**, *273*, 9797−9803.
(232) Kreitzer, G.; Liao, G.; Gundersen, G. G. Detyrosination of Tubulin Regulates the Interaction of Intermediate Filaments with Microtubules in Vivo Via a Kinesin-Dependent Mechanism. *Mol. Biol. Cell* **1999**, *10*, 1105−1118.
(233) Svitkina, T. M.; Verkhovsky, A. B.; Borisy, G. G. Plectin Sidearms Mediate Interaction of Intermediate Filaments with Microtubules and Other Components of the Cytoskeleton. *J. Cell Biol.* **1996**, *135*, 991−1007.
(234) Burke, B.; Stewart, C. L. The Nuclear Lamins: Flexibility in Function. *Nat. Rev. Mol. Cell Biol.* **2013**, *14*, 13−24.
(235) de Leeuw, R.; Gruenbaum, Y.; Medalia, O. Nuclear Lamins: Thin Filaments with Major Functions. *Trends Cell Biol.* **2018**, *28*, 34−45.
(236) Zullo, J. M.; Demarco, I. A.; Piqué-Regi, R.; Gaffney, D. J.; Epstein, C. B.; Spooner, C. J.; Luperchio, T. R.; Bernstein, B. E.; Pritchard, J. K.; Reddy, K. L.; et al. DNA Sequence-Dependent Compartmentalization and Silencing of Chromatin at the Nuclear Lamina. *Cell* **2012**, *149*, 1474−1487.
(237) Guo, M.; Ehrlicher, A. J.; Jensen, M. H.; Renz, M.; Moore, J. R.; Goldman, R. D.; Lippincott-Schwartz, J.; Mackintosh, F. C.; Weitz, D. A. Probing the Stochastic, Motor-Driven Properties of the Cytoplasm Using Force Spectrum Microscopy. *Cell* **2014**, *158*, 822−832.
(238) Hannezo, E.; Heisenberg, C.-P. Mechanochemical Feedback Loops in Development and Disease. *Cell* **2019**, *178*, 12−25.
(239) Fuchs, E.; Cleveland, D. W. A Structural Scaffolding of Intermediate Filaments in Health and Disease. *Science* **1998**, *279*, 514−519.
(240) Kelley, L. C.; Chi, Q.; Cáceres, R.; Hastie, E.; Schindler, A. J.; Jiang, Y.; Matus, D. Q.; Plastino, J.; Sherwood, D. R. Adaptive F-Actin Polymerization and Localized Atp Production Drive Basement Membrane Invasion in the Absence of Mmps. *Dev. Cell* **2019**, *48*, 313−328.
(241) Chan, C. E.; Odde, D. J. Traction Dynamics of Filopodia on Compliant Substrates. *Science* **2008**, *322*, 1687−1691.
(242) Adebowale, K.; Gong, Z.; Hou, J. C.; Wisdom, K. M.; Garbett, D.; Lee, H.-p.; Nam, S.; Meyer, T.; Odde, D. J.; Shenoy, V. B.; et al. Enhanced Substrate Stress Relaxation Promotes Filopodia-Mediated Cell Migration. *Nat. Mater.* **2021**, *20*, 1290−1299.
(243) Kim, M.-C.; Silberberg, Y. R.; Abeyaratne, R.; Kamm, R. D.; Asada, H. H. Computational Modeling of Three-Dimensional Ecm-Rigidity Sensing to Guide Directed Cell Migration. *Proc. Natl. Acad. Sci. U. S. A.* **2018**, *115*, E390−E399.
(244) Bornschlögl, T.; Romero, S.; Vestergaard, C. L.; Joanny, J.-F.; Van Nhieu, G. T.; Bassereau, P. Filopodial Retraction Force Is Generated by Cortical Actin Dynamics and Controlled by Reversible Tethering at the Tip. *Proc. Natl. Acad. Sci. U. S. A.* **2013**, *110*, 18928−18933.
(245) Deng, L.; Trepat, X.; Butler, J. P.; Millet, E.; Morgan, K. G.; Weitz, D. A.; Fredberg, J. J. Fast and Slow Dynamics of the Cytoskeleton. *Nat. Mater.* **2006**, *5*, 636−640.
(246) Wei, X.; Fang, C.; Gong, B.; Yao, J.; Qian, J.; Lin, Y. Viscoelasticity of 3d Actin Networks Dictated by the Mechanochemical Characteristics of Cross-Linkers. *Soft Matter* **2021**, *17*, 10177−10185.
(247) Wei, X.; Fang, C.; Gong, B.; Shao, X.; Sun, F.; Qian, J.; Lin, Y. Time-Dependent Response of Bio-Polymer Networks Regulated by Catch and Slip Bond-Like Kinetics of Cross-Linkers. *Journal of the Mechanics and Physics of Solids* **2021**, *147*, 104267.
(248) Lieleg, O.; Kayser, J.; Brambilla, G.; Cipelletti, L.; Bausch, A. R. Slow Dynamics and Internal Stress Relaxation in Bundled Cytoskeletal Networks. *Nat. Mater.* **2011**, *10*, 236−242.
(249) Cocucci, E.; Aguet, F.; Boulant, S.; Kirchhausen, T. The First Five Seconds in the Life of a Clathrin-Coated Pit. *Cell* **2012**, *150*, 495−507.
(250) Cheng, X.; Chen, K.; Dong, B.; Yang, M.; Filbrun, S. L.; Myoung, Y.; Huang, T.-X.; Gu, Y.; Wang, G.; Fang, N. Dynamin-Dependent Vesicle Twist at the Final Stage of Clathrin-Mediated Endocytosis. *Nat. Cell Biol.* **2021**, *23*, 859−869.
(251) Bucher, D.; Frey, F.; Sochacki, K. A.; Kummer, S.; Bergeest, J.-P.; Godinez, W. J.; Kräusslich, H.-G.; Rohr, K.; Taraska, J. W.; Schwarz, U. S.; et al. Clathrin-Adaptor Ratio and Membrane Tension Regulate the Flat-to-Curved Transition of the Clathrin Coat during Endocytosis. *Nat. Commun.* **2018**, *9*, 1109.
(252) Hatit, M. Z. C.; Dobrowolski, C. N.; Lokugamage, M. P.; Loughrey, D.; Ni, H.; Zurla, C.; Da Silva Sanchez, A. J.; Radmand, A.; Huayamares, S. G.; Zenhausern, R.; Paunovska, K.; Peck, H. E.; Kim, J.; Sato, M.; Feldman, J. I.; Rivera, M.-A.; Cristian, A.; Kim, Y.; Santangelo, P. J.; Dahlman, J. E. Nanoparticle Stereochemistry-Dependent Endocytic Processing Improves in Vivo Mrna Delivery. *Nat. Chem.* **2023**, *15*, 508−515.
(253) Mitchell, M. J.; Billingsley, M. M.; Haley, R. M.; Wechsler, M. E.; Peppas, N. A.; Langer, R. Engineering Precision Nanoparticles for Drug Delivery. *Nat. Rev. Drug Discovery* **2021**, *20*, 101−124.
(254) Hou, X.; Zaks, T.; Langer, R.; Dong, Y. Lipid Nanoparticles for Mrna Delivery. *Nature Reviews Materials* **2021**, *6*, 1078−1094.
(255) Riley, R. S.; June, C. H.; Langer, R.; Mitchell, M. J. Delivery Technologies for Cancer Immunotherapy. *Nat. Rev. Drug Discovery* **2019**, *18*, 175−196.
(256) Zhang, S.; Gao, H.; Bao, G. Physical Principles of Nanoparticle Cellular Endocytosis. *ACS Nano* **2015**, *9*, 8655−8671.
(257) Hui, Y.; Yi, X.; Hou, F.; Wibowo, D.; Zhang, F.; Zhao, D.; Gao, H.; Zhao, C.-X. Role of Nanoparticle Mechanical Properties in Cancer Drug Delivery. *ACS Nano* **2019**, *13*, 7410−7424.
(258) Shen, Z.; Ye, H.; Yi, X.; Li, Y. Membrane Wrapping Efficiency of Elastic Nanoparticles during Endocytosis: Size and Shape Matter. *ACS Nano* **2019**, *13*, 215−228.
(259) Walani, N.; Torres, J.; Agrawal, A. Endocytic Proteins Drive Vesicle Growth Via Instability in High Membrane Tension Environment. *Proc. Natl. Acad. Sci. U. S. A.* **2015**, *112*, E1423−E1432.
(260) Gao, H.; Shi, W.; Freund, L. B. Mechanics of Receptor-Mediated Endocytosis. *Proc. Natl. Acad. Sci. U. S. A.* **2005**, *102*, 9469−9474.
(261) Yi, X.; Shi, X.; Gao, H. Cellular Uptake of Elastic Nanoparticles. *Phys. Rev. Lett.* **2011**, *107*, 098101.

https://doi.org/10.1021/acsnano.4c12599
ACS Nano 2024, 18, 29311−29336

(262) Rafiq, N. B. M.; Nishimura, Y.; Plotnikov, S. V.; Thiagarajan, V.; Zhang, Z.; Shi, S.; Natarajan, M.; Viasnoff, V.; Kanchanawong, P.; Jones, G. E.; et al. A Mechano-Signalling Network Linking Microtubules, Myosin Iia Filaments and Integrin-Based Adhesions. *Nat. Mater.* **2019**, *18*, 638−649.
(263) Fritsch, A.; Höckel, M.; Kiessling, T.; Nnetu, K. D.; Wetzel, F.; Zink, M.; Käs, J. A. Are Biomechanical Changes Necessary for Tumour Progression? *Nat. Phys.* **2010**, *6*, 730−732.
(264) Isomursu, A.; Park, K.-Y.; Hou, J.; Cheng, B.; Mathieu, M.; Shamsan, G. A.; Fuller, B.; Kasim, J.; Mahmoodi, M. M.; Lu, T. J.; et al. Directed Cell Migration Towards Softer Environments. *Nat. Mater.* **2022**, *21*, 1081−1090.
(265) Chaudhuri, O.; Cooper-White, J.; Janmey, P. A.; Mooney, D. J.; Shenoy, V. B. Effects of Extracellular Matrix Viscoelasticity on Cellular Behaviour. *Nature* **2020**, *584*, 535−546.
(266) Gong, Z.; Szczesny, S. E.; Caliari, S. R.; Charrier, E. E.; Chaudhuri, O.; Cao, X.; Lin, Y.; Mauck, R. L.; Janmey, P. A.; Burdick, J. A.; et al. Matching Material and Cellular Timescales Maximizes Cell Spreading on Viscoelastic Substrates. *Proc. Natl. Acad. Sci. U. S. A.* **2018**, *115*, E2686−E2695.
(267) Bangasser, B. L.; Shamsan, G. A.; Chan, C. E.; Opoku, K. N.; Tüzel, E.; Schlichtmann, B. W.; Kasim, J. A.; Fuller, B. J.; McCullough, B. R.; Rosenfeld, S. S.; et al. Shifting the Optimal Stiffness for Cell Migration. *Nat. Commun.* **2017**, *8*, 15313.
(268) Bonnans, C.; Chou, J.; Werb, Z. Remodelling the Extracellular Matrix in Development and Disease. *Nat. Rev. Mol. Cell Biol.* **2014**, *15*, 786−801.
(269) Elosegui-Artola, A.; Gupta, A.; Najibi, A. J.; Seo, B. R.; Garry, R.; Tringides, C. M.; de Lázaro, I.; Darnell, M.; Gu, W.; Zhou, Q.; et al. Matrix Viscoelasticity Controls Spatiotemporal Tissue Organization. *Nat. Mater.* **2023**, *22*, 117−127.
(270) Ingber, D. E.; Wang, N.; Stamenović, D. Tensegrity, Cellular Biophysics, and the Mechanics of Living Systems. *Rep. Prog. Phys.* **2014**, *77*, 046603.
(271) Wang, N.; Naruse, K.; Stamenović, D.; Fredberg, J. J.; Mijailovich, S. M.; Tolić-Nørrelykke, I. M.; Polte, T.; Mannix, R.; Ingber, D. E. Mechanical Behavior in Living Cells Consistent with the Tensegrity Model. *Proc. Natl. Acad. Sci. U. S. A.* **2001**, *98*, 7765−7770.
(272) Sun, S.-Y.; Zhang, L.-Y.; Chen, X.; Feng, X.-Q. Biochemo-mechanical Tensegrity Model of Cytoskeletons. *Journal of the Mechanics and Physics of Solids* **2023**, *175*, 105288.
(273) Holmes, D. F.; Yeung, C.-Y. C.; Garva, R.; Zindy, E.; Taylor, S. H.; Lu, Y.; Watson, S.; Kalson, N. S.; Kadler, K. E. Synchronized Mechanical Oscillations at the Cell-Matrix Interface in the Formation of Tensile Tissue. *Proc. Natl. Acad. Sci. U. S. A.* **2018**, *115*, No. E9288.
(274) Yin, S.; Li, B.; Feng, X.-Q. Three-Dimensional Chiral Morphodynamics of Chemomechanical Active Shells. *Proc. Natl. Acad. Sci. U. S. A.* **2022**, *119*, No. e2206159119.
(275) Rozman, J.; Krajnc, M.; Ziherl, P. Collective Cell Mechanics of Epithelial Shells with Organoid-Like Morphologies. *Nat. Commun.* **2020**, *11*, 3805.
(276) Tang, W.; Das, A.; Pegoraro, A. F.; Han, Y. L.; Huang, J.; Roberts, D. A.; Yang, H.; Fredberg, J. J.; Kotton, D. N.; Bi, D.; et al. Collective Curvature Sensing and Fluidity in Three-Dimensional Multicellular Systems. *Nat. Phys.* **2022**, *18*, 1371−1378.
(277) Farhadifar, R.; Röper, J.-C.; Aigouy, B.; Eaton, S.; Jülicher, F. The Influence of Cell Mechanics, Cell-Cell Interactions, and Proliferation on Epithelial Packing. *Curr. Biol.* **2007**, *17*, 2095−2104.
(278) Lin, S.-Z.; Li, B.; Lan, G.; Feng, X.-Q. Activation and Synchronization of the Oscillatory Morphodynamics in Multicellular Monolayer. *Proc. Natl. Acad. Sci. U. S. A.* **2017**, *114*, 8157−8162.
(279) Chen, Y.; Gao, Q.; Li, J.; Mao, F.; Tang, R.; Jiang, H. Activation of Topological Defects Induces a Brittle-to-Ductile Transition in Epithelial Monolayers. *Phys. Rev. Lett.* **2022**, *128*, 018101.
(280) Pinheiro, D.; Hannezo, E.; Herszterg, S.; Bosveld, F.; Gaugue, I.; Balakireva, M.; Wang, Z.; Cristo, I.; Rigaud, S. U.; Markova, O.; et al. Transmission of Cytokinesis Forces Via E-Cadherin Dilution and Actomyosin Flows. *Nature* **2017**, *545*, 103−107.
(281) Lin, S.-Z.; Li, Y.; Ji, J.; Li, B.; Feng, X.-Q. Collective Dynamics of Coherent Motile Cells on Curved Surfaces. *Soft Matter* **2020**, *16*, 2941−2952.
(282) Luciano, M.; Xue, S.-L.; De Vos, W. H.; Redondo-Morata, L.; Surin, M.; Lafont, F.; Hannezo, E.; Gabriele, S. Cell Monolayers Sense Curvature by Exploiting Active Mechanics and Nuclear Mechanoa-daptation. *Nat. Phys.* **2021**, *17*, 1382−1390.
(283) Fang, C.; Shao, X.; Tian, Y.; Chu, Z.; Lin, Y. Size-Dependent Response of Cells in Epithelial Tissue Modulated by Contractile Stress Fibers. *Biophys. J.* **2023**, *122*, 1315−1324.
(284) López-Gay, J. M.; Nunley, H.; Spencer, M.; Di Pietro, F.; Guirao, B.; Bosveld, F.; Markova, O.; Gaugue, I.; Pelletier, S.; Lubensky, D. K.; et al. Apical Stress Fibers Enable a Scaling between Cell Mechanical Response and Area in Epithelial Tissue. *Science* **2020**, *370*, No. eabb2169.
(285) Devany, J.; Sussman, D. M.; Yamamoto, T.; Manning, M. L.; Gardel, M. L. Cell Cycle-Dependent Active Stress Drives Epithelia Remodeling. *Proc. Natl. Acad. Sci. U. S. A.* **2021**, *118*, No. e1917853118.
(286) Wang, X.; Merkel, M.; Sutter, L. B.; Erdemci-Tandogan, G.; Manning, M. L.; Kasza, K. E. Anisotropy Links Cell Shapes to Tissue Flow during Convergent Extension. *Proc. Natl. Acad. Sci. U. S. A.* **2020**, *117*, 13541−13551.
(287) Hang, J.-T.; Xu, G.-K.; Gao, H. Frequency-Dependent Transition in Power-Law Rheological Behavior of Living Cells. *Science Advances* **2022**, *8*, No. eabn6093.
(288) Hang, J.-T.; Kang, Y.; Xu, G.-K.; Gao, H. A Hierarchical Cellular Structural Model to Unravel the Universal Power-Law Rheological Behavior of Living Cells. *Nat. Commun.* **2021**, *12*, 6067.
(289) Mullard, A. 2020 Fda Drug Approvals. *Nat. Rev. Drug Discovery* **2021**, *20*, 85−91.
(290) Schuhmacher, A.; Hinder, M.; Boger, N.; Hartl, D.; Gassmann, O. The Significance of Blockbusters in the Pharmaceutical Industry. *Nat. Rev. Drug Discovery* **2023**, *22*, 177−178.
(291) Kreitz, J.; Friedrich, M. J.; Guru, A.; Lash, B.; Saito, M.; Macrae, R. K.; Zhang, F. Programmable Protein Delivery with a Bacterial Contractile Injection System. *Nature* **2023**, *616*, 357−364.
(292) Madani, A.; Krause, B.; Greene, E. R.; Subramanian, S.; Mohr, B. P.; Holton, J. M.; Olmos, J. L.; Xiong, C.; Sun, Z. Z.; Socher, R.; Fraser, J. S.; Naik, N. Large Language Models Generate Functional Protein Sequences across Diverse Families. *Nat. Biotechnol.* **2023**, *41*, 1099−1106.
(293) Lu, H.; Zhou, Q.; He, J.; Jiang, Z.; Peng, C.; Tong, R.; Shi, J. Recent Advances in the Development of Protein-Protein Interactions Modulators: Mechanisms and Clinical Trials. *Signal transduction and targeted therapy* **2020**, *5*, 213.
(294) Case, D. A.; Aktulga, H. M.; Belfon, K.; Ben-Shalom, I.; Brozell, S. R.; Cerutti, D. S.; Cheatham, I. I. I.; T, E.; Cruzeiro, V. W. D.; Darden, T. A.; Duke, R. E. *Amber 2021*; University of California, San Francisco, 2021.
(295) Conibear, A. C. Deciphering Protein Post-Translational Modifications Using Chemical Biology Tools. *Nature Reviews Chemistry* **2020**, *4*, 674−695.
(296) Ramazi, S.; Zahiri, J. Post-Translational Modifications in Proteins: Resources, Tools and Prediction Methods. *Database* **2021**, *2021*, baab012.
(297) Bedford, M. T.; Richard, S. Arginine Methylation: An Emerging Regulatorof Protein Function. *Mol. Cell* **2005**, *18*, 263−272.
(298) Balchin, D.; Hayer-Hartl, M.; Hartl, F. U. In Vivo Aspects of Protein Folding and Quality Control. *Science* **2016**, *353*, aac4354.
(299) Jumper, J.; Evans, R.; Pritzel, A.; Green, T.; Figurnov, M.; Ronneberger, O.; Tunyasuvunakool, K.; Bates, R.; Žídek, A.; Potapenko, A.; et al. Highly Accurate Protein Structure Prediction with Alphafold. *Nature* **2021**, *596*, 583−589.
(300) Baek, M.; DiMaio, F.; Anishchenko, I.; Dauparas, J.; Ovchinnikov, S.; Lee, G. R.; Wang, J.; Cong, Q.; Kinch, L. N.; Schaeffer, R. D.; et al. Accurate Prediction of Protein Structures and Interactions Using a Three-Track Neural Network. *Science* **2021**, *373*, 871−876.

https://doi.org/10.1021/acsnano.4c12599
ACS Nano 2024, 18, 29311−29336

(301) Mirdita, M.; Schütze, K.; Moriwaki, Y.; Heo, L.; Ovchinnikov, S.; Steinegger, M. Colabfold: Making Protein Folding Accessible to All. *Nat. Methods* **2022**, *19*, 679−682.
(302) Nguyen, H.; Maier, J.; Huang, H.; Perrone, V.; Simmerling, C. Folding Simulations for Proteins with Diverse Topologies Are Accessible in Days with a Physics-Based Force Field and Implicit Solvent. *J. Am. Chem. Soc.* **2014**, *136*, 13959−13962.
(303) Insco, M. L.; Abraham, B. J.; Dubbury, S. J.; Kaltheuner, I. H.; Dust, S.; Wu, C.; Chen, K. Y.; Liu, D.; Bellaousov, S.; Cox, A. M.; et al. Oncogenic Cdk13 Mutations Impede Nuclear Rna Surveillance. *Science* **2023**, *380*, No. eabn7625.
(304) Guarnera, E.; Berezovsky, I. N. Allosteric Drugs and Mutations: Chances, Challenges, and Necessity. *Curr. Opin. Struct. Biol.* **2020**, *62*, 149−157.
(305) Doudna, J. A. The Promise and Challenge of Therapeutic Genome Editing. *Nature* **2020**, *578*, 229−236.
(306) Allen, A. G.; Khan, S. Q.; Margulies, C. M.; Viswanathan, R.; Lele, S.; Blaha, L.; Scott, S. N.; Izzo, K. M.; Gerew, A.; Pattali, R.; Cochran, N. R.; Holland, C. S.; Zhao, A. H.; Sherman, S. E.; Jaskolka, M. C.; Wu, M.; Wilson, A. C.; Sun, X.; Ciulla, D. M.; Zhang, D.; et al. A Highly Efficient Transgene Knock-in Technology in Clinically Relevant Cell Types. *Nat. Biotechnol.* **2023**, 458−469.
(307) Abramson, J.; Adler, J.; Dunger, J.; Evans, R.; Green, T.; Pritzel, A.; Ronneberger, O.; Willmore, L.; Ballard, A. J.; Bambrick, J.; Bodenstein, S. W.; Evans, D. A.; Hung, C.-C.; O'Neill, M.; Reiman, D.; Tunyasuvunakool, K.; Wu, Z.; Žemgulytė, A.; Arvaniti, E.; Beattie, C.; et al. Accurate Structure Prediction of Biomolecular Interactions with Alphafold 3. *Nature* **2024**, *630*, 493−500.
(308) Tsaban, T.; Varga, J. K.; Avraham, O.; Ben-Aharon, Z.; Khramushin, A.; Schueler-Furman, O. Harnessing Protein Folding Neural Networks for Peptide-Protein Docking. *Nat. Commun.* **2022**, *13*, 176.
(309) Evans, R.; O'Neill, M.; Pritzel, A.; Antropova, N.; Senior, A.; Green, T.; Žídek, A.; Bates, R.; Blackwell, S.; Yim, J. Protein complex prediction with AlphaFold-Multimer. *BioRxiv* **2021**, 2021.10.04.463034.
(310) Fang, X.; Wang, F.; Liu, L.; He, J.; Lin, D.; Xiang, Y.; Zhu, K.; Zhang, X.; Wu, H.; Li, H.; Song, L. A Method for Multiple-Sequence-Alignment-Free Protein Structure Prediction Using a Protein Language Model. *Nature Machine Intelligence* **2023**, *5*, 1087−1096.
(311) Wang, J. Y.; Doudna, J. A. Crispr Technology: A Decade of Genome Editing Is Only the Beginning. *Science* **2023**, *379*, No. eadd8643.
(312) Stenson, P. D.; Mort, M.; Ball, E. V.; Chapman, M.; Evans, K.; Azevedo, L.; Hayden, M.; Heywood, S.; Millar, D. S.; Phillips, A. D.; et al. The Human Gene Mutation Database (Hgmd®): Optimizing Its Use in a Clinical Diagnostic or Research Setting. *Hum. Genet.* **2020**, *139*, 1197−1207.
(313) Haradhvala, N. J.; Leick, M. B.; Maurer, K.; Gohil, S. H.; Larson, R. C.; Yao, N.; Gallagher, K. M.; Katsis, K.; Frigault, M. J.; Southard, J.; et al. Distinct Cellular Dynamics Associated with Response to Car-T Therapy for Refractory B Cell Lymphoma. *Nat. Med.* **2022**, *28*, 1848−1859.
(314) Guo, A.; Huang, H.; Zhu, Z.; Chen, M. J.; Shi, H.; Yuan, S.; Sharma, P.; Connelly, J. P.; Liedmann, S.; Dhungana, Y.; et al. Cbaf Complex Components and Myc Cooperate Early in Cd8+ T Cell Fate. *Nature* **2022**, *607*, 135−141.
(315) Larson, R. C.; Kann, M. C.; Bailey, S. R.; Haradhvala, N. J.; Llopis, P. M.; Bouffard, A. A.; Scarfó, I.; Leick, M. B.; Grauwet, K.; Berger, T. R.; et al. Car T Cell Killing Requires the Ifnγr Pathway in Solid but Not Liquid Tumours. *Nature* **2022**, *604*, 563−570.
(316) Jo, S.; Das, S.; Williams, A.; Chretien, A.-S.; Pagliardini, T.; Le Roy, A.; Fernandez, J. P.; Le Clerre, D.; Jahangiri, B.; Chion-Sotinel, I.; et al. Endowing Universal Car T-Cell with Immune-Evasive Properties Using Talen-Gene Editing. *Nat. Commun.* **2022**, *13*, 3453.
(317) Rafiq, S.; Hackett, C. S.; Brentjens, R. J. Engineering Strategies to Overcome the Current Roadblocks in Car T Cell Therapy. *Nature reviews Clinical oncology* **2020**, *17*, 147−167.
(318) Marofi, F.; Motavalli, R.; Safonov, V. A.; Thangavelu, L.; Yumashev, A. V.; Alexander, M.; Shomali, N.; Chartrand, M. S.; Pathak, Y.; Jarahian, M.; et al. Car T Cells in Solid Tumors: Challenges and Opportunities. *Stem cell research & therapy* **2021**, *12*, 81.
(319) Zinn, S.; Vazquez-Lombardi, R.; Zimmermann, C.; Sapra, P.; Jermutus, L.; Christ, D. Advances in Antibody-Based Therapy in Oncology. *Nature Cancer* **2023**, *4*, 165−180.
(320) Zhang, Z.; Zhou, L.; Xie, N.; Nice, E. C.; Zhang, T.; Cui, Y.; Huang, C. Overcoming Cancer Therapeutic Bottleneck by Drug Repurposing. *Signal Transduction and Targeted Therapy* **2020**, *5*, 113.
(321) Yang, D.; Zhou, Q.; Labroska, V.; Qin, S.; Darbalaei, S.; Wu, Y.; Yuliantie, E.; Xie, L.; Tao, H.; Cheng, J.; et al. G Protein-Coupled Receptors: Structure-and Function-Based Drug Discovery. *Signal transduction and targeted therapy* **2021**, *6*, 7.
(322) Nero, T. L.; Morton, C. J.; Holien, J. K.; Wielens, J.; Parker, M. W. Oncogenic Protein Interfaces: Small Molecules, Big Challenges. *Nat. Rev. Cancer* **2014**, *14*, 248−262.
(323) Dobson, C. M. Chemical Space and Biology. *Nature* **2004**, *432*, 824−828.
(324) Singh, I.; Seth, A.; Billesbølle, C. B.; Braz, J.; Rodriguiz, R. M.; Roy, K.; Bekele, B.; Craik, V.; Huang, X.-P.; Boytsov, D.; et al. Structure-Based Discovery of Conformationally Selective Inhibitors of the Serotonin Transporter. *Cell* **2023**, *186*, 2160−2175.
(325) Sadybekov, A. A.; Sadybekov, A. V.; Liu, Y.; Iliopoulos-Tsoutsouvas, C.; Huang, X.-P.; Pickett, J.; Houser, B.; Patel, N.; Tran, N. K.; Tong, F.; et al. Synthon-Based Ligand Discovery in Virtual Libraries of over 11 Billion Compounds. *Nature* **2022**, *601*, 452−459.
(326) Gentile, F.; Yaacoub, J. C.; Gleave, J.; Fernandez, M.; Ton, A.-T.; Ban, F.; Stern, A.; Cherkasov, A. Artificial Intelligence-Enabled Virtual Screening of Ultra-Large Chemical Libraries with Deep Docking. *Nat. Protoc.* **2022**, *17*, 672−697.
(327) Olivecrona, M.; Blaschke, T.; Engkvist, O.; Chen, H. Molecular De-Novo Design through Deep Reinforcement Learning. *Journal of cheminformatics* **2017**, *9*, 48.
(328) Wang, Y.; Wang, J.; Cao, Z.; Barati Farimani, A. Molecular Contrastive Learning of Representations Via Graph Neural Networks. *Nature Machine Intelligence* **2022**, *4*, 279−287.
(329) Graff, D. E.; Shakhnovich, E. I.; Coley, C. W. Accelerating High-Throughput Virtual Screening through Molecular Pool-Based Active Learning. *Chemical science* **2021**, *12*, 7866−7881.
(330) Chen, S.; Gao, J.; Chen, J.; Xie, Y.; Shen, Z.; Xu, L.; Che, J.; Wu, J.; Dong, X. Clusterx: A Novel Representation Learning-Based Deep Clustering Framework for Accurate Visual Inspection in Virtual Screening. *Brief. Bioinform.* **2023**, *24*, bbad126.
(331) Corso, G.; Stärk, H.; Jing, B.; Barzilay, R.; Jaakkola, T. Diffdock: Diffusion Steps, Twists, and Turns for Molecular Docking. *arXiv.* **2022**, 2210.01776.
(332) Watson, J. L.; Juergens, D.; Bennett, N. R.; Trippe, B. L.; Yim, J.; Eisenach, H. E.; Ahern, W.; Borst, A. J.; Ragotte, R. J.; Milles, L. F.; Wicky, B. I. M.; Hanikel, N.; Pellock, S. J.; Courbet, A.; Sheffler, W.; Wang, J.; Venkatesh, P.; Sappington, I.; Torres, S. V.; Lauko, A.; et al. De Novo Design of Protein Structure and Function with Rfdiffusion. *Nature* **2023**, *620*, 1089−1100.
(333) Ingraham, J. B.; Baranov, M.; Costello, Z.; Barber, K. W.; Wang, W.; Ismail, A.; Frappier, V.; Lord, D. M.; Ng-Thow-Hing, C.; Van Vlack, E. R.; Tie, S.; Xue, V.; Cowles, S. C.; Leung, A.; Rodrigues, J. V.; Morales-Perez, C. L.; Ayoub, A. M.; Green, R.; Puentes, K.; Oplinger, F.; et al. Illuminating Protein Space with a Programmable Generative Model. *Nature* **2023**, *623*, 1070−1078.
(334) Atance, S. R.; Diez, J. V.; Engkvist, O.; Olsson, S.; Mercado, R. De Novo Drug Design Using Reinforcement Learning with Graph-Based Deep Generative Models. *J. Chem. Inf. Model.* **2022**, *62*, 4863−4872.
(335) Segler, M. H.; Kogej, T.; Tyrchan, C.; Waller, M. P. Generating Focused Molecule Libraries for Drug Discovery with Recurrent Neural Networks. *ACS central science* **2018**, *4*, 120−131.

https://doi.org/10.1021/acsnano.4c12599
ACS Nano 2024, 18, 29311−29336

(336) Cho, K.; Van Merriënboer, B.; Bahdanau, D.; Bengio, Y. On the Properties of Neural Machine Translation: Encoder-Decoder Approaches. *arXiv.* **2014**, 1409.1259.
(337) Li, Y.; Zhang, L.; Liu, Z. Multi-Objective De Novo Drug Design with Conditional Graph Generative Model. *Journal of cheminformatics* **2018**, *10*, 1−24.
(338) Gómez-Bombarelli, R.; Wei, J. N.; Duvenaud, D.; Hernández-Lobato, J. M.; Sánchez-Lengeling, B.; Sheberla, D.; Aguilera-Iparraguirre, J.; Hirzel, T. D.; Adams, R. P.; Aspuru-Guzik, A. Automatic Chemical Design Using a Data-Driven Continuous Representation of Molecules. *ACS central science* **2018**, *4*, 268−276.
(339) Jin, W.; Barzilay, R.; Jaakkola, T. Hierarchical Generation of Molecular Graphs Using Structural Motifs. In *International conference on machine learning*, 2020; PMLR: pp 4839−4848.
(340) Ma, T.; Chen, J.; Xiao, C. Constrained Generation of Semantically Valid Graphs Via Regularizing Variational Autoencoders. *Advances in Neural Information Processing Systems* **2018**, *31*, 7113−7124.
(341) De Cao, N.; Kipf, T. Molgan: An Implicit Generative Model for Small Molecular Graphs. *arXiv.* **2018**, 1805.11973.
(342) Goodfellow, I.; Pouget-Abadie, J.; Mirza, M.; Xu, B.; Warde-Farley, D.; Ozair, S.; Courville, A.; Bengio, Y. Generative Adversarial Networks. *Communications of the ACM* **2020**, *63*, 139−144.
(343) Arús-Pous, J.; Johansson, S. V.; Prykhodko, O.; Bjerrum, E. J.; Tyrchan, C.; Reymond, J.-L.; Chen, H.; Engkvist, O. Randomized Smiles Strings Improve the Quality of Molecular Generative Models. *Journal of cheminformatics* **2019**, *11*, 71.
(344) Arús-Pous, J.; Patronov, A.; Bjerrum, E. J.; Tyrchan, C.; Reymond, J.-L.; Chen, H.; Engkvist, O. Smiles-Based Deep Generative Scaffold Decorator for De-Novo Drug Design. *Journal of cheminformatics* **2020**, *12*, 38.
(345) Yang, K.; Swanson, K.; Jin, W.; Coley, C.; Eiden, P.; Gao, H.; Guzman-Perez, A.; Hopper, T.; Kelley, B.; Mathea, M.; et al. Analyzing Learned Molecular Representations for Property Prediction. *J. Chem. Inf. Model.* **2019**, *59*, 3370−3388.
(346) Atz, K.; Grisoni, F.; Schneider, G. Geometric Deep Learning on Molecular Representations. *Nature Machine Intelligence* **2021**, *3*, 1023−1032.
(347) Mercado, R.; Rastemo, T.; Lindelöf, E.; Klambauer, G.; Engkvist, O.; Chen, H.; Bjerrum, E. J. Graph Networks for Molecular Design. *Machine Learning: Science and Technology* **2021**, *2*, 025023.
(348) Guan, J.; Qian, W. W.; Peng, X.; Su, Y.; Peng, J.; Ma, J. 3d Equivariant Diffusion for Target-Aware Molecule Generation and Affinity Prediction. *arXiv.* **2023**, 2303.03543.
(349) Xu, M.; Yu, L.; Song, Y.; Shi, C.; Ermon, S.; Tang, J. Geodiff: A Geometric Diffusion Model for Molecular Conformation Generation. *arXiv.* **2022**, 2203.02923.
(350) Seath, C. P.; Burton, A. J.; Sun, X.; Lee, G.; Kleiner, R. E.; MacMillan, D. W. C.; Muir, T. W. Tracking Chromatin State Changes Using Nanoscale Photo-Proximity Labelling. *Nature* **2023**, *616*, 574−580.
(351) Gainza, P.; Wehrle, S.; Van Hall-Beauvais, A.; Marchand, A.; Scheck, A.; Harteveld, Z.; Buckley, S.; Ni, D.; Tan, S.; Sverrisson, F.; Goverde, C.; Turelli, P.; Raclot, C.; Teslenko, A.; Pacesa, M.; Rosset, S.; Georgeon, S.; Marsden, J.; Petruzzella, A.; Liu, K.; et al. De Novo Design of Protein Interactions with Learned Surface Fingerprints. *Nature* **2023**, *617*, 176−184.
(352) Bryant, P.; Pozzati, G.; Elofsson, A. Improved Prediction of Protein-Protein Interactions Using Alphafold2. *Nat. Commun.* **2022**, *13*, 1265.
(353) Gao, Z.; Jiang, C.; Zhang, J.; Jiang, X.; Li, L.; Zhao, P.; Yang, H.; Huang, Y.; Li, J. Hierarchical Graph Learning for Protein-Protein Interaction. *Nat. Commun.* **2023**, *14*, 1093.
(354) Chen, S.-J.; Hassan, M.; Jernigan, R. L.; Jia, K.; Kihara, D.; Kloczkowski, A.; Kotelnikov, S.; Kozakov, D.; Liang, J.; Liwo, A.; et al. Protein Folds Vs. Protein Folding: Differing Questions, Different Challenges. *Proc. Natl. Acad. Sci. U. S. A.* **2023**, *120*, No. e2214423119.
(355) Nussinov, R.; Zhang, M.; Liu, Y.; Jang, H. Alphafold, Allosteric, and Orthosteric Drug Discovery: Ways Forward. *Drug Discovery Today* **2023**, *28*, 103551.
(356) Wang, Y.; Yan, J.; Goult, B. T. Force-Dependent Binding Constants. *Biochemistry* **2019**, *58*, 4696−4709.
(357) Del Rio, A.; Perez-Jimenez, R.; Liu, R.; Roca-Cusachs, P.; Fernandez, J. M.; Sheetz, M. P. Stretching Single Talin Rod Molecules Activates Vinculin Binding. *Science* **2009**, *323*, 638−641.
(358) Mondal, S.; Johnston, J. M.; Wang, H.; Khelashvili, G.; Filizola, M.; Weinstein, H. Membrane Driven Spatial Organization of Gpcrs. *Sci. Rep.* **2013**, *3*, 2909.
(359) Reynolds, M. J.; Hachicho, C.; Carl, A. G.; Gong, R.; Alushin, G. M. Bending Forces and Nucleotide State Jointly Regulate F-Actin Structure. *Nature* **2022**, *611*, 380−386.
(360) Oosterheert, W.; Klink, B. U.; Belyy, A.; Pospich, S.; Raunser, S. Structural Basis of Actin Filament Assembly and Aging. *Nature* **2022**, *611*, 374−379.
(361) Strohmeyer, N.; Bharadwaj, M.; Costell, M.; Fässler, R.; Müller, D. J. Fibronectin-Bound A5β1 Integrins Sense Load and Signal to Reinforce Adhesion in Less Than a Second. *Nat. Mater.* **2017**, *16*, 1262−1270.
(362) Li, J.; Springer, T. A. Integrin Extension Enables Ultrasensitive Regulation by Cytoskeletal Force. *Proc. Natl. Acad. Sci. U. S. A.* **2017**, *114*, 4685−4690.
(363) Newton, M. D.; Taylor, B. J.; Driessen, R. P.; Roos, L.; Cvetesic, N.; Allyjaun, S.; Lenhard, B.; Cuomo, M. E.; Rueda, D. S. DNA Stretching Induces Cas9 Off-Target Activity. *Nat. Struct. Mol. Biol.* **2019**, *26*, 185−192.
(364) Pradhan, B.; Kanno, T.; Umeda Igarashi, M.; Loke, M. S.; Baaske, M. D.; Wong, J. S. K.; Jeppsson, K.; Björkegren, C.; Kim, E. The Smc5/6 Complex Is a DNA Loop-Extruding Motor. *Nature* **2023**, *616*, 843−848.
(365) Davidson, I. F.; Barth, R.; Zaczek, M.; van der Torre, J.; Tang, W.; Nagasaka, K.; Janissen, R.; Kerssemakers, J.; Wutz, G.; Dekker, C.; Peters, J.-M. Ctcf Is a DNA-Tension-Dependent Barrier to Cohesin-Mediated Loop Extrusion. *Nature* **2023**, *616*, 822−827.
(366) Brouwer, I.; Kerklingh, E.; van Leeuwen, F.; Lenstra, T. L. Dynamic Epistasis Analysis Reveals How Chromatin Remodeling Regulates Transcriptional Bursting. *Nat. Struct. Mol. Biol.* **2023**, *30*, 692−702.
(367) Risca, V. I.; Wang, E. B.; Chaudhuri, O.; Chia, J. J.; Geissler, P. L.; Fletcher, D. A. Actin Filament Curvature Biases Branching Direction. *Proc. Natl. Acad. Sci. U. S. A.* **2012**, *109*, 2913−2918.
(368) Svitkina, T. M. Actin Bends over Backward for Directional Branching. *Proc. Natl. Acad. Sci. U. S. A.* **2012**, *109*, 2693−2694.
(369) McCafferty, C. L.; Pennington, E. L.; Papoulas, O.; Taylor, D. W.; Marcotte, E. M. Does Alphafold2Model Proteins' Intracellular Conformations? An Experimental Test Using Cross-Linking Mass Spectrometry of Endogenous Ciliary Proteins. *Communications Biology* **2023**, *6*, 421.
(370) Ayaz, P.; Lyczek, A.; Paung, Y.; Mingione, V. R.; Iacob, R. E.; de Waal, P. W.; Engen, J. R.; Seeliger, M. A.; Shan, Y.; Shaw, D. E. Structural Mechanism of a Drug-Binding Process Involving a Large Conformational Change of the Protein Target. *Nat. Commun.* **2023**, *14*, 1885.
(371) Pan, A. C.; Jacobson, D.; Yatsenko, K.; Sritharan, D.; Weinreich, T. M.; Shaw, D. E. Atomic-Level Characterization of Protein-Protein Association. *Proc. Natl. Acad. Sci. U. S. A.* **2019**, *116*, 4244−4249.
(372) Lindorff-Larsen, K.; Piana, S.; Palmo, K.; Maragakis, P.; Klepeis, J. L.; Dror, R. O.; Shaw, D. E. Improved Side-Chain Torsion Potentials for the Amber Ff99sb Protein Force Field. *Proteins: Struct., Funct., Bioinf.* **2010**, *78*, 1950−1958.
(373) Grosdidier, A.; Zoete, V.; Michielin, O. Fast Docking Using the Charmm Force Field with Eadock Dss. *J. Comput. Chem.* **2011**, *32*, 2149−2159.
(374) Zhu, X.; Lopes, P. E.; MacKerell, A. D., Jr Recent Developments and Applications of the Charmm Force Fields. *Wiley*

https://doi.org/10.1021/acsnano.4c12599
ACS Nano 2024, 18, 29311−29336

Interdisciplinary Reviews: Computational Molecular Science **2012**, *2*, 167−185.
(375) Goossens, K.; De Winter, H. Molecular Dynamics Simulations of Membrane Proteins: An Overview. *J. Chem. Inf. Model.* **2018**, *58*, 2193−2202.
(376) Schmid, N.; Eichenberger, A. P.; Choutko, A.; Riniker, S.; Winger, M.; Mark, A. E.; Van Gunsteren, W. F. Definition and Testing of the Gromos Force-Field Versions 54a7 and 54b7. *Eur. Biophys. J.* **2011**, *40*, 843−856.
(377) Diem, M.; Oostenbrink, C. Hamiltonian Reweighing to Refine Protein Backbone Dihedral Angle Parameters in the Gromos Force Field. *J. Chem. Inf. Model.* **2020**, *60*, 279−288.
(378) Robertson, M. J.; Tirado-Rives, J.; Jorgensen, W. L. Improved Peptide and Protein Torsional Energetics with the Opls-Aa Force Field. *J. Chem. Theory Comput.* **2015**, *11*, 3499−3509.
(379) Robertson, M. J.; Skiniotis, G. Development of Opls-Aa/M Parameters for Simulations of G Protein-Coupled Receptors and Other Membrane Proteins. *J. Chem. Theory Comput.* **2022**, *18*, 4482−4489.
(380) Souza, P. C. T.; Alessandri, R.; Barnoud, J.; Thallmair, S.; Faustino, I.; Grünewald, F.; Patmanidis, I.; Abdizadeh, H.; Bruininks, B. M. H.; Wassenaar, T. A.; Kroon, P. C.; Melcr, J.; Nieto, V.; Corradi, V.; Khan, H. M.; Domański, J.; Javanainen, M.; Martinez-Seara, H.; Reuter, N.; Best, R. B.; et al. Martini 3: A General Purpose Force Field for Coarse-Grained Molecular Dynamics. *Nat. Methods* **2021**, *18*, 382−388.
(381) Monticelli, L.; Kandasamy, S. K.; Periole, X.; Larson, R. G.; Tieleman, D. P.; Marrink, S.-J. The Martini Coarse-Grained Force Field: Extension to Proteins. *J. Chem. Theory Comput.* **2008**, *4*, 819−834.
(382) Bernardi, R. C.; Melo, M. C.; Schulten, K. Enhanced Sampling Techniques in Molecular Dynamics Simulations of Biological Systems. *Biochimica et Biophysica Acta (BBA)-General Subjects* **2015**, *1850*, 872−877.
(383) Beedle, A. E.; Garcia-Manyes, S. The Role of Single-Protein Elasticity in Mechanobiology. *Nature Reviews Materials* **2023**, *8*, 10−24.
(384) Donaldson, J. G.; Jackson, C. L. Arf Family G Proteins and Their Regulators: Roles in Membrane Transport, Development and Disease. *Nat. Rev. Mol. Cell Biol.* **2011**, *12*, 362−375.
(385) Park, S.; Schulten, K. Calculating Potentials of Mean Force from Steered Molecular Dynamics Simulations. *J. Chem. Phys.* **2004**, *120*, 5946−5961.
(386) Wang, E.; Sun, H.; Wang, J.; Wang, Z.; Liu, H.; Zhang, J. Z.; Hou, T. End-Point Binding Free Energy Calculation with Mm/Pbsa and Mm/Gbsa: Strategies and Applications in Drug Design. *Chem. Rev.* **2019**, *119*, 9478−9508.
(387) Crean, R. M.; Pudney, C. R.; Cole, D. K.; Van der Kamp, M. W. Reliable in Silico Ranking of Engineered Therapeutic Tcr Binding Affinities with Mmpb/Gbsa. *J. Chem. Inf. Model.* **2022**, *62*, 577−590.
(388) Kumari, R.; Kumar, R.; Lynn, A. G_Mmpbsa-a Gromacs Tool for High-Throughput Mm-Pbsa Calculations. *J. Chem. Inf. Model.* **2014**, *54*, 1951−1962.
(389) Miller, B. R., III; McGee, T. D., Jr; Swails, J. M.; Homeyer, N.; Gohlke, H.; Roitberg, A. E. Mmpbsa. Py: An Efficient Program for End-State Free Energy Calculations. *J. Chem. Theory Comput.* **2012**, *8*, 3314−3321.
(390) Sharp, K. A.; Honig, B. Calculating Total Electrostatic Energies with the Nonlinear Poisson-Boltzmann Equation. *J. Phys. Chem.* **1990**, *94*, 7684−7692.
(391) Wang, C.; Greene, D. A.; Xiao, L.; Qi, R.; Luo, R. Recent Developments and Applications of the Mmpbsa Method. *Frontiers in molecular biosciences* **2018**, *4*, 87.
(392) Tan, C.; Tan, Y.-H.; Luo, R. Implicit Nonpolar Solvent Models. *J. Phys. Chem. B* **2007**, *111*, 12263−12274.
(393) Duan, L.; Liu, X.; Zhang, J. Z. Interaction Entropy: A New Paradigm for Highly Efficient and Reliable Computation of Protein-Ligand Binding Free Energy. *J. Am. Chem. Soc.* **2016**, *138*, 5722−5728.
(394) Valdés-Tresanco, M. S.; Valdés-Tresanco, M. E.; Valiente, P. A.; Moreno, E. Gmx_Mmpbsa: A New Tool to Perform End-State Free Energy Calculations with Gromacs. *J. Chem. Theory Comput.* **2021**, *17*, 6281−6291.
(395) Chipot, C.; Pohorille, A. Calculating Free Energy Differences Using Perturbation Theory. In *Free Energy Calculations: Theory and Applications in Chemistry and Biology*; Springer, 2007; pp 33−75.
(396) Liu, P.; Dehez, F. o.; Cai, W.; Chipot, C. A Toolkit for the Analysis of Free-Energy Perturbation Calculations. *J. Chem. Theory Comput.* **2012**, *8*, 2606−2616.
(397) Wang, L.; Wu, Y.; Deng, Y.; Kim, B.; Pierce, L.; Krilov, G.; Lupyan, D.; Robinson, S.; Dahlgren, M. K.; Greenwood, J.; et al. Accurate and Reliable Prediction of Relative Ligand Binding Potency in Prospective Drug Discovery by Way of a Modern Free-Energy Calculation Protocol and Force Field. *J. Am. Chem. Soc.* **2015**, *137*, 2695−2703.
(398) Jorgensen, W. L.; Thomas, L. L. Perspective on Free-Energy Perturbation Calculations for Chemical Equilibria. *J. Chem. Theory Comput.* **2008**, *4*, 869−876.
(399) Bennett, C. H. Efficient Estimation of Free Energy Differences from Monte Carlo Data. *J. Comput. Phys.* **1976**, *22*, 245−268.
(400) Zhu, F.; Bourguet, F. A.; Bennett, W. F.; Lau, E. Y.; Arrildt, K. T.; Segelke, B. W.; Zemla, A. T.; Desautels, T. A.; Faissol, D. M. Large-Scale Application of Free Energy Perturbation Calculations for Antibody Design. *Sci. Rep.* **2022**, *12*, 12489.
(401) Shaw, D. E.; Adams, P. J.; Azaria, A.; Bank, J. A.; Batson, B.; Bell, A.; Bergdorf, M.; Bhatt, J.; Butts, J. A.; Correia, T. Anton 3: Twenty Microseconds of Molecular Dynamics Simulation before Lunch. In *Proceedings of the International Conference for High Performance Computing, Networking, Storage and Analysis*, 2021; pp 1−11.
(402) Ridley, A. J.; Schwartz, M. A.; Burridge, K.; Firtel, R. A.; Ginsberg, M. H.; Borisy, G.; Parsons, J. T.; Horwitz, A. R. Cell Migration: Integrating Signals from Front to Back. *Science* **2003**, *302*, 1704−1709.
(403) Fürthauer, S.; Lemma, B.; Foster, P. J.; Ems-McClung, S. C.; Yu, C.-H.; Walczak, C. E.; Dogic, Z.; Needleman, D. J.; Shelley, M. J. Self-Straining of Actively Crosslinked Microtubule Networks. *Nat. Phys.* **2019**, *15*, 1295−1300.
(404) Wang, X.; Zhu, H.; Lu, Y.; Wang, Z.; Kennedy, D. The Elastic Properties and Deformation Mechanisms of Actin Filament Networks Crosslinked by Filamins. *J. Mech. Behav. Biomed. Mater.* **2020**, *112*, 104075.
(405) Wang, X.; Zhu, H.; Song, B.; Chen, X.; Kennedy, D.; Shi, Y. Nonlinear Elastic Behaviors and Deformation Mechanisms of Nano-Structured Crosslinked Biopolymer Networks. *Extreme Mechanics Letters* **2023**, *61*, 102017.
(406) Aroush, D. R.-B.; Ofer, N.; Abu-Shah, E.; Allard, J.; Krichevsky, O.; Mogilner, A.; Keren, K. Actin Turnover in Lamellipodial Fragments. *Curr. Biol.* **2017**, *27*, 2963−2973.
(407) Civalek, Ö.; Demir, Ç. Bending Analysis of Microtubules Using Nonlocal Euler-Bernoulli Beam Theory. *Applied Mathematical Modelling* **2011**, *35*, 2053−2067.
(408) Hutchinson, J. Shear Coefficients for Timoshenko Beam Theory. *J. Appl. Mech.* **2001**, *68*, 87−92.
(409) Reddy, J. N. *Introduction to the Finite Element Method*; McGraw-Hill Education, 2019.
(410) Mund, M.; van der Beek, J. A.; Deschamps, J.; Dmitrieff, S.; Hoess, P.; Monster, J. L.; Picco, A.; Nédélec, F.; Kaksonen, M.; Ries, J. Systematic Nanoscale Analysis of Endocytosis Links Efficient Vesicle Formation to Patterned Actin Nucleation. *Cell* **2018**, *174*, 884−896.
(411) Scott, B. L.; Sochacki, K. A.; Low-Nam, S. T.; Bailey, E. M.; Luu, Q.; Hor, A.; Dickey, A. M.; Smith, S.; Kerkvliet, J. G.; Taraska, J. W.; Hoppe, A. D. Membrane Bending Occurs at All Stages of Clathrin-Coat Assembly and Defines Endocytic Dynamics. *Nat. Commun.* **2018**, *9*, 419.

https://doi.org/10.1021/acsnano.4c12599
ACS Nano 2024, 18, 29311−29336

(412) Buschmann, M. D.; Carrasco, M. J.; Alishetty, S.; Paige, M.; Alameh, M. G.; Weissman, D. Nanomaterial Delivery Systems for Mrna Vaccines. *Vaccines* **2021**, *9*, 65.
(413) Wang, M. S.; Hu, Y.; Sanchez, E. E.; Xie, X.; Roy, N. H.; de Jesus, M.; Winer, B. Y.; Zale, E. A.; Jin, W.; Sachar, C.; et al. Mechanically Active Integrins Target Lytic Secretion at the Immune Synapse to Facilitate Cellular Cytotoxicity. *Nat. Commun.* **2022**, *13*, 3222.
(414) Zheng, X.; Hou, Z.; Qian, Y.; Zhang, Y.; Cui, Q.; Wang, X.; Shen, Y.; Liu, Z.; Zhou, Y.; Fu, B.; et al. Tumors Evade Immune Cytotoxicity by Altering the Surface Topology of Nk Cells. *Nat. Immunol.* **2023**, *24*, 802−813.
(415) Molinie, N.; Gautreau, A. The Arp2/3 Regulatory System and Its Deregulation in Cancer. *Physiol. Rev.* **2018**, *98*, 215−238.
(416) Zhao, K.; Wang, D.; Zhao, X.; Wang, C.; Gao, Y.; Liu, K.; Wang, F.; Wu, X.; Wang, X.; Sun, L.; et al. Wdr63 Inhibits Arp2/3-Dependent Actin Polymerization and Mediates the Function of P53 in Suppressing Metastasis. *EMBO Rep.* **2020**, *21*, No. e49269.
(417) Dang, I.; Gorelik, R.; Sousa-Blin, C.; Derivery, E.; Guérin, C.; Linkner, J.; Nemethova, M.; Dumortier, J. G.; Giger, F. A.; Chipysheva, T. A.; et al. Inhibitory Signalling to the Arp2/3 Complex Steers Cell Migration. *Nature* **2013**, *503*, 281−284.
(418) Fregoso, F. E.; van Eeuwen, T.; Simanov, G.; Rebowski, G.; Boczkowska, M.; Zimmet, A.; Gautreau, A. M.; Dominguez, R. Molecular Mechanism of Arp2/3 Complex Inhibition by Arpin. *Nat. Commun.* **2022**, *13*, 628.
(419) Newick, K.; O'Brien, S.; Moon, E.; Albelda, S. M. Car T Cell Therapy for Solid Tumors. *Annu. Rev. Med.* **2017**, *68*, 139−152.
(420) Caruana, I.; Savoldo, B.; Hoyos, V.; Weber, G.; Liu, H.; Kim, E. S.; Ittmann, M. M.; Marchetti, D.; Dotti, G. Heparanase Promotes Tumor Infiltration and Antitumor Activity of Car-Redirected T Lymphocytes. *Nat. Med.* **2015**, *21*, 524−529.
(421) Denais, C. M.; Gilbert, R. M.; Isermann, P.; McGregor, A. L.; Te Lindert, M.; Weigelin, B.; Davidson, P. M.; Friedl, P.; Wolf, K.; Lammerding, J. Nuclear Envelope Rupture and Repair during Cancer Cell Migration. *Science* **2016**, *352*, 353−358.
(422) Raab, M.; Gentili, M.; de Belly, H.; Thiam, H.-R.; Vargas, P.; Jimenez, A. J.; Lautenschlaeger, F.; Voituriez, R.; Lennon-Duménil, A.-M.; Manel, N.; et al. Escrt Iii Repairs Nuclear Envelope Ruptures during Cell Migration to Limit DNA Damage and Cell Death. *Science* **2016**, *352*, 359−362.
(423) Bushweller, J. H. Targeting Transcription Factors in Cancer—from Undruggable to Reality. *Nat. Rev. Cancer* **2019**, *19*, 611−624.
(424) Hie, B. L.; Shanker, V. R.; Xu, D.; Bruun, T. U. J.; Weidenbacher, P. A.; Tang, S.; Wu, W.; Pak, J. E.; Kim, P. S. Efficient Evolution of Human Antibodies from General Protein Language Models. *Nat. Biotechnol.* **2023**, *42*, 275−283.
(425) Mayor-Ruiz, C.; Bauer, S.; Brand, M.; Kozicka, Z.; Siklos, M.; Imrichova, H.; Kaltheuner, I. H.; Hahn, E.; Seiler, K.; Koren, A.; Petzold, G.; Fellner, M.; Bock, C.; Müller, A. C.; Zuber, J.; Geyer, M.; Thomä, N. H.; Kubicek, S.; Winter, G. E. Rational Discovery of Molecular Glue Degraders Via Scalable Chemical Profiling. *Nat. Chem. Biol.* **2020**, *16*, 1199−1207.
(426) Békés, M.; Langley, D. R.; Crews, C. M. Protac Targeted Protein Degraders: The Past Is Prologue. *Nat. Rev. Drug Discovery* **2022**, *21*, 181−200.
(427) Cao, L.; Coventry, B.; Goreshnik, I.; Huang, B.; Sheffler, W.; Park, J. S.; Jude, K. M.; Marković, I.; Kadam, R. U.; Verschueren, K. H. G.; Verstraete, K.; Walsh, S. T. R.; Bennett, N.; Phal, A.; Yang, A.; Kozodoy, L.; DeWitt, M.; Picton, L.; Miller, L.; Strauch, E.-M.; et al. Design of Protein-Binding Proteins from the Target Structure Alone. *Nature* **2022**, *605*, 551−560.

https://doi.org/10.1021/acsnano.4c12599
ACS Nano 2024, 18, 29311−29336